

Physik Department
der Technische Universität München
Lehrstuhl für Biophysik E22

Establishment of a New Plasma Membrane Model with Well-Defined Polymer Spacers

Oliver Purrucker

Vollständiger Abdruck der von der Fakultät für Physik der Technische Universität München zur Erlangung des akademischen Grades eines

Doktors der Naturwissenschaften (Dr. rer. nat.)

genehmigten Dissertation.

Vorsitzender:	Univ.-Prof. Dr. H. Friedrich
Prüfer der Dissertation:	1. Univ.-Prof. Dr. E. Sackmann, em. 2. Hon.-Prof. Dr. P. Fromherz

Die Dissertation wurde am 10.08.2004 bei der Technischen Universität München eingereicht und durch die Fakultät für Physik am 07.09.2004 angenommen.

Meinen Eltern und meiner Oma.

Table of Contents

Summary	ix
Introduction	1
1 Materials and Methods	7
1.1 Materials	7
1.1.1 Poly(2-oxazoline) Lipopolymers	7
1.1.2 Lipids	8
1.1.3 Transmembrane Cell Receptor Integrin $\alpha_{\text{IIb}}\beta_3$	9
1.1.4 Substrates	10
1.1.5 Chemicals and Buffer Solutions	11
1.2 Film Balance and Langmuir-Blodgett Technique	12
1.2.1 Physical Principles of the Film Balance Technique	12
1.2.2 Pressure-Area-Isotherms	13
1.2.3 Langmuir-Blodgett Deposition	13
1.2.4 Fluorescence Film Balance	14
1.3 Fluorescence Microscopy	15
1.4 Lipid Vesicle Preparation and Vesicle Fusion	16
1.5 Diffusion Measurements	17
1.5.1 Continuous Bleaching	17
1.5.2 Fluorescence Recovery after Photobleaching (FRAP)	19
1.6 Fluorescence Interference Contrast Microscopy (FLIC)	22
1.7 X-Ray Scattering	24
2 Polymer-Tethered Lipid Bilayer Membranes	27
2.1 Introduction	27
2.2 Langmuir Isotherms of Lipid/Lipopolymer Monolayers	30
2.3 Langmuir-Blodgett Deposition of Lipid/Lipopolymer Monolayers	32
2.4 Spreading of Top Layers by Vesicle Fusion	34
2.5 Incorporation of Integrin $\alpha_{\text{IIb}}\beta_3$ into Polymer-Tethered Membranes	37
2.6 Diffusion Measurements in Polymer-Tethered Membranes	39
2.6.1 Theory of Diffusion	39
2.6.2 Diffusion of Lipids	42
2.6.3 Diffusion of Transmembrane Cell Receptors	46
2.7 Determination of Frictional Coupling	50
2.8 Measurement of Membrane-Substrate Distance by FLIC	53
2.9 Function of Integrin in Polymer-Tethered Membranes	56
2.10 Limitations of the Membrane Model	60
2.11 Conclusion	61

2.12 Outlook	63
3 Dissipative Structures in Lipid/Lipopolymer LB Monolayers	65
3.1 Introduction	65
3.2 Lipid/Lipopolymer Monolayers at the Air/Water Interface	67
3.3 Influence of Monolayer Constituents on Pattern Formation	69
3.3.1 Influence of Hydrophobic Mismatch	69
3.3.2 Influence of the Polymer Chain	70
3.4 Influence of Preparation Conditions on Pattern Formation	74
3.4.1 Influence of Transfer Velocity	74
3.4.2 Influence of Subphase Viscosity	75
3.5 Confirmation of Demixing of Lipid/Lipopolymer LB Monolayers	77
3.6 Mechanisms of Micropattern Formation	79
3.7 Confinement of Transmembrane Cell Receptors into Micropatterns	82
3.8 Conclusion	84
3.9 Outlook	85
A Appendix	87
A.1 Estimation of Protein/Lipid Ratio in Proteoliposomes	87
A.2 X-ray Scattering of Lipid/Lipopolymer Dispersions	90
A.3 Lipids	96
A.4 Poly(2-oxazoline) Lipopolymers	97
A.5 Abbreviations	99
A.6 Symbols	100
Bibliography	101
Acknowledgements	115
Curriculum Vitae	116
Publications	117

The surface was invented by the devil.

Wolfgang Pauli

Summary

In this thesis, a new model of the plasma membrane was established, where a lipid membrane is separated from a planar, solid substrate via hydrated polymer spacers with defined length and density, which play the role of the glycocalyx. This amphiphilic membrane tether consists of hydrophobic lipid anchors, a poly(2-methyl-2-oxazoline) spacer, and a trimethoxysilane coupling group. The supported membranes separated from the solid by polymer films possess the following advantages compared to conventional model membranes directly deposited onto planar substrates: (i) the distance between membrane and substrate can be adjusted by the length of the polymer spacer, and (ii) the average viscosity of the polymer interlayer can be controlled by the lateral tether density. This polymer film provides a bio-analog environment for membrane spanning proteins.

Supported membranes were prepared by the following two steps: (i) the proximal membrane leaflet was deposited by Langmuir-Blodgett (LB) transfer of a suitable lipid/lipopolymer mixture onto a solid substrate, and (ii) the distal leaflet was prepared by fusion of lipid vesicles onto the dry LB monolayer. Optimization of both preparation steps resulted in the formation of stable and defect-free membranes over large areas in cm^2 range.

Impacts of the spacer length and the lipopolymer fraction on the lateral diffusivity of lipids were systematically compared by fluorescence recovery after photobleaching (FRAP). At a ratio of 5 mol% lipopolymers, the diffusion was independent from the length of the polymer tether, exhibiting diffusion coefficients of $D = 1.4\text{-}1.6 \mu\text{m}^2\text{s}^{-1}$ and mobile fractions of $R \approx 98\%$. However, the introduction of 50 mol% of lipopolymers in the proximal layer resulted in the reduction of D to $0.4 \mu\text{m}^2\text{s}^{-1}$.

The distance d between membrane and underlying substrate was quantitatively measured as a function of polymer chain length ($n = 14\text{-}104$) using fluorescence interference contrast microscopy (FLIC). The distance was found to be uniform for all polymer tethers in spite of the low tether density (average distance ≈ 12 nm), owing to the well-defined polymer chain length. The increase in spacer length from $n = 33$ to $n = 104$ led to an increase in the distance from $d = (2.3 \pm 0.7)$ nm to $d = (4.8 \pm 0.6)$ nm, which is much larger than d of solid supported membranes ($d \approx 2$ nm).

The functionality and the usefulness of the membrane model was tested by reconstitution of the transmembrane cell receptor integrin $\alpha_{IIb}\beta_3$ into the polymer-tethered membrane. Homogeneity of integrin distribution in the membrane was found to be dependent on the length of the lipopolymer spacer, which seems to be plausible from FLIC analysis of the membrane-substrate distance. Moreover, the diffusion coefficient D and mobile fraction R of integrin were found to increase with decreasing tether density and with increasing membrane-substrate distance. Applying long lipopolymer spacers ($n = 104$) at a low molar fraction (0.5%), the measured values were $D = (0.13 \pm 0.06) \mu\text{m}^2\text{s}^{-1}$ and $R = (24 \pm 8) \%$, respectively.

Based on the obtained membrane-substrate distances d and the diffusion coefficients D , the effect of two parameters, the length and density of polymer spacers, on the friction coefficient b_s between integrins and solid substrates were discussed according to the theory of Evans and Sackmann. Dependent on the tether length and density, b_s varied between 1.5 and $2.7 \times 10^8 \text{Nsm}^{-3}$. Using d obtained from FLIC measurements, the viscosity of the water reservoir η_l was estimated to be in the range of 0.4 to 0.7Nsm^{-2} . This indicates the advantage of the strategy to systematically control the hydrated polymer interlayers.

The functionality of integrin $\alpha_{IIb}\beta_3$ in polymer-tethered membranes was evaluated by quantitative measurements of the free energy of adhesion of giant vesicles with synthetic ligands (cyclic hexapeptide containing the RGD sequence coupled to lipid anchors, which is specifically recognized by integrin). The estimated free energy of adhesion was approximately 30 times larger than the corresponding value on solid supported membranes without tethers. Thus, the obtained results clearly demonstrate that polymer tethers with well-defined length and density facilitate the significant improvement in homogeneity, lateral mobility, and functionality of transmembrane proteins by providing a lubricant layer with an adjustable viscosity.

In the last part, an interesting phenomenon observed through the optimization of preparation methods is discussed, where stripe-like heterogeneities were observed as a result from LB transfer of the proximal leaflet. These structures do not coincide with any defect in the film but with the demixing of lipopolymer tethers and matrix lipids. In preliminary experiments, integrin $\alpha_{IIb}\beta_3$ tends to be incorporated into lipopolymer-rich domains, resulting in patterns of membrane proteins with tuneable width. This finding suggests a large potential towards the confinement of various transmembrane proteins in quasi two dimensional stripe micropatterns with thickness in the order of nm.

Introduction

One of the most important components of living cells is the plasma membrane, which enables the separation of their interior from the surrounding environment under preservation of selective material exchange between the inner and outer cellular space. The membrane can be understood as a quasi two-dimensional, supramolecular assembly consisting of amphiphilic lipids, supported by biopolymer layers (cytoskeleton, glycocalyx and extracellular matrix), associated with various integral and peripheral proteins. On the cytoplasmic side of the cell, the membrane binds to the cytoskeleton that provides mechanical stability and drives the cellular motion. On the outer leaflet of the membrane, the extracellular matrix controls the cell-cell communication and adhesion activities (Figure 1).

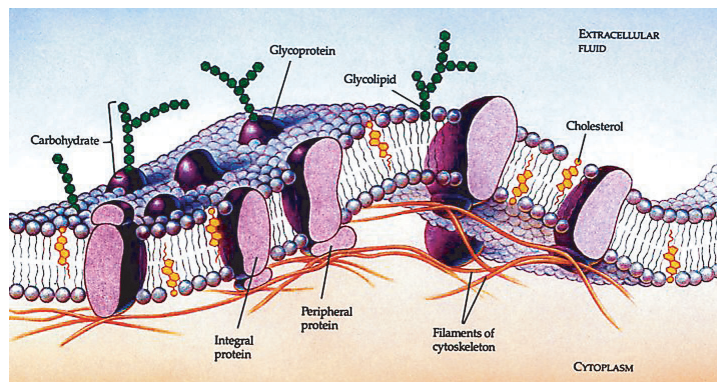


Figure 1: Schematic illustration of the cell plasma membrane (from [Campbell et al., 1999]).

In the *fluid mosaic model* [Singer & Nicolson, 1972], the cell membrane is described as a “two dimensional oriented solution of integral proteins in the viscous phospholipid bilayer solvent.” The model has been improved over years by taking into account lateral phase separation within multi-component membranes, binding of proteins to cytoskeleton or extracellular matrices, confinement of proteins to domains by the cytoskeleton and tight junctions, and the formation of large protein-lipid aggregates as functional complexes [Scalettar & Abney, 1991, Jacobson et al., 1995].

In contrast to other artificial membrane models, such as spherical lipid vesicles [Sackmann, 1995] and free standing black lipid membranes [Müller et al., 1962, Müller & Rudin, 1968], model cell membranes deposited onto planar, solid supports

(called supported membranes in the following, Figure 2) posses excellent mechanical and thermodynamical stability [Tamm & McConnell, 1985, Plant, 1993]. The planar geometries further allow for the application of various surface sensitive techniques to characterize the structures and functions of lipid-protein composite membranes in a quantitative manner.

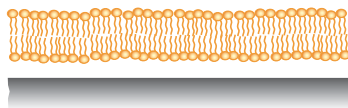


Figure 2: Sketch of a membrane supported by a solid substrate.

One of the crucial steps to introduce biological functions to supported membranes is the incorporation of transmembrane proteins, e.g. cell adhesion receptors and ion channels. A commonly used method is direct spreading of proteoliposomes (spherical lipid vesicles with integral proteins) onto solid substrates. However, the typical distance of 1-3 nm between solid supported membrane and substrate [Johnson et al., 1991, Koenig et al., 1996, Lambacher & Fromherz, 2002] does not provide a sufficient water reservoir to prevent denaturing of proteins, whose extracellular domains can be larger than 10 nm [Sackmann & Bruinsma, 2002]. To circumvent this problem, hydrophilic polymer interlayers can be introduced, such as polymer *cushions* [Sackmann, 1996, Sackmann & Tanaka, 2000] or polymer *tethers* [Knoll et al., 2000], which can supply a more “fluid” environment for proteins.

The cushions are composed of various types of hydrated polymer films (Figure 3): polyacrylamide [Kühner et al., 1994, Théato & Zentel, 2000], dextran [Elender et al., 1996, Kühner & Sackmann, 1996], agarose [Dietrich & Tampe, 1995], polyethyleneimine [Majewski et al., 1998, Wong et al., 1999], and cellulose derivatives [Schaub et al., 1993, Sigl et al., 1997]. Especially, it has been demonstrated that Langmuir-Blodgett (LB) films of regenerated cellulose (thickness: 5-10 nm) can serve as a good template for the deposition of artificial [Hillebrandt et al., 1999, Gönnerwein et al., 2003] and native cell membranes [Tanaka et al., 2001, Tanaka et al., 2004]. However, in spite of the

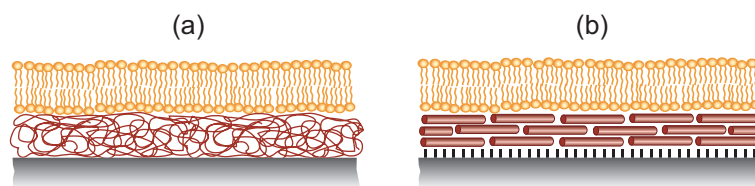


Figure 3: (a) Sketch of a supported membrane on a hydrated polymer cushion. (b) Sketch of a membrane supported by a Langmuir-Blodgett film of cellulose.

remarkable progress, it is still difficult to tune physical properties of the polymer layers in a systematic manner.

An alternative strategy to decouple a lipid membrane from a solid support without impeding the stability is the use of hydrophilic lipopolymer brushes [Häussling et al., 1991, Heyse et al., 1995, Heibel et al., 1998, Knoll et al., 2000]. Such tethers are equipped with surface coupling groups for attachment to the solid surface, lipid anchors for insertion into the membrane, and a connecting hydrophilic and flexible polymer chain that keeps a certain distance between the membrane and the substrate (Figure 4).

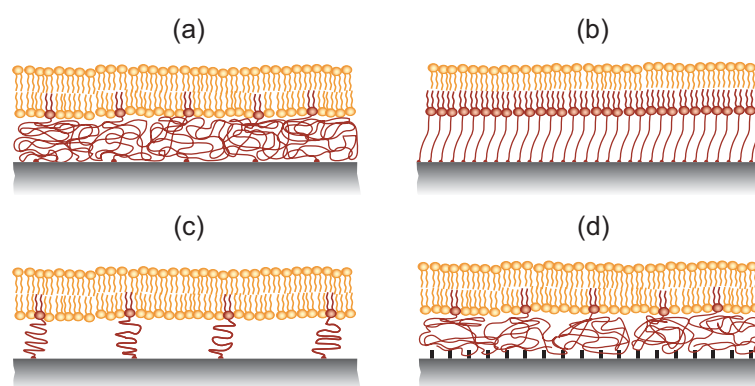


Figure 4: Schematic illustrations of tethered membranes. (a) The membrane is tethered by a random terpolymer. (b) The whole proximal layer of the membrane is tethered. (c) The tether molecule consists of lipid anchors, a polymer or peptide spacer, and a surface coupling group. (d) The lipopolymer spacer is randomly tethered to a pre-functionalized surface.

Fabrication of homogeneous and stable membranes demands quantitative control of length and lateral density of the polymer spacers, as well as the clear separation between hydrophilic polymer chains and hydrophobic membrane anchors. The first point is important to control the thickness and viscosity of the water reservoir between the substrate and the membrane, while the second, the selective hydration of the polymer spacer, is crucial to avoid formation of local defects due to the negative spreading pressure [Brochard-Wyart & de Gennes, 1992, Elender & Sackmann, 1994].

One of the possible macromolecular architectures is a random terpolymer of functional monomers (Figure 4(a)) [Spinke et al., 1992, Erdelen et al., 1994, Seitz et al., 2000, Théato & Zentel, 2000]. The polymer consists of monomers with a surface coupling group, hydrophilic monomers as spacers, and monomers with lipid anchors. The final morphology depends on the ratio between these three monomers. However, it was still difficult to control the phase separation between

hydrophobic and hydrophilic layers due to the random distribution of each building block, which often resulted in local defects.

Another possibility is the incorporation of lipopolymers with defined spacers [Häussling et al., 1991]. This well-defined molecular architecture was realized for functional polymers based on oligo(ethylene oxide) [Lang et al., 1994, Cornell et al., 1997, Raguse et al., 1998, Schiller et al., 2003], poly(ethylene oxide) [Wagner & Tamm, 2000, Wagner & Tamm, 2001], oligopeptides with thiol groups [Bunjes et al., 1997, Schmidt et al., 1998, Naumann et al., 1999], or poly(ethyloxazoline) spacers [Shen et al., 2001, Naumann et al., 2002].

Oligo(ethylene oxide) and oligopeptide spacers possess several drawbacks: due to the grafting of the molecules by self-assembly, the tether density is undefined. This can lead to a tethering of the whole proximal leaflet of the membrane (Figure 4(b)) [Schiller et al., 2003], which might impede the incorporation and unobstructed mobility of transmembrane proteins. Even if the tether density is reduced by introducing lateral spacers [Cornell et al., 1997, Raguse et al., 1998] (Figure 4(c)), the length of the tethers prevents the formation of a sufficient water reservoir between membrane and substrate. Furthermore, the rigidity of the short spacers does not allow for a soft and flexible membrane support.

In the work of Shen et al. [Shen et al., 2001] and Naumann et al. [Naumann et al., 2002], the poly(2-ethyl-2-oxazoline) lipopolymers did not carry a surface-reactive group at the end of the polymer chain. Instead of this, the surface was modified by deposition of benzophenone derivatives and the polymer was randomly grafted to these molecules by a photo-crosslinking reaction (Figure 4(d)). Hence, the distance between the surface coupling point and lipid anchors is not defined, which results in no control in membrane-substrate spacing.

In 2000, Wagner and Tamm [Wagner & Tamm, 2000] reported the deposition of supported membranes with silane-functionalized poly(ethylene oxide) (PEO) tethers ($n = 77$) on glass substrates. A mixed monolayer of lipids and lipopolymers was transferred onto a substrate by Langmuir-Blodgett (LB) deposition, followed by the fusion of vesicle suspensions to form the distal leaflet of a lipid bilayer. In comparison to grafting of tether molecules by self-assembly, the LB deposition has the advantage of precise adjustment of the tether density within the proximal leaflet (Figure 4(c)). Furthermore, PEO tethers increase the water reservoir thickness significantly compared to solid supported membranes [Kiessling & Tamm, 2003]. Moreover, this system was tested for the incorporation of several transmembrane proteins

(cytochrome b5 and annexin V [Wagner & Tamm, 2000], Syntaxin1A/SNAP25 [Wagner & Tamm, 2001, Kiessling & Tamm, 2003]). But it also bears crucial disadvantages: PEO is known to possess some hydrophobic character and it forms monolayers at the air/water interface [Kjellander & Florin, 1981, Israelachvili, 1997]. Therefore PEO is not the polymer of choice to exhibit a clear separation between polymer headgroups and lipid anchors. This can generate defects in polymer-tethered membranes, which were reported in previous studies [Wagner & Tamm, 2000]. Moreover, a systematic control of the length and density of polymer tethers is missing. Tamm and coworkers stick to one molar fraction (3%) and one length ($n = 77$) of PEO lipopolymers in all of their studies.

The primary aim of this thesis was the establishment of a new artificial plasma membrane model. As membrane tethers, poly(2-methyl-2-oxazoline) lipopolymers were used. The lipopolymers were synthesized by living cationic ring-opening polymerization (by the group of R. Jordan, Lehrstuhl für Makromolekulare Stoffe, Technische Universität München), which allows for a high flexibility in the used surface coupling group, length and side functionalities of the spacers. Furthermore, this polymerization is advantageous to realize a significantly low polydispersity index for the polymer chains so that the spacer length can be precisely controlled [Jordan et al., 1996]. The alkyl chains can be inserted into the proximal leaflet of a lipid bilayer, while the other end of the lipopolymers can be used to covalently graft the tethers onto the surface. In this study, hydrophilic poly(2-methyl-2-oxazoline)s with defined degrees of polymerization ($n = 14$ to 104) were used as polymer spacers, which have a high water storage capability [Rehfeldt et al., 2002] and an excellent resistance against nonspecific protein adsorption [Velandar et al., 1992, Woodle et al., 1994, Lasic & Needham, 1995, Lehmann & Rühle, 1999].

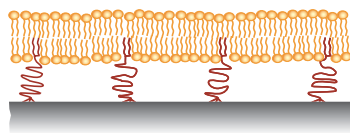


Figure 5: Sketch of a membrane tethered with poly(2-methyl-2-oxazoline) lipopolymers.

The homogeneous distribution, lateral mobility, and functionality of transmembrane proteins in polymer-tethered membranes were tested by incorporating cell adhesion receptors integrin $\alpha_{\text{IIb}}\beta_3$. This major transmembrane glycoprotein on human blood platelets plays an important role in thrombosis and hemostasis [Hynes, 1992, González-Rodríguez et al., 1994]. It is composed of an $\alpha\beta$ heterodimer

with a molecular weight of ≈ 230 kDa. Integrin exhibits a large extracellular domain with a size of $\approx 8 \times 12$ nm², two α -helical transmembrane domains with a particular radius of 0.45 nm, and two short cytoplasmic C-terminal tails (20-50 residues each) [Hynes, 1992, González-Rodríguez et al., 1994]. The extracellular domain binds to proteins of the insoluble extracellular matrix (ECM) or to counter-receptors on other cells [Schwartz et al., 1995, Ruoslahti, 1996]. This is accomplished by binding sites for the tripeptide sequence Arg-Gly-Asp (RGD) present in fibronectin, vitronectin, van Willebrandt factor, fibrinogen, and thrombospondin. Also an alternative ligand sequence KQAGDV from fibrinogen is recognized [Hynes, 1992, Ruoslahti, 1996]. The cytoplasmic domains of integrin form links with the cytoskeletal elements [Schwartz et al., 1995, Ruoslahti, 1996].

In contrast to solid supported membranes, it was demonstrated that the homogeneous distribution of integrins was significantly improved by introduction of relatively long ($n \geq 33$) polymer spacers. The measurements of lateral diffusion coefficients and mobile fractions postulated the clear influence of the length and density of spacers on the viscosity of the interlayer between the membrane and the substrate. Furthermore, the functionality of integrins in polymer-tethered membranes (evaluated by the adhesion free energy to giant lipid vesicles with synthetic RGD ligands) was remarkably enhanced with respect to that in solid supported membranes. The obtained results strongly suggest a large potential of this plasma membrane model both towards scientific (quantitative study of protein functions and cell adhesion) and practical (fast screening templates for drug discovery) applications.

1. Materials and Methods

For the establishment of polymer-tethered membranes as model system, the following materials, preparation methods, and characterization techniques were applied.

1.1 Materials

1.1.1 Poly(2-oxazoline) Lipopolymers

In this study, lipid bilayer membranes were supported by poly(2-oxazoline) lipopolymer tethers. The synthesis was performed by Anton Förtig and Rainer Jordan (Lehrstuhl für Makromolekulare Stoffe, TU München, Germany), details can be found in recent publications [Jordan et al., 1996, Jordan et al., 2001a, Förtig et al., 2003, Förtig et al., 2004, Purruicker et al., 2004a, Purruicker et al., 2004b].

The advantage of the used “living cationic ring-opening polymerization“ of 2-alkyl-2-oxazolines is the variability in the synthesis: the linear polymer chains have an adjustable degree of polymerization, a low polydispersity, and a quantitative end-functionalization at both ends of the polymer [Jordan et al., 2001a]. Throughout this study, lipopolymers composed of a distearoyl lipid moiety, a hydrophilic poly(2-methyl-2-oxazoline) polymer spacer, and a trimethoxysilane surface coupling group were used predominantly after careful optimization of the polymer-tethered membrane system (see Figure 1.1).

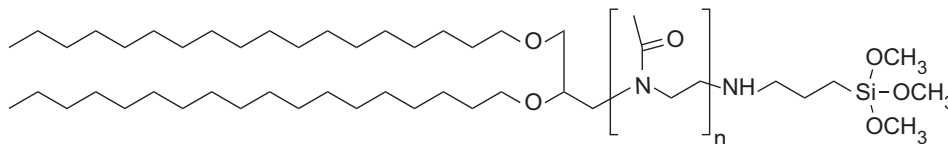


Figure 1.1: Chemical structure of poly(2-methyl-2-oxazoline) lipopolymer with distearoyl lipid moiety and trimethoxysilane coupling group (DS-PMO_{x_n}-Si).

The double chain lipid moiety with ether instead of ester linkages is stable against hydrolysis - analog to lipids found in archaea [Woese & Fox, 1977]. The importance of the ether linkage for preparation of stable membranes was recently postulated by several groups [Mathai et al., 2001, Schiller et al., 2003]. In contrast to earlier accounts of Jordan et al., 2-methyl-2-oxazoline instead of 2-

ethyl-2-oxazoline was used as the monomer. Both monomers resulted in hydrophilic polymers with similar swelling behavior [Rehfeldt et al., 2002], which suppress unspecific adsorption to proteins [Velandar et al., 1992, Woodle et al., 1994, Lasic & Needham, 1995, Lehmann & R uhe, 1999]. However, recent studies revealed adsorption of poly(2-ethyl-2-oxazoline) to the air/water interface, which might result in poorer separation between lipid anchors and polymer spacers [Baekmark et al., 1997, Baekmark et al., 1998, Foreman et al., 2003]. In the synthesis, also trimethoxysilane groups instead of dimethylmethoxysilane groups were used for surface coupling. Although both are suitable coupling groups to oxide surfaces, tri-functional silanes guarantee more effective coupling reaction and higher stability towards hydrolysis. Since the lipopolymers were deposited at relatively low grafting densities, a polycondensation of the silane end groups during or after the Langmuir-Blodgett transfer (see Section 1.2.3) is negligible.

For the characterization of the membrane model system, further lipopolymers with different lipid moieties and end-functionalizations were used, which can be seen in detail in Appendix A.4.

1.1.2 Lipids

In this study, the following lipids were used without further purification:

abbreviation	full name	fluorescence ex. / em.
SOPC ¹	1-stearoyl-2-oleoyl- <i>sn</i> -glycero-3-phosphocholine	-
DPhPC ¹	1,2-diphytanoyl- <i>sn</i> -glycero-3-phosphocholine	-
DMPC ¹	1,2-dimyristoyl- <i>sn</i> -glycero-3-phosphocholine	-
DSPC ²	1,2-distearoyl- <i>sn</i> -glycero-3-phosphocholine	-
DMPG ¹	1,2-dimyristoyl- <i>sn</i> -glycero-3-[phospho-rac-(1-glycerol)]	-
SOPG ¹	1-stearoyl-2-oleoyl- <i>sn</i> -glycero-3-[phospho-rac-(1-glycerol)]	-
NBD-PE ¹	1,2-dimyristoyl- <i>sn</i> -glycero-3-phosphoethanolamine-N-(7-nitro-1-1,3-benzoxadiazol-4-yl)	460 nm / 534 nm
NBD-PC ¹	1-oleoyl-2-[12-[(7-nitro-2-1,3-benzoxadiazol-4-yl)amino]dodecanoyl]- <i>sn</i> -glycero-3-phosphocholine	460 nm / 534 nm
Texas Red-PE ³	1,2-dihexadecanoyl- <i>sn</i> -glycero-3-phosphoethanolamine triethylammonium salt	582 nm / 601 nm
DiI ³	1,1'-dioctadecyl-3,3',3'-tetramethylindocarbocyanine perchlorate	549 nm / 565 nm
purchased from	¹ Avanti Polar Lipids (Alabaster, USA), ² Sigma-Aldrich (Munich, Germany) ³ Molecular Probes (Leiden, Netherlands)	

Details of the chemical structure can be seen in Appendix A.3.

1.1.3 Transmembrane Cell Receptor Integrin $\alpha_{\text{IIb}}\beta_3$

Integrin $\alpha_{\text{IIb}}\beta_3$ is the major transmembrane glycoprotein on human blood platelets and plays an important role in thrombosis and hemostasis [Hynes, 1992, González-Rodríguez et al., 1994]. It is composed of an $\alpha\beta$ heterodimer with a molecular weight of ≈ 230 kDa. The extracellular domain exhibits a size of $\approx 8 \times 12$ nm², the transmembrane domain of the heterodimer is composed of two α -helices (particular radius 0.45 nm), and the cytoplasmic part consists of two short C-terminal tails (20-50 residues each) [Hynes, 1992, González-Rodríguez et al., 1994]. The extracellular domain binds to proteins of the insoluble extracellular matrix (ECM) or to counter-receptors on other cells [Schwartz et al., 1995, Ruoslahti, 1996]. This is accomplished by binding sites for the tripeptide sequence Arg-Gly-Asp (RGD) present in fibronectin, vitronectin, van Willebrandt factor, fibrinogen, and thrombospondin. Also an alternative ligand sequence KQAGDV from fibrinogen is recognized [Hynes, 1992, Ruoslahti, 1996]. The cytoplasmic domains of integrin form links with the cytoskeletal elements [Schwartz et al., 1995, Ruoslahti, 1996].

Here, the extraction and incorporation of integrin into lipid vesicles is presented in brief:

Integrin $\alpha_{\text{IIb}}\beta_3$ was extracted from outdated human blood platelets of the local blood bank using Triton X-100 (Sigma-Aldrich, Munich, Germany), following the protocol of Fitzgerald et al. [Fitzgerald et al., 1985], whose specific function was checked by enzyme-linked immunosorbent assay (ELISA) tests. For reconstitution of integrins into lipid vesicles, Triton X-100 was removed by Bio-Beads SM2 adsorbents from Bio-Rad Laboratories (Hercules, USA), as described previously [Erb et al., 1997, Müller et al., 1993, Hu et al., 2000].

As matrix lipids, 1:1 mixtures (molar) of DMPC and DMPG, or SOPC and SOPG were used. The proteoliposomes were separated from pure lipid vesicles and pure protein aggregates by centrifugation in a sucrose gradient, and dialyzed to Tris-buffer (see Section 1.1.5).

For fluorescence microscopy and FRAP experiments, integrins were labelled with 5-(and-6)-carboxytetramethylrhodamine, succinimidyl ester (5(6)-TAMRA-SE, ex. 540 nm, em. 565 nm, Molecular Probes, Leiden, Netherlands), whose labelling efficiency was quantified to be 100% [Hu et al., 2000]. The labelled and unlabelled proteins were mixed to yield a final molar fraction of labelled proteins of 10%.

The incorporation of integrin $\alpha_{\text{IIb}}\beta_3$ into polymer-tethered membranes was carried out by spreading of proteoliposomes onto the dry, hydrophobic LB monolayers, ana-

log to Section 1.4. The liposomes were incubated for one hour at 40 °C (see Figure 1.2), and the supernatant solution was removed by intensive rinsing with Tris-buffer or Hepes-buffer solution (see Section 1.1.5).

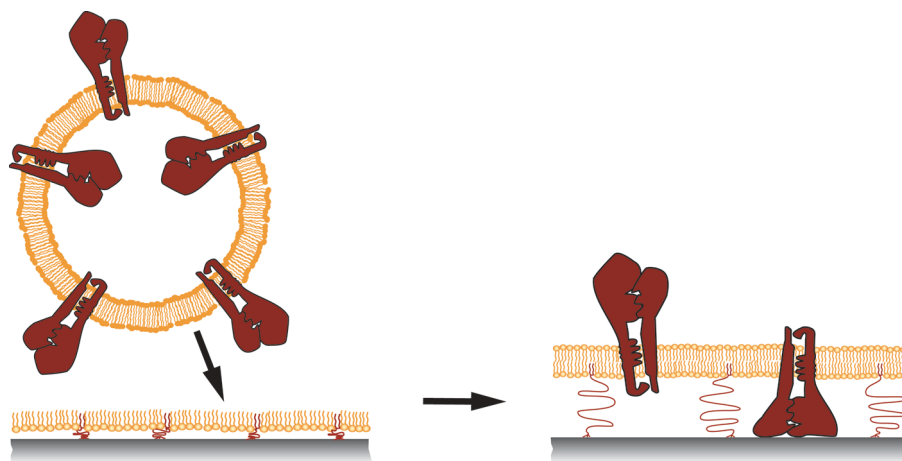


Figure 1.2: Sketch of the proteoliposome fusion procedure. Liposome suspensions were directly deposited onto the dry LB monolayers (left). This resulted in polymer-tethered lipid bilayer membranes with incorporated transmembrane cell receptors (right).

1.1.4 Substrates

As solid supports, glass cover slides (24 × 24 mm, thickness 0.17 mm) from Karl Hecht KG (Sondheim, Germany) were used. Prior to the film deposition, they were cleaned in the following manner:

- Ultrasonication (3 min) and subsequent rinsing with acetone and methanol.
- Ultrasonication in a solution of 1 : 1 : 5 (v/v) H₂O₂ (30 %) : NH₄OH (30 %) : water for 5 min, and
- soaking in the same solution for another 30 min at 60 °C [Kern & Puotinen, 1970].
- Finally, they were rinsed intensively with water, dried at 70 °C, and stored in sealed glass boxes.

1.1.5 Chemicals and Buffer Solutions

Where not stated otherwise, all chemicals were purchased from Sigma-Aldrich (Munich, Germany) and used without further purification.

For all aqueous solutions, water from a Millipore purification system ($R > 18 \text{ M}\Omega\text{cm}$, Millipore, Molsheim, France) was used.

The following buffer solutions were used, which were thoroughly degassed before the experiments:

- As *standard buffer*, an aqueous solution of 10 mM 4-(2-hydroxyethyl) piperazine-1-ethanesulfonic acid (Hepes) with 50 mM NaCl was used (pH 7.5).
- *Tris-buffer* was composed of 20 mM tris-(hydroxymethyl)-aminomethane (Tris), purchased from Roth GmbH (Karlsruhe, Germany), 150 mM NaCl, 1 mM CaCl_2 , 1 mM MgCl_2 , 1 mM NaN_3 (pH 7.4).
- For removing of proteoliposomes, *Hepes-buffer*, containing 10 mM Hepes, 100 mM NaCl, 1 mM CaCl_2 , 1 mM MgCl_2 , 1 mM NaN_3 , was used (pH 7.4).

1.2 Film Balance and Langmuir-Blodgett Technique

1.2.1 Physical Principles of the Film Balance Technique

To investigate the properties of lipid/lipopolymer monolayers at the air/water interface, the film balance technique according to Wilhelmy in combination with a Langmuir trough was used [Gaines, 1966]. In Figure 1.3, the general design of a Langmuir film balance is illustrated. Amphiphilic molecules can be spread onto the water subphase of the trough, and the area per molecule can be changed by moving the barrier.

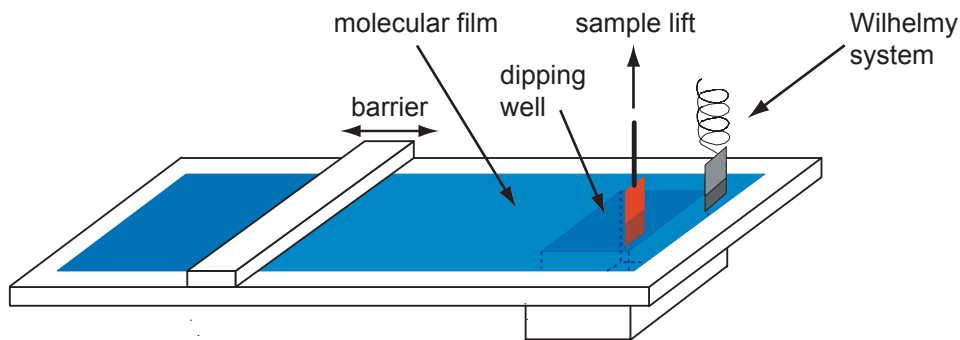


Figure 1.3: Sketch of a Langmuir-Blodgett film balance. Compared to a normal film balance, it is equipped additionally with a dipping well and a film lift, with which the monolayer can be transferred onto a solid substrate.

The surface tension of water γ_0 is decreased to γ by these amphiphiles. This reduction is denoted as surface pressure Π :

$$\Pi = \gamma_0 - \gamma \quad , \quad (1.1)$$

which can be measured by the Wilhelmy method. There, a thin plate connected to a spring is dragged towards the air/water interface by the surface tension γ . Knowing the elongation of the spring, the spring constant, and the geometry of the plate, γ can be calculated. In addition, also buoyancy and gravity are acting at the plate:

$$\vec{F}(\gamma) = mg + 2\gamma(a + b) \cos \alpha - \rho g h a b \quad , \quad (1.2)$$

where α is the contact angle between plate and water, a is the thickness, b the width, and m the mass of the Wilhelmy plate, h the height of the plate covered with water, and ρ the density of water. Since in general $a \ll b$ and $\alpha = 0$ when a thin, wettable filter paper as Wilhelmy plate is taken, the formula can be simplified to:

$$\vec{F}(\gamma) = mg + 2\gamma b \quad . \quad (1.3)$$

Therefore, the surface pressure Π can be determined from the difference in forces acting on the plate:

$$\Pi = -\Delta\gamma = -\frac{\Delta\vec{F}}{2b} . \quad (1.4)$$

1.2.2 Pressure-Area-Isotherms

Using the film balance technique, the surface pressure Π as a function of area per molecule A is measured at constant temperature to characterize amphiphilic monolayers in terms of phase behavior, compressibility, etc. First measurements of Π - A -isotherms of phospholipid monolayers were performed in the 1960s [van Deenen et al., 1962, Phillips & Chapman, 1968], and extensive and thorough experiments were carried out by Albrecht et al. [Albrecht et al., 1978, Albrecht et al., 1981]. Reviews of phospholipid monolayers were written by H. Möhwald [Möhwald, 1990, Möhwald, 1995].

For Π - A -isotherms of lipid/lipopolymer monolayers, an appropriate mixture was spread from chloroform stock solutions onto the air/water interface of a self-built Langmuir trough (subphase area: 1008 cm²) (see Figure 1.3), and the temperature was kept at 20 °C by an external thermostat (Julabo, Seelbach, Germany). After evaporation of the solvent, the monolayer was compressed by moving the barrier (barrier velocity: 50 μms^{-1}). Additionally, the lateral pressure and the barrier position was monitored.

1.2.3 Langmuir-Blodgett Deposition

For the deposition of lipid/lipopolymer monolayers onto solid substrates, the Langmuir-Blodgett (LB) technique was used [Blodgett, 1934, Blodgett, 1935, Blodgett & Langmuir, 1937]. The cleaned, hydrophilic substrates were immersed into the subphase before spreading of the monolayer onto the air/water interface. After spreading, solvent evaporation, and compression of the monolayer to a lateral pressure of $\Pi = 30 \text{ mNm}^{-1}$, the amphiphilic film was deposited onto the substrates at various transfer velocities ($\sim 50 - 500 \mu\text{ms}^{-1}$) (Figure 1.4). During the LB transfer, the surface pressure was kept constant with an electronic feedback circuit. The transfer ratio of 1:1 verified the successful transfer of the monolayer.

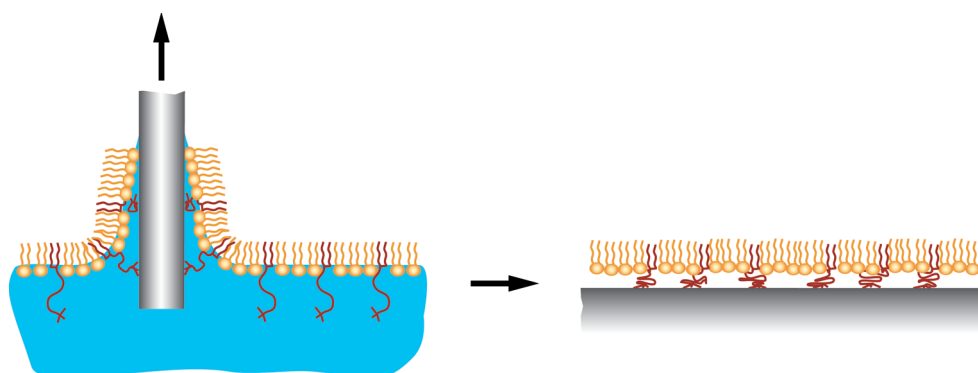


Figure 1.4: Scheme of the Langmuir-Blodgett deposition. After compression of the Langmuir monolayer, the hydrophilic substrates were withdrawn from the subphase at constant velocity (left), which resulted in dry, supported monolayers (right).

1.2.4 Fluorescence Film Balance

To investigate the phase behavior of lipid/lipopolymer monolayers at the air/water interface by optical methods, a Langmuir film balance (KSV Instruments, Helsinki, Finland) coupled to an inverted microscope (Axiovert 200, Carl Zeiss, Göttingen, Germany, see Section 1.3 for details) was used. In Figure 1.5, the setup of the fluorescence film balance is illustrated. The monolayer (with fluorescence dye tracers) is illuminated from the bottom through a quartz window using a $20\times$ long distance objective. The fluorescence emission of the dye is monitored analog to Section 1.3.

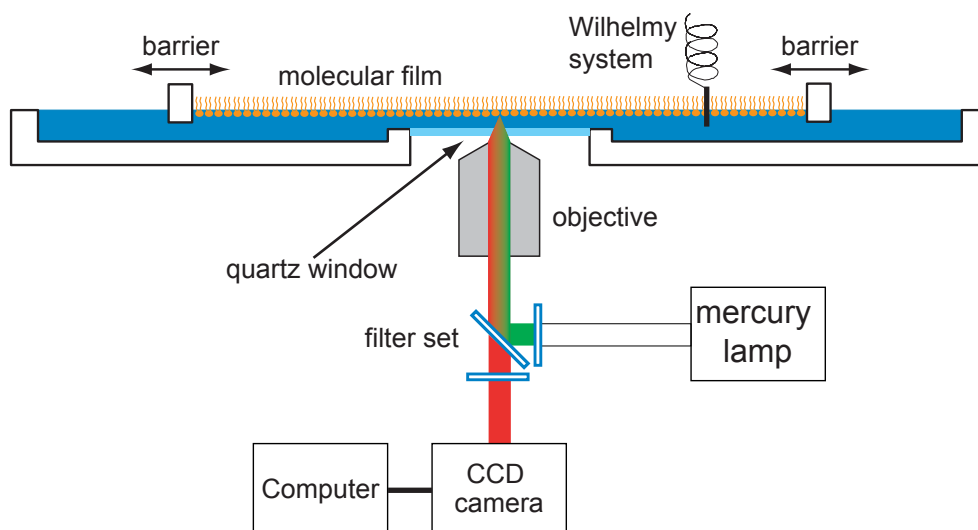


Figure 1.5: Sketch of a fluorescence film balance.

1.3 Fluorescence Microscopy

For fluorescence studies, an inverted microscope was used (Axiovert 200, Carl Zeiss, Göttingen, Germany), equipped with the following objectives:

- 63× long distance objective (Achromplan, N.A. 0.75), and
- 10× long distance objective (Achromplan, N.A. 0.25) for fluorescence images of supported lipid/lipopolymer monolayers and bilayers,
- 20× long distance objective (Achromplan, N.A. 0.40) for fluorescence images of lipid/lipopolymer monolayers at the air/water interface,

all purchased from Carl Zeiss. As a light source, a high pressure mercury lamp (HBO 100, Osram, Munich, Germany) was installed. Fluorescence filter sets were adapted to the fluorescence dye tracers incorporated in the membrane:

- For NBD, a combination of exciter (440/21 nm), dichroic (455 nm), and emitter (510/23 nm) was used (Omega Filters, , USA),
- for Texas Red, a combination of exciter (560/40 nm), dichroic (585 nm), and emitter (630/75 nm) was used (Carl Zeiss), and
- for DiI, TRITC, and TAMRA, a combination of exciter (525/45 nm), dichroic (560 nm), and emitter (595/60 nm) was used (Omega Filters).

Images and movies were taken by a cooled CCD camera (Orca ER, Hamamatsu Photonics, Herrsching, Germany), digitized by a frame-grabber card (Stemmer Imaging, Puchheim, Germany), and processed by a home-made imaging software “Open Box“ [Keller et al., 2001, Schilling, 2004].

1.4 Lipid Vesicle Preparation and Vesicle Fusion

For the preparation of polymer-tethered membranes, lipid vesicle suspensions were directly deposited onto the dry, hydrophobic LB monolayers [Kalb et al., 1992, Plant, 1993]. These suspensions in buffer solution were prepared in the following manner:

- Appropriate amounts of lipids from chloroform stock solutions were put into a glass flask.
- The solvent was evaporated by nitrogen flow with subsequent storing in a vacuum chamber over night.
- Buffer solution was added to obtain a total lipid concentration of about 1 mg mL^{-1} .
- The lipid suspension was sonicated with a tip sonifier (Bachhofer GmbH, Reutlingen, Germany) for 10 min to create small unilamellar vesicles (SUVs), which were centrifuged at 2500 min^{-1} for 5 min to remove titanium debris from the sonicator tip.
- The vesicle suspension was deposited onto the LB monolayer, and incubated for one hour at 40°C . After that, the remaining vesicles were removed by intensive rinsing with buffer solution.

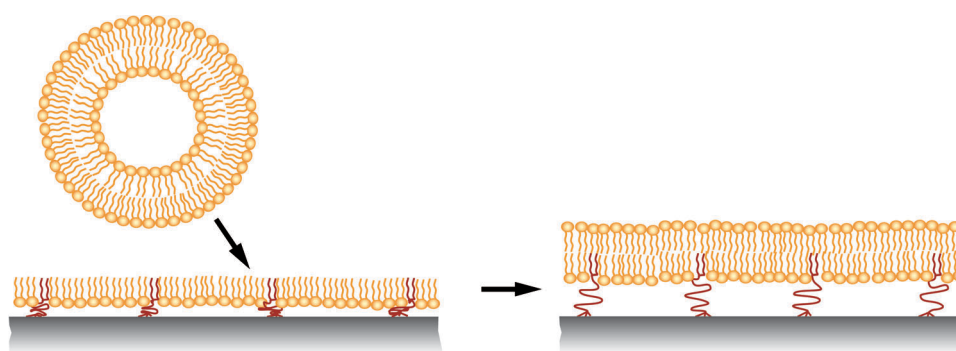


Figure 1.6: Sketch of the vesicle fusion procedure. Lipid vesicle suspensions were directly deposited onto the dry LB monolayers (left). This resulted in polymer-tethered lipid bilayer membranes (right).

1.5 Diffusion Measurements

In nature, the lipid bilayer of the cell membrane provides a fluid environment for transmembrane proteins [Singer & Nicolson, 1972, Jacobson et al., 1995], where the lateral mobility of lipids and proteins play an important role for the function of membrane components. Since this work deals with the establishment of an artificial membrane model on planar supports, measurements of diffusivity and mobility of lipids and proteins were carried out to prove the functionality of the system. Here, two measurement techniques are introduced, namely the so-called *continuous bleaching* technique and the *fluorescence recovery after photobleaching (FRAP)* technique. Further details of diffusion in membranes are presented in Section 2.6.

To estimate the diffusion coefficient and mobility of lipids in the polymer-tethered membrane, the proximal leaflet (underlayer) and the distal leaflet (toplayer) of the membrane were selectively labelled with fluorescent dyes. The underlayer was labelled by doping with 1 mol% NBD-PC in the LB monolayer, followed by spreading of unlabelled SOPC vesicles, whereas SOPC vesicles with 1 mol% NBD-PC were spread on the unlabelled monolayers to label the toplayer (see Section 1.1.2).

For investigation of mobility and diffusivity of transmembrane cell receptors, the proteins itself were stained with fluorescence dyes (see Section 1.1.3), whereby no fluorescence lipid tracers were included in the membrane.

1.5.1 Continuous Bleaching

Continuous bleaching introduced by Dietrich et al. [Dietrich & Tampe, 1995, Dietrich et al., 1997] is a convenient technique to evaluate diffusion coefficients using a standard fluorescence microscope setup, as introduced in Section 1.3. There, an area of the fluorescently labelled lipid membrane defined by the aperture of the microscope (diameter $\sim 200 \mu\text{m}$) was continuously illuminated by the high pressure mercury lamp of the microscope (Figure 1.7(a)). This resulted in photobleaching of the dye molecules and a continuous decrease in brightness, where diffusion of unbleached dye molecules into the illuminated area led to a spatial concentration profile at the edges of the illuminated area (Figure 1.7(b)).

In this type of experiments, the diffusion equation has to be extended by an additional term which describes photobleaching:

$$\frac{dc(x, y)}{dt} = D \cdot \nabla^2 c(x, y) - B(x, y) \cdot c(x, y) \quad . \quad (1.5)$$

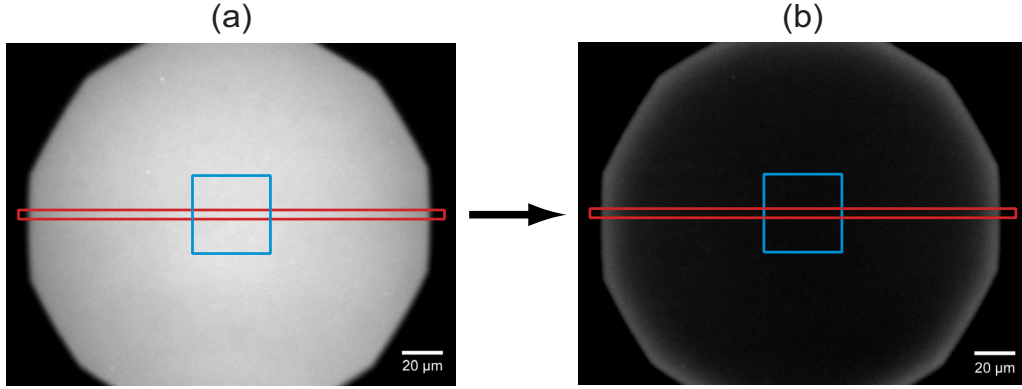


Figure 1.7: (a) Fluorescence image of a polymer tethered lipid membrane at $t = 0$ s. (b) Fluorescence image of the same area after prolonged illumination. The red boxes illustrate the area of the taken line profiles. The blue boxes denote the center area, from which the average brightness was extracted.

c denotes the concentration of tracers, D is the diffusion constant, and $B(x, y)$ is the rate of photobleaching, which is dependent on the light intensity, the chemical nature of the dye, and its environment. In the case of the experiments performed in this study, photobleaching can be treated as a stochastic decomposition process with a constant decomposition rate B_0 .

Assuming an illuminated half-plane and a constant B_0 , the concentration $c(x, t)$ of dyes within the illuminated area after long times can be written as

$$c(x, t) = A(t) \cdot e^{-\frac{x}{\lambda}} + e^{-B_0 \cdot t} . \quad (1.6)$$

Where

$$\lambda = \sqrt{\frac{D}{B_0}} \quad (1.7)$$

is the characteristic decay length. Here, only the form of the profile is stationary (mono-exponential with the decay length λ), whereas the prefactor $A(t)$ never approaches a stationary value. Knowing the bleaching rate B_0 , the diffusion constant D can be calculated from the decay length λ .

The bleaching rate B_0 was taken from the decrease in average brightness at the center of the aperture (area $\sim 1000 \mu\text{m}^2$, blue boxes in Figure 1.7, fit in Figure 1.8(b)). The decay length λ was extracted from the exponential decrease of fluorescence intensity at the rim (red boxes in Figure 1.7, line profiles in Figures 1.8(a)). The average brightness and the line profiles were extracted with the imaging software ‘‘Open Box’’.

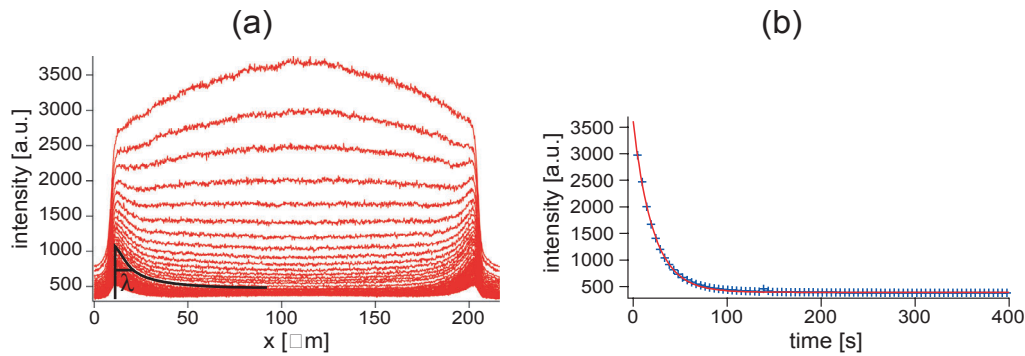


Figure 1.8: (a) Line profiles across the illuminated area which illustrate the decrease in fluorescence with time. From the exponential decay at the rim, λ was extracted. (b) Obtained average brightness (fluorescence intensity) of the center of the illuminate area. The bleaching rate B_0 was evaluated from the exponential fit.

1.5.2 Fluorescence Recovery after Photobleaching (FRAP)

Lateral diffusion coefficients and mobile fractions of lipids and transmembrane cell receptors in polymer-tethered membranes were evaluated by FRAP, introduced by Axelrod et al. [Axelrod et al., 1976].

The setup for FRAP measurements can be seen in Figure 1.9. There, the beam of an argon ion laser (power ~ 700 mW, Innova 70, Coherent, Santa Clara, CA, USA) was divided into a bleaching beam and an observation beam (1000 \times attenuated), and focussed onto the sample (spot diameter $9.3 \mu\text{m}$, see Figure 1.10) through a microscope oil immersion objective (Fluar 100 \times , N.A. 1.3, Carl Zeiss, Göttingen, Germany). The dye molecules were bleached by a short laser pulse (typically 200–400 ms), and recovery of the fluorescence intensity according to the diffusion of

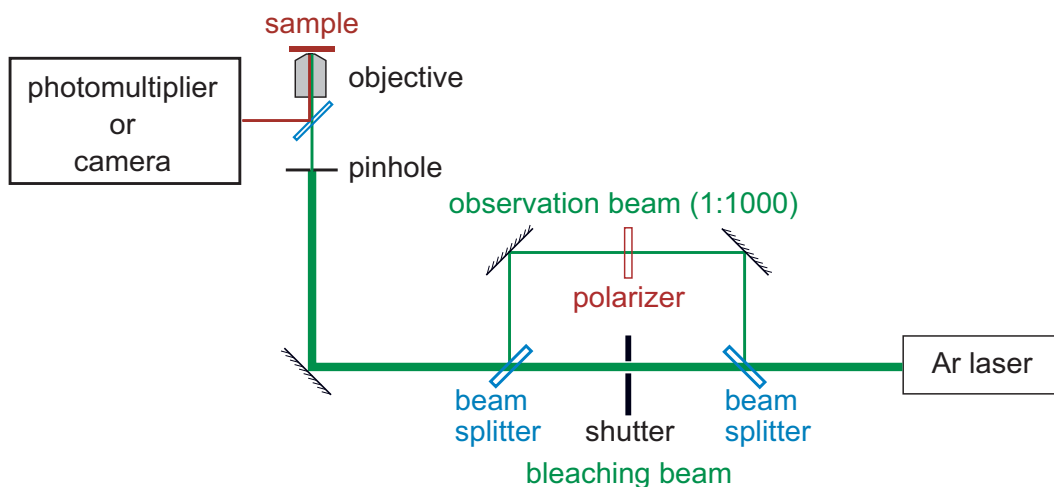


Figure 1.9: Sketch of the FRAP setup.

unbleached dyes was monitored by a RCA 31034-04 photomultiplier. To eliminate effects of drift of the optical path, the quality of the focus (in lateral and horizontal plane) was checked after each measurement with a SIT-camera (Hamamatsu Photonics, Munich, Germany) (see also [Merkel et al., 1989, Kühner et al., 1994] for details of the setup).

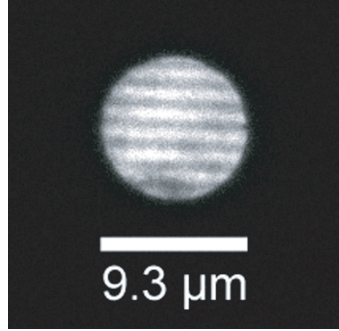


Figure 1.10: Image of a fluorescently labelled lipid membrane, illuminated by an Ar laser via the pinhole.

The lateral diffusion coefficient D and the mobile fraction R were calculated from the measured fluorescence recovery curves (see Figure 1.11), following the method reported by Soumpasis [Soumpasis, 1983], which holds for a rectangular intensity profile of the bleaching light.

From the experimental recovery curves, the characteristic time constant τ can be evaluated by fitting the following analytical expression to the intensity:

$$F(t) = F(\infty) - (F_0 - F(\infty)) \cdot \left\{ 1 - \exp\left(-\frac{2\tau}{t}\right) \left[I_0\left(\frac{2\tau}{t}\right) - I_1\left(\frac{2\tau}{t}\right) \right] \right\} , \quad (1.8)$$

with the initial fluorescence intensity F_0 , integrated over the bleaching area. $F(0)$ denotes the intensity measured directly after the bleaching pulse, and $F(\infty)$ the intensity recovered at the end of the experiment (see Figure 1.11). I_0 and I_1 are spherical Bessel functions of first and second order, respectively.

The lateral diffusion coefficient D can then be obtained by:

$$D = \frac{r^2}{4\tau} , \quad (1.9)$$

where r is the radius of the bleaching spot.

In addition, the FRAP experiments yield the relative fluorescence recovery R corresponding to the fraction of mobile fluorescence dyes within the membrane. This

parameter is defined as

$$R = \frac{F(\infty) - F(0)}{F_0 - F(0)} . \quad (1.10)$$

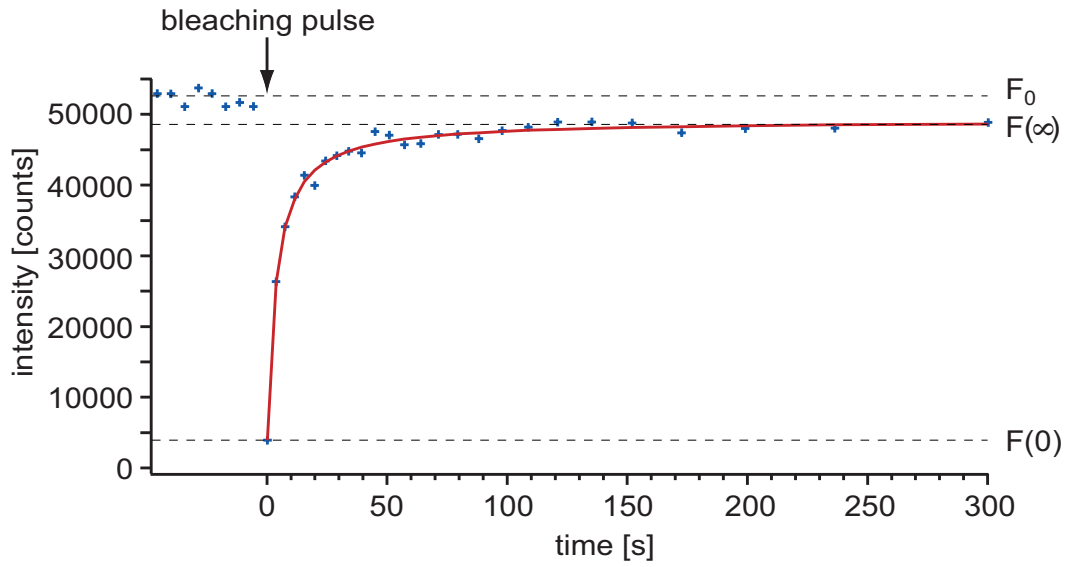


Figure 1.11: Typical fluorescence intensity recovery curve, the line illustrates the fit of the data. The arrow denotes the moment of the bleaching pulse at $t=0$ s, where the dashed lines indicate the fluorescence intensities before (F_0) the laser pulse, directly after the pulse ($F(0)$), and after recovery of the fluorescence ($F(\infty)$).

1.6 Fluorescence Interference Contrast Microscopy (FLIC)

The distance between the polymer-tethered lipid membrane and the substrate was estimated by FLIC [Lambacher & Fromherz, 1996, Braun & Fromherz, 1997, Lambacher & Fromherz, 2002].

There, the polymer-tethered membrane, doped with the fluorescent cyanine dye DiI (see Appendix A.3) in both membrane leaflets, was deposited by the LB technique (see Section 1.2.3) and subsequent vesicle fusion (see Section 1.4) onto regularly structured Si/SiO₂ chips. The silicon dioxide thickness varies in 16 steps, ranging from ~ 30 to 320 nm with a size of $2.5 \times 2.5 \mu\text{m}$ (see Figure 1.12).

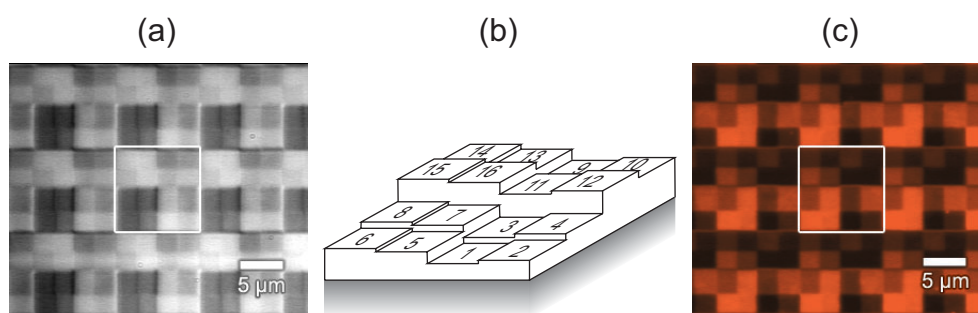


Figure 1.12: (a) Bright field image of the stepped FLIC substrate with 16 different oxide thicknesses. (b) Sketch of the 16 steps with consecutively numbered step heights. (c) Fluorescence image of the same FLIC substrate, covered with a polymer tethered membrane. The white frame denotes the 16 related steps.

Assuming a constant distance d between fluorescently labelled lipid membrane and SiO₂, the position of the dyes above the reflecting Si/SiO₂ interface varies with the oxide thickness. Since the excitation light forms standing waves above the Si, the excitation probability of the dye changes strongly with the position. The same holds for the fluorescence emission of the dyes (Figure 1.13(a)).

Therefore, the detected fluorescence depends on the excitation wavelength, the emission spectrum of the dye, the chosen fluorescence filter set and the aperture of the objective (Figure 1.12(c)). For a quantitative analysis of the fluorescence intensity, also the direction and polarization of the excitation and emission light, the orientation of the chromophore with respect to the membrane normal, its quantum yield, and the fluorescence life time have to be taken into account. Furthermore, the optical parameters of the layer system have to be known, namely the refractive indices of Si, SiO₂, water, and the lipid membrane.

To match the theoretical fluorescence intensity $F_{th}(d)$ with the experimentally ob-

tained intensity $F_{exp}(d)$ three parameters have to be adjusted: the distance d between membrane and substrate, the background fluorescence b , and the scaling factor a .

$$F_{exp}(d) = a \cdot F_{th}(d) + b \quad . \quad (1.11)$$

The experiments were carried out in the lab of Prof. P. Fromherz (Membran- und Neurophysik, MPI für Biochemie, Martinsried, Germany). An upright microscope (Axioskop) equipped with a 100× water immersion objective (Achromplan, N.A. 1.0) was used (Carl Zeiss, Göttingen, Germany). Images were taken with a CCD camera (SIS1-s285, Theta-System, Gröbenzell, Germany) and transferred by a frame-grabber card (ITEX AFG, Stemmer-Imaging, Puchheim, Germany) to a computer.

For the measurements with DiI, a combination of excitation filter (bandpass 546/10 nm, Andover, Salem, N.H.), dichroic mirror (565 nm, AHF Analysentechnik, Tübingen, Germany), and emission filter (bandpass 610/70 nm, AHF Analysentechnik) was used. The oxide thickness of the 16 steps was evaluated at large reference steps by ellipsometry (Plasmos, Munich, Germany) .

The measured fluorescence intensity was related to the oxide thickness by taking a reference image in bright field light (see Figure 1.12(a)). In FLIC theory, the distance d was estimated by the obtained intensity maxima, where the standard deviations of intensities and oxide thicknesses gives the error of the distance.

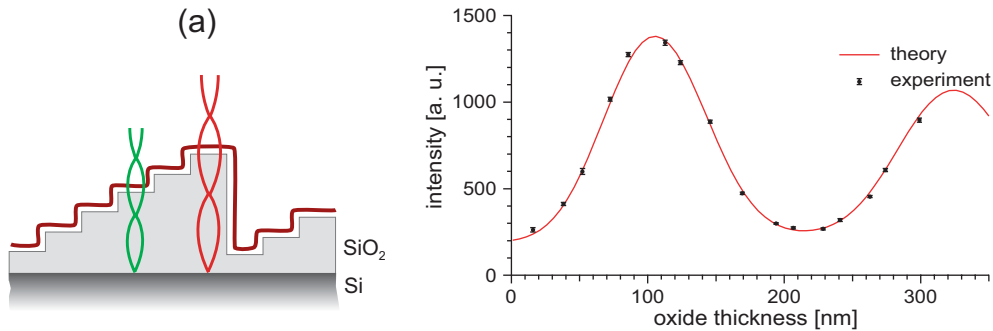


Figure 1.13: (a) Sketch of a FLIC substrate with deposited lipid membrane (dark red line). The standing waves of fluorescence excitation (green) and emission (red) are illustrated. (b) Typical curve of obtained fluorescence intensity vs. oxide thickness. The line denotes the fitted FLIC theory to fluorescence intensity.

1.7 X-Ray Scattering

Conventional static X-ray diffraction methods have been used to study the structure of lipid/water systems of relevance to biological membranes [Luzzati, 1968, Shipley, 1973, Blaurock, 1982]. Both the small angle X-ray scattering (SAXS) from the three-dimensional molecular packing array and the wide angle X-ray scattering (WAXS) of the two-dimensional packing subcell of the alkyl chains can be monitored.

Lipid/Water diffraction patterns

Regarding the diffraction of X-rays, the lipid/water dispersions investigated here are equivalent to powder samples that are composed of many randomly oriented microcrystals. Thus, Bragg's condition is automatically fulfilled, and all possible diffraction peaks are simultaneously recorded. While the positions of the diffraction peaks are related to periodic distances within the lyotropic lipid mesophase, their sharpness or width reflects the extent of this periodicity over large distances. The measured reciprocal spacings are given by

$$s = \frac{2}{\lambda} \sin \theta \quad , \quad (1.12)$$

where 2θ is the scattering angle, and λ the wavelength of radiation. If a lipid/water phase is lacking any periodic structure, diffuse small-angle scattering is observed only.

The most common mesophases that are observed in lipids are the lamellar, the hexagonal, and the cubic phase. The lamellar phase (denoted as L or P) consists of alternating layers of lipid and water molecules. This quasi-one-dimensional periodic structure exhibits diffraction patterns in the small-angle regime that are described by the equation

$$s_n = n \frac{1}{d} \quad (1.13)$$

where $n = 1, 2, 3, \dots$ and d is the lamellar repeat unit, which consists of the sum of the water and lipid layer thickness.

The common hexagonal phase among non-lamellar phases found in lipids of biological relevance is the inverse hexagonal lipid/water mesophase (denoted as H_{II}), where cylindrical water rods are surrounded by lipid monolayers. The rods are packed in a two-dimensional hexagonal lattice with Bragg peaks positioned at

$$s_{hk} = \frac{2}{\sqrt{3}a} \sqrt{h^2 + k^2 + hk} \quad , \quad (1.14)$$

where a is the distance between the centers of two neighboring rods (lattice constant) and h , k are the Miller indices. In small-angle diffraction patterns hexagonal lipid phases are easily distinguished from lamellar phases by their ratio of Bragg peak positions, which is $1:\sqrt{3}:2:\dots$

In a diffraction experiment, Bragg peaks of cubic structures may be observed at

$$s_{hkl} = \frac{1}{a} \sqrt{h^2 + k^2 + l^2} \quad , \quad (1.15)$$

where a is the cubic lattice constant. The Miller indices h , k , and l depend on the lattice type (primitive, body-centered, face-centered) and the symmetry elements of the cubic structure.

The pattern of X-ray scattering in the WAXS region can provide information on the state of order and packing of the hydrocarbon substituents of the mesophase, and the different packing arrangements characterize different lipid phases, like the lamellar crystal phase L_c , the lamellar gel phase L_β , the ripple phase P_β , and the lamellar fluid phase L_α [Cunningham et al., 1994, Seddon & Templer, 1995, Winter, 2002].

Experimental Setup

Figure 1.14 shows a sketch of the used setup at the beamline A2 (HASY-Lab) at DESY (Deutsches Elektronen Synchrotron, Hamburg, Germany). The beam of the X-ray source hits the sample, which is scattered at an angle of 2θ with respect to the direct beam, according to Bragg's law. SAXS and WAXS were simultaneously recorded with two different linear detectors, which were calibrated with scatters from RTT and Tripalmitin samples, respectively. The resolution of the SAXS corresponds to ~ 4 to 10 nm which therefore resolves the lattice spacing, and WAXS is suited for the investigation of in-plane correlation in the range of a few nm down to 1 \AA . As samples, lipid/lipopolymer dispersions in water (concentration ~ 20 wt% water) were used, which were filled into quartz capillaries (Hilgenberg, Malsfeld, Germany).

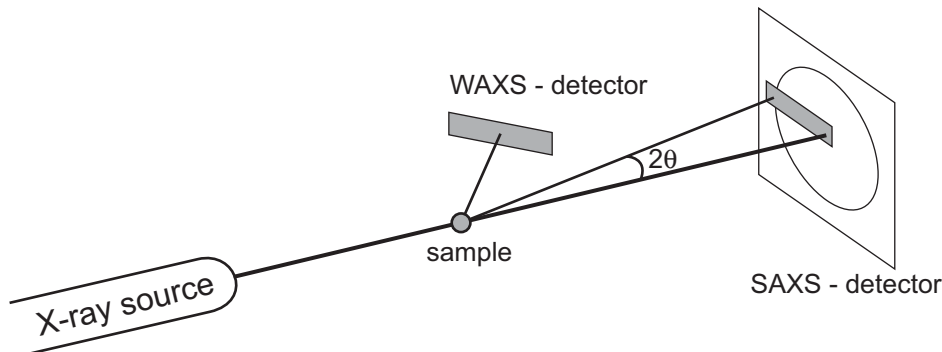


Figure 1.14: Schematic drawing of the used setup at DESY (Hamburg, Germany).

2. Polymer-Tethered Lipid Bilayer Membranes

2.1 Introduction

For the establishment of polymer-tethered lipid membranes, different preparation methods were applied, all consisting of a two-step procedure: After deposition of the proximal lipid monolayer adjacent to the substrate, the distal layer was prepared by vesicle fusion. In the beginning, the “grafting from“ method [Jordan & Ulman, 1998, Jordan et al., 2001b], and the “grafting onto“ method [Rehfeldt et al., 2002] were applied.

In the “grafting from“ process (Figure 2.1(a)), the polymer layer is established stepwise from the surface, on which initiator groups for the polymerization were coupled in advance. Suited monomers are transformed to the corresponding polymers by the initiator. As termination agent of the reaction, a lipid moiety is used. The resulted lipopolymer monolayer is pre-organized, and high grafting densities can be achieved.

The “grafting onto“ method (Figure 2.1(b)) consists of a synthesis of the whole lipopolymer in solution, including lipid moiety and surface coupling group, and the subsequent coupling to the surface in a second step. Compared to the “grafting from“ procedure, the lipopolymer layer exhibits a lower surface density and a poorer separation into hydrophilic polymer and hydrophobic lipid layers.

Both procedures resulted in brush-like polymer monolayers with high grafting densities. Immediately after the grafting reaction, the polymer layer was found to be homogenous and unstructured. A single submersion in water and consecutive exposure towards air at room temperature causes a self-organization of the lipopolymer layer into a hydrated polymer interlayer and an upper hydrophobic alkyl layer. In all cases, no crystallization of alkyl chains were observed in the polymer supported alkyl monolayer.

For construction of the supported bilayer, dry polymer monolayers prepared by the “grafting from“ or “grafting onto“ method were immersed to a solution of lipid vesicles in water. However, a formation of lipid bilayers could not be observed. Also numerous modifications of the procedure using different lipids and lipopolymers

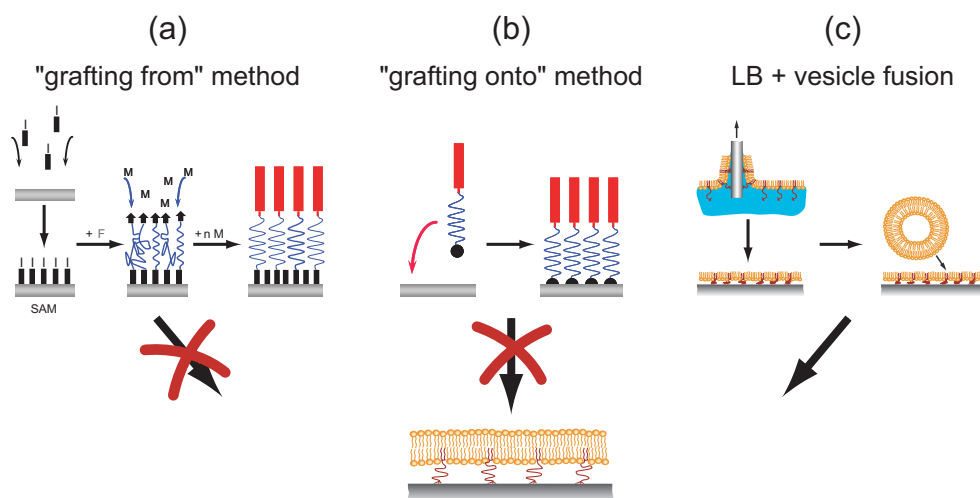


Figure 2.1: Schematic drawing of the different grafting methods of lipopolymers applied throughout this study. The methods (a) “grafting from“, and (b) “grafting onto“ did not lead to polymer-tethered lipid bilayer membranes. Only method (c), the two-step preparation of Langmuir-Blodgett transfer with subsequent vesicle fusion succeeded in homogeneous, functional polymer-tethered lipid membranes.

failed. Presumably, the exposure to water reorganizes the amphiphilic lipopolymer monolayer and vesicle fusion did not occur.

Encouraged by the work of Wagner et al. [Wagner & Tamm, 2000], the lipid/lipopolymer monolayer was pre-organized at the air/water interface of a Langmuir-Blodgett trough and transferred onto solid substrates, which allowed a defined grafting densities of the lipopolymer tether. However, instead of a homogeneous distribution of the fluorescence dye tracer within the lipid/lipopolymer monolayer, stripe-like micropatterns aligned parallel to the transfer direction were observed (Figure 2.2(a)). These dissipated structures could be circumvented by changing the transfer velocity to values $\geq 400 \mu\text{m s}^{-1}$ (Figure 2.2(b)). The underlying mechanisms of this pattern formation will be discussed in Chapter 3.

After the optimization of the preparation procedure of the first membrane leaflet, homogenous and uniform layers for different lipopolymer/lipid compositions were obtained (presented in Sections 2.2 and 2.3). The consecutive deposition of the upper lipid leaflet by fusion of vesicles was also improved till optimal results were exhibited (see Section 2.4). Therefore, the preparation of polymer-tethered membranes were carried out by the combination of LB and subsequent vesicle fusion (Figure 2.1(c)).

Since we started with lipopolymers composed of a single chain lipophilic moiety and a short polymer spacer (Ph-PMOx₁₂-Si), the hydrophilic/lipophilic balance (HLB) was shifted to an hydrophilic overweight when the length of the polymer spacer was

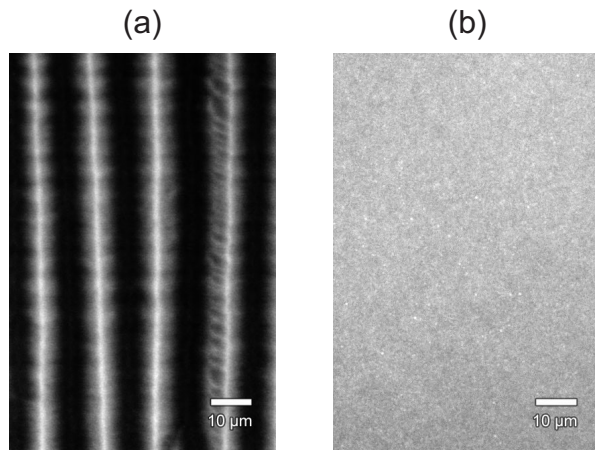


Figure 2.2: Fluorescence images of a transferred LB monolayer composed of 10 mol% Ph-PMO_{x12}-Si, 89.8 mol% DPhPC, and 0.2 mol% Texas Red-PE. The monolayers were deposited at $\Pi = 30 \text{ mNm}^{-1}$, a temperature of $20 \text{ }^\circ\text{C}$, and with a transfer velocity of (a) $\sim 80 \mu\text{ms}^{-1}$, and (b) $\sim 400 \mu\text{ms}^{-1}$.

increased (Ph-PMO_{x21}-Si). This led to unstable lipid/lipopolymer monolayers at the air/water interface, which made a successful LB transfer impossible (see Section 2.10).

Therefore, the establishment of the polymer-tethered membrane system was carried out with lipopolymers equipped with a double chain lipid moiety, DS-PMO_{xn}-Si (see Section 1.1.1).

The incorporation of transmembrane cell receptors is presented in Section 2.5, where the influence of the length of the polymer spacer is evaluated.

At this system, the diffusion coefficients and mobile fractions of lipids and proteins were estimated (Section 2.6), as well as the frictional coupling of the proteins to the substrate (Section 2.7). The membrane-substrate distance was obtained by FLIC (Section 2.8), and the functionality of incorporated transmembrane receptors was also evaluated (Section 2.9).

2.2 Langmuir Isotherms of Lipid/Lipopolymer Monolayers

As the first step, Langmuir isotherms of various lipid/lipopolymer (DS-PMO_{x14}-Si) mixtures were measured to determine the optimal mixing ratios (Figure 2.3). With increasing molar fractions of lipopolymer, we observed an increase in average area per molecule, corresponding to the larger hydrophilic moiety of the lipopolymers in comparison to matrix lipids. At lipopolymer concentrations above 20 mol%, a shoulder-like region appeared, caused by polymer-polymer interactions at surface pressures of $\Pi \approx 20 \text{ mNm}^{-1}$. Although there is a distinct hydrophobic mismatch between lipid anchors of matrix lipid (stearoyl-oleoyl chains) and those of lipopolymer (distearoyl chains), no phase separation could be observed by fluorescence microscopy at the air/water interface (see Section 3.2).

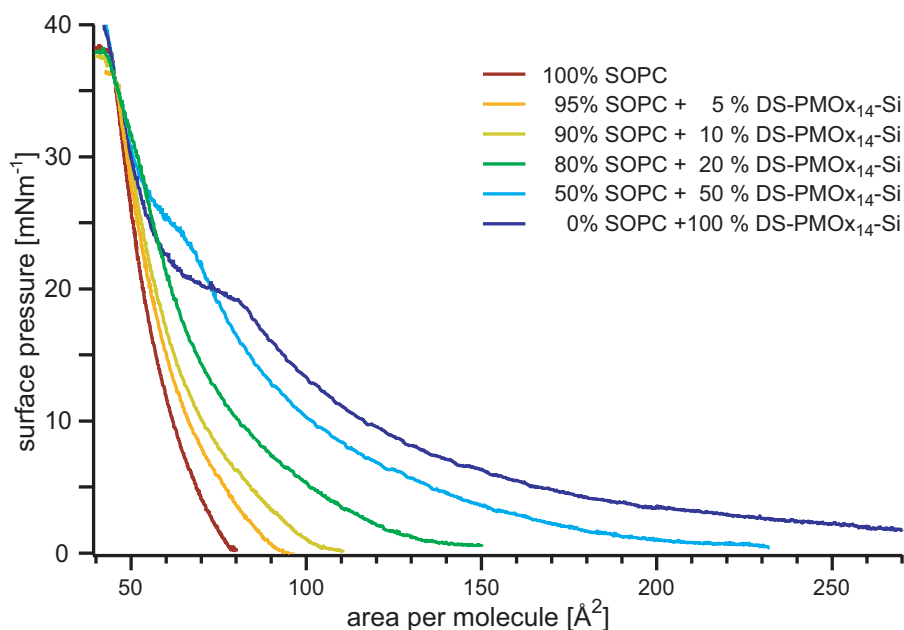


Figure 2.3: Langmuir isotherms of various lipid/lipopolymer (DS-PMO_{x14}-Si) mixtures recorded at 20 °C. Molar fractions of the lipopolymer ranged between 0 and 100 mol%, indicating that polymer-polymer interaction is negligible when the lipopolymer fraction is ≤ 20 mol%.

To investigate the influence of the polymer chain length on the lateral cooperativity within the monolayer, Langmuir isotherms of SOPC monolayers with 5 mol% lipopolymers were measured for DS-PMO_{x18}-Si and DS-PMO_{x33}-Si (Figure 2.4). At this low molar fraction of lipopolymer, the stretching of polymer chains only appeared near the onset of the increase in surface pressure (inset, Figure 2.4). When the film was compressed to higher surface pressures, the isotherms overlapped

with each other up to $\Pi \approx 40 \text{ mNm}^{-1}$. The obtained results indicate that polymer-polymer interaction is also negligible for DS-PMO_{x18}-Si and DS-PMO_{x33}-Si, if the molar fraction of the lipopolymer was kept at 5 mol%. Since no phase separation could be observed neither from isotherms nor by fluorescence microscopy, one can assume a random distribution of the lipopolymers in the polymer/lipid monolayer.

Therefore, the average distance between the lipopolymers can be approximated from the average molecular area measured at $\Pi = 30 \text{ mNm}^{-1}$ ($A \approx 55 \text{ \AA}^2$), and from the molar fraction of lipopolymers ($f = 0.05 - 0.20$) to be $d = \sqrt{A/f}$. Since the radius of gyration R_g scales with \sqrt{N} , one can approximate R_g from previous light scattering study of Chen et al. [Chen et al., 1990] to $R_g \approx 1.7 \text{ nm}$ for DS-PMO_{x14}-Si, 1.9 nm for DS-PMO_{x18}-Si, and 2.5 nm for DS-PMO_{x33}-Si, respectively. Although the mean distance $d \approx 1.7 \text{ nm}$ at a lipopolymer fraction of 20 mol% matches with $R_g \approx 1.7 \text{ nm}$ for DS-PMO_{x14}-Si, no polymer-polymer interaction was observed in the isotherms at this molar ratio (Figure 2.3), since these values are approximations. Furthermore, as suggested from the isotherms (Figure 2.4), interactions between the longer polymer chains (DS-PMO_{x18}-Si and DS-PMO_{x33}-Si) are also negligible at a lipopolymer fraction of 5 mol% because the expected distance between polymer chains ($d \approx 3.3 \text{ nm}$) is larger than R_g . This also excludes a polycondensation via the trimethoxysilane end groups of the lipopolymers prior to the deposition.

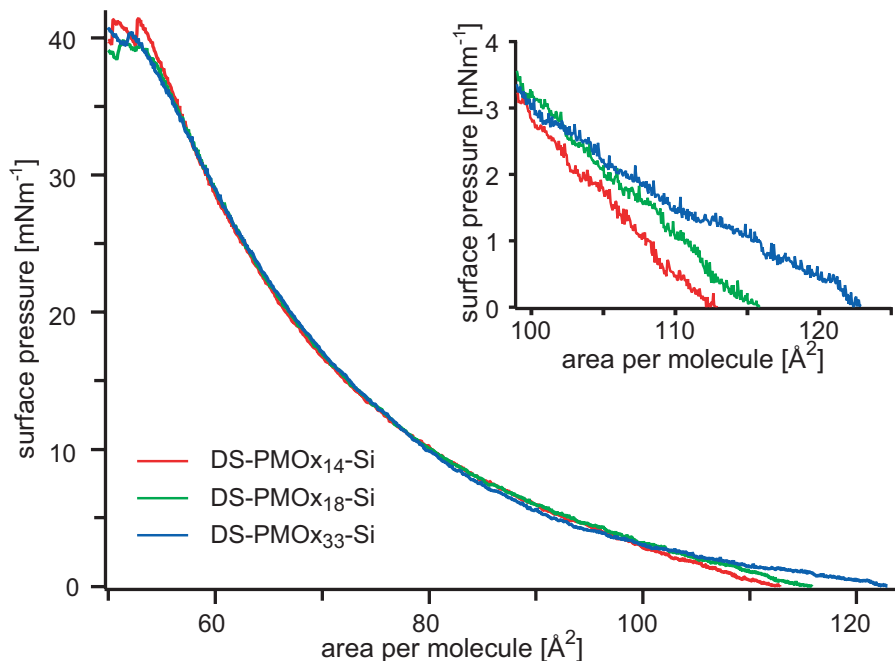


Figure 2.4: Langmuir isotherms of SOPC monolayers with 5 mol% lipopolymer (DS-PMO_{x14}-Si, DS-PMO_{x18}-Si, and DS-PMO_{x33}-Si), recorded at 20 °C. Little deviation among different polymer lengths could be seen at low surface pressures, presented in the inset.

2.3 Langmuir-Blodgett Deposition of Lipid/Lipopolymer Monolayers

After the compression, the monolayer was transferred from the air/water interface onto a solid substrate at constant velocity. The transfer ratio, i.e. ratio between the decrease in the subphase area and the area of the substrate, was found to be 1:1 for all samples. However, when the monolayer was transferred at a low transfer velocity (e.g. $50 \mu\text{ms}^{-1}$), stripe-like patterns were observed (see Figure 2.5(a)). These stripes were always aligned parallel to the transfer direction, as indicated by an arrow in the figure. It should be noted that such patterns are not formed due to a phase separation under thermodynamic equilibrium, because the fluorescence image of the same monolayer at air/water interface appeared homogeneous before the transfer (see Section 3.2). Furthermore, fluorescence labelling of lipopolymers confirmed that such stripe-like heterogeneities are formed by demixing of lipids and lipopolymers, but not by the segregation of fluorescence lipids (see Section 3.5). These findings strongly suggest that hydrodynamic conditions in the vicinity of the wetting front play a dominant role. When the transfer velocity was increased, these microscopic stripes became thinner and disappeared at a very high velocity ($\geq 400 \mu\text{ms}^{-1}$) (see Section 3.4.1). As shown in Figure 2.5(b), the fluorescence image of the monolayer with 5 mol% of DS-PMO_{x14}-Si was homogeneous over the entire substrate, but the transfer ratio still remained 1:1. Fluorescence images of the monolayers transferred at this condition were found to be homogeneous at various lipopolymer fractions between 0 and 50 mol%.

Furthermore, the homogeneous distribution of lipopolymers within the monolayer was verified by experiments using analog lipid/lipopolymer mixtures with fluorescence labelled lipopolymers (see Figure 2.6). Although the morphology of these stripe-like domains differed slightly, an increase in the transfer velocity led to a “thinning” of the stripe patterns. Indeed, for all the lipid/lipopolymer mixtures, we could prepare homogeneous monolayers without any loss of materials.

Heterogeneous “stripes” and “holes” either due to phase separation or to local defects have been reported in some of the previous studies [Wagner & Tamm, 2000, Naumann et al., 2002]. For example, Wagner and Tamm observed holes and stripe-like defects in the first lipid/lipopolymer layer with poly(ethylene oxide) lipopolymers, which could only be healed to some extent by spreading of the top layer. Naumann et al. used poly(2-ethyl-2-oxazoline) lipopolymers that were randomly grafted onto the surface by cross-linking to benzophenone groups. They also found macro-

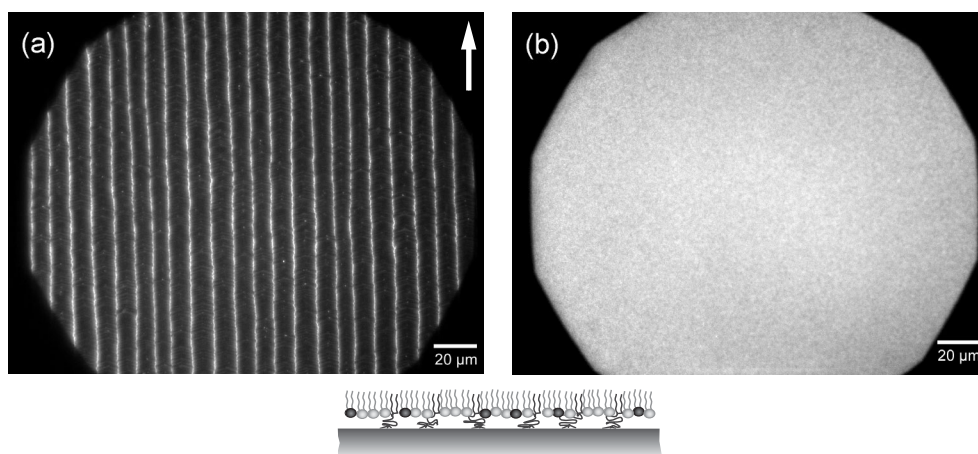


Figure 2.5: Fluorescence images of SOPC monolayers with 5 mol% DS-PMO_{x14}-Si. The monolayers were transferred at velocities of (a) $50 \mu\text{ms}^{-1}$ and (b) $400 \mu\text{ms}^{-1}$. The arrow denotes the direction of film transfer. Schematic illustration of the film is given at the bottom, representing fluorescence probes in black.

scopic defects and phase separations at a lipopolymer concentration of 20 mol%. In contrast to these approaches, it was demonstrated that systematic control of the hydrodynamic conditions during the transfer (i.e. transfer velocity) enables one to deposit homogeneous lipid/lipopolymer monolayers for various spacer lengths and concentrations.

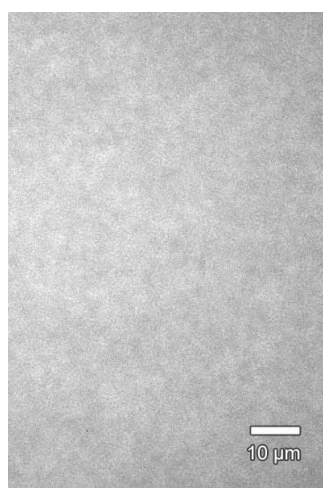


Figure 2.6: Fluorescence images of a LB monolayer composed of 0.2 mol% DS-PMO_{x13}-TRITC, 4.8 mol% DS-PMO_{x18}-Si, 94 mol% SOPC, and 1 mol% NBD-PE, observed with a TRITC fluorescence filter. The monolayer was transferred at a velocity of $500 \mu\text{ms}^{-1}$.

2.4 Spreading of Top Layers by Vesicle Fusion

To verify the “self-healing” of heterogeneities in the underlayer as reported by Wagner and Tamm [Wagner & Tamm, 2000], we spread unlabelled SOPC vesicles on the labelled monolayer with stripe-like heterogeneities (Figure 2.7(a)). For the direct comparison, the monolayer was prepared under the same conditions as that presented in Figure 2.5(a). As apparent from the figure, the spreading of the top layer as well as the swelling of polymer spacers seemed to induce the diffusion and mixing of lipids and lipopolymers, but a distinct heterogeneity in the underlayer still remains. Since the lipopolymers are most likely covalently attached to the surface and enriched in one of the domains, it is understandable that lateral diffusion of lipids cannot perfectly heal the “imprinted” heterogeneity. On the other hand, homogeneity of the monolayer prepared under the same conditions as that in Figure 2.5(b) was not disturbed by spreading of unlabelled SOPC vesicles (Figure 2.7(b)).

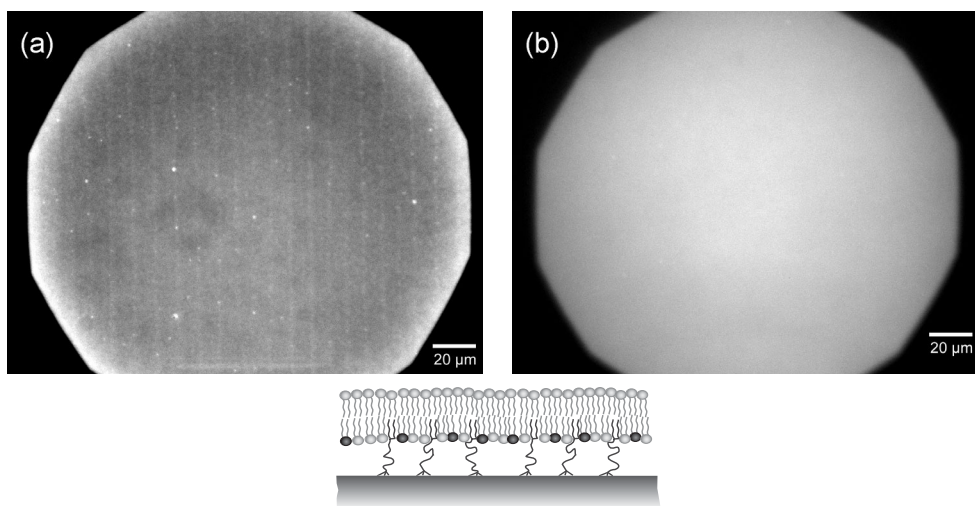


Figure 2.7: Fluorescence images of SOPC monolayers with 5 mol% DS-PMO_{x14}-Si. The underlayer was labelled with 0.2 mol% Texas Red-PE, and unlabelled SOPC vesicles were spread onto the dry monolayers. Transfer velocities: (a) 50 μms^{-1} , and (b) 400 μms^{-1} . Schematic illustration of the bilayer is given at the bottom, representing fluorescence probes in black.

As the next step, labelled SOPC vesicles were spread onto the unlabelled underlayers. When the labelled vesicles were fused on a heterogeneous surface as described before, stripe-like domains could clearly be observed (Figure 2.8(a)). This strongly denotes that underlying heterogeneities in the underlayer disturb the homogeneous spreading of the toplayer. To explain such a significant impact of the underlayer, there are two possible scenarios: (i) demixing of lipids and lipopolymers causes the mismatch in the lateral density of alkyl chains in lipid-enriched and lipopolymer-enriched domains that might even cause local defects, or (ii) lateral diffusion of the lipids is disturbed

by the high local concentration of grafted lipopolymer tethers. However, when the labelled vesicles were spread on a uniformly mixed lipid/lipopolymer monolayer, the toplayer coated the entire surface homogeneously (Figure 2.8(b)).

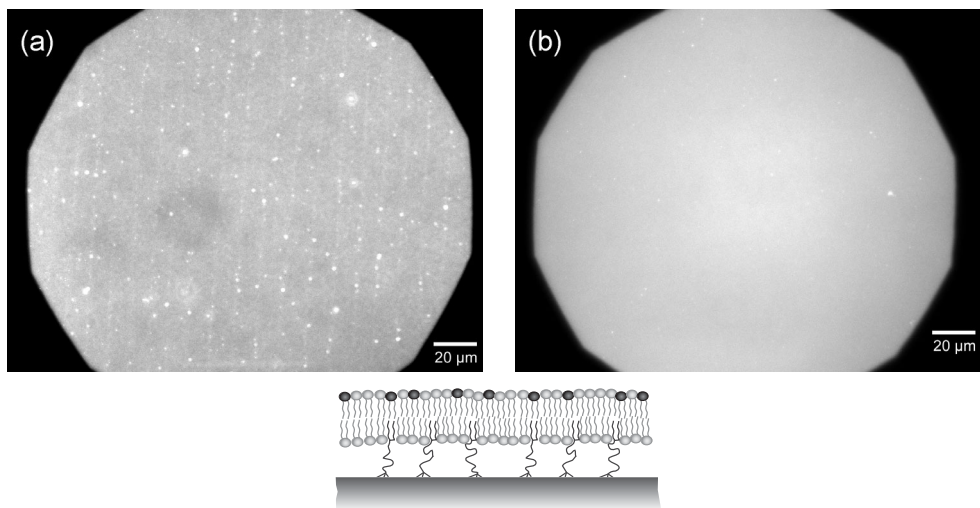


Figure 2.8: Fluorescence image of polymer-tethered membranes with 5 mol% DS-PMO_{x14}-Si. The underlayer was unlabelled, and SOPC vesicles labelled with 0.2 mol% Texas Red-PE were spread onto the dry monolayers. Transfer velocities: (a) 50 μms^{-1} , and (b) 400 μms^{-1} . Schematic illustration of the bilayer is given at the bottom, representing fluorescence probes in black.

To achieve a good homogeneity of polymer-tethered membranes, further preparation conditions have to be optimized, like the incubation time of vesicle suspensions, the method of spreading the suspension onto the dry LB monolayers, and the rinsing method for removing vesicle suspension.

The incubation time of the vesicle suspension can be quite short. Even after just 5 min of incubation, homogeneous bilayer membranes were observed (Figure 2.9(a)). Nevertheless, the coverage is not complete, there were still some small, uncovered regions. Increasing the incubation time up to one hour, 100% of the underlying LB monolayer has received its second leaflet. After an incubation time $\gtrsim 12$ h, large vesicle clusters adhered on the membrane surface, which could hardly be removed by intensive rinsing with buffer solution (Figure 2.9(b)). Furthermore, after prolonged incubation also strand-like constructs can evolve (length $\sim 10 - 20 \mu\text{m}$), swaying by the convection of aqueous bulk above (Figure 2.9(c)).

Additionally, the spreading process itself influences the homogeneity of bilayer membranes. The propagating front of the vesicle suspension on the LB monolayer can generate circle like defects within the membrane (Figure 2.10(a), (b)), which also can arise by spreading of proteoliposomes (Figure 2.10(c)). The release of the sus-

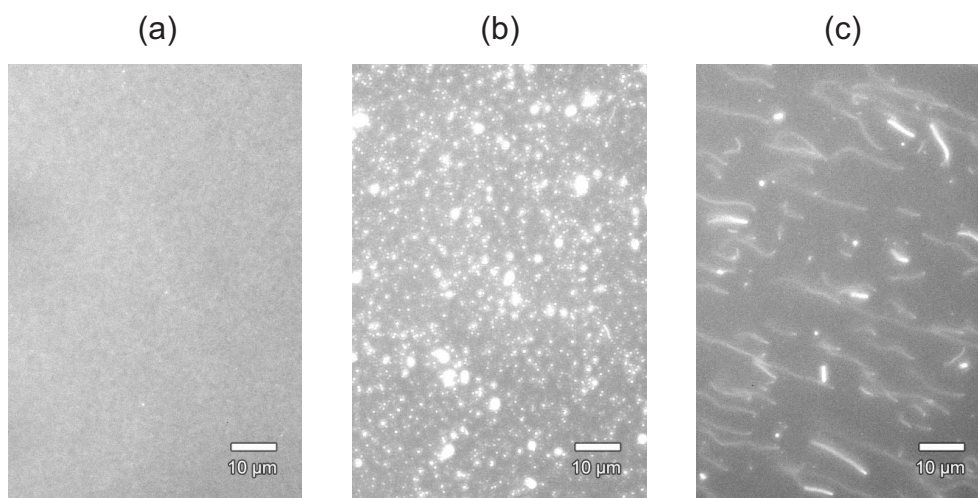


Figure 2.9: Fluorescence image of polymer-tethered membranes. (a) A LB monolayer (5 mol% DS-PMO_{x33}-Si, 95 mol% SOPC) was incubated for 5 min with a vesicle suspension (99.8 mol% SOPC and 0.2 mol% Texas Red-PE). (b) After prolonged incubation with a vesicle suspension (99 mol% SOPC and 1 mol% NBD-PC), vesicle clusters were not able to be removed by intensive rinsing (LB monolayer: 10 mol% DS-PMO_{x14}-Si, 90 mol% SOPC). (c) After prolonged incubation, also floating strands (length $\sim 10 - 20 \mu\text{m}$) evolved, swaying by convection of bulk water (underlayer: 20 mol% DS-PMO_{x14}-Si, 78.5 mol% SOPC, 1.5 mol% NBD-PC; toplayer: 100 mol% SOPC).

pension from the syringe or pipette should be performed in close proximity to the dry monolayer.

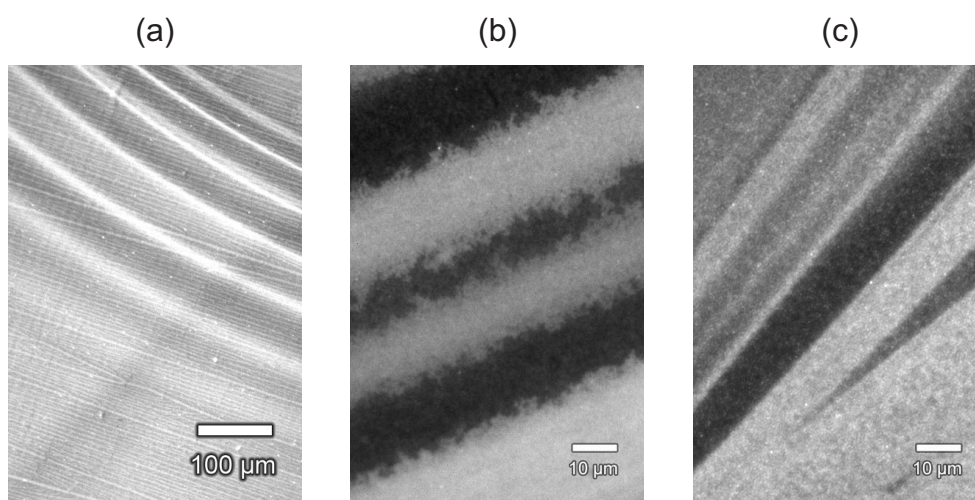


Figure 2.10: Fluorescence images of polymer-tethered membranes. All defects arose from the propagating spreading wave of the dropped vesicle suspension. (a) $10\times$ LD objective image of labelled vesicles (99.8 mol% SOPC and 0.2 mol% Texas Red-PE) spread onto LB monolayer with micropatterns (10 mol% DS-PMO_{x33}-Si, 90 mol% SOPC). (b) A LB monolayer (5 mol% DS-PMO_{x33}-Si, 95 mol% SOPC) was incubated for 5 min with a vesicle suspension (99.8 mol% SOPC and 0.2 mol% Texas Red-PE). (c) Proteoliposomes with TAMRA-labelled integrins were spread onto a LB monolayer (0.5 mol% DS-PMO_{x33}-Si, 99.5 mol% SOPC).

2.5 Incorporation of Integrin $\alpha_{\text{IIb}}\beta_3$ into Polymer-Tethered Membranes

To test the feasibility and potential of the polymer-tethered membrane construct, experiments to incorporate transmembrane proteins within the bilayer were performed. Proteoliposomes with integrin $\alpha_{\text{IIb}}\beta_3$ were spread onto underlayers with 5 mol% of DS-PMO_{x14}-Si, DS-PMO_{x18}-Si, or DS-PMO_{x33}-Si. For evaluation of the layer quality, the integrins were labelled with 5(6)-TAMRA-SE prior to the preparation of proteoliposomes.

Again, as a control experiment, proteoliposomes were firstly spread on a glass substrate, resulting in fragmented domains of proteins (Figure 2.11(a)). Prolonged incubation time could not increase the homogeneity of the protein distribution, indicating that the local defects cannot be healed by the fusion of single patches [Gönnenwein et al., 2003].

When proteoliposomes were incubated on an underlayer with 5 mol% DS-PMO_{x14}-Si, one could clearly see fluorescent “circles“ on the surface, whose diameter are approx. 10 μm (Figure 2.11(b)). At present, it is unclear whether these “circles“ correspond to fused proteoliposomes adherent to the surface or to the clusters of integrins.

Spreading of proteoliposomes onto underlayers with 5 mol% of DS-PMO_{x18}-Si or DS-PMO_{x33}-Si resulted in a very different picture (Figure 2.11(c + d)). A homogeneous distribution of integrins on the surface was visible. Although one could still observe small clusters that might correspond to locally aggregating integrins, the entire surface is uniformly coated with polymer-tethered membranes containing integrins. The macroscopically homogeneous distribution of integrins in the membranes with longer polymer spacers (DS-PMO_{x18}-Si and DS-PMO_{x33}-Si) suggests that the substrate-membrane distance is one of the key parameters for successful incorporation of transmembrane receptors. Nevertheless, the results obtained here strongly suggest the potential of tethered membranes with well-defined length and distribution of soft polymer spacers for stress-free incorporation of transmembrane receptors with large extracellular domains.

Even a decrease in lipopolymer concentration to 0.5 mol%, which corresponds to an average tether distance of $d = \sqrt{A/f} \sim 11 \text{ nm}$, did not lead to an decrease in homogeneity of the distribution of integrin $\alpha_{\text{IIb}}\beta_3$. In Figures 2.11(e) and (f), homogeneous fluorescence images of TAMRA-labelled integrin incorporated into membranes with 0.5 mol% DS-PMO_{x33}-Si and accordingly 0.5 mol% DS-PMO_{x104}-Si in the under-

layer are presented.

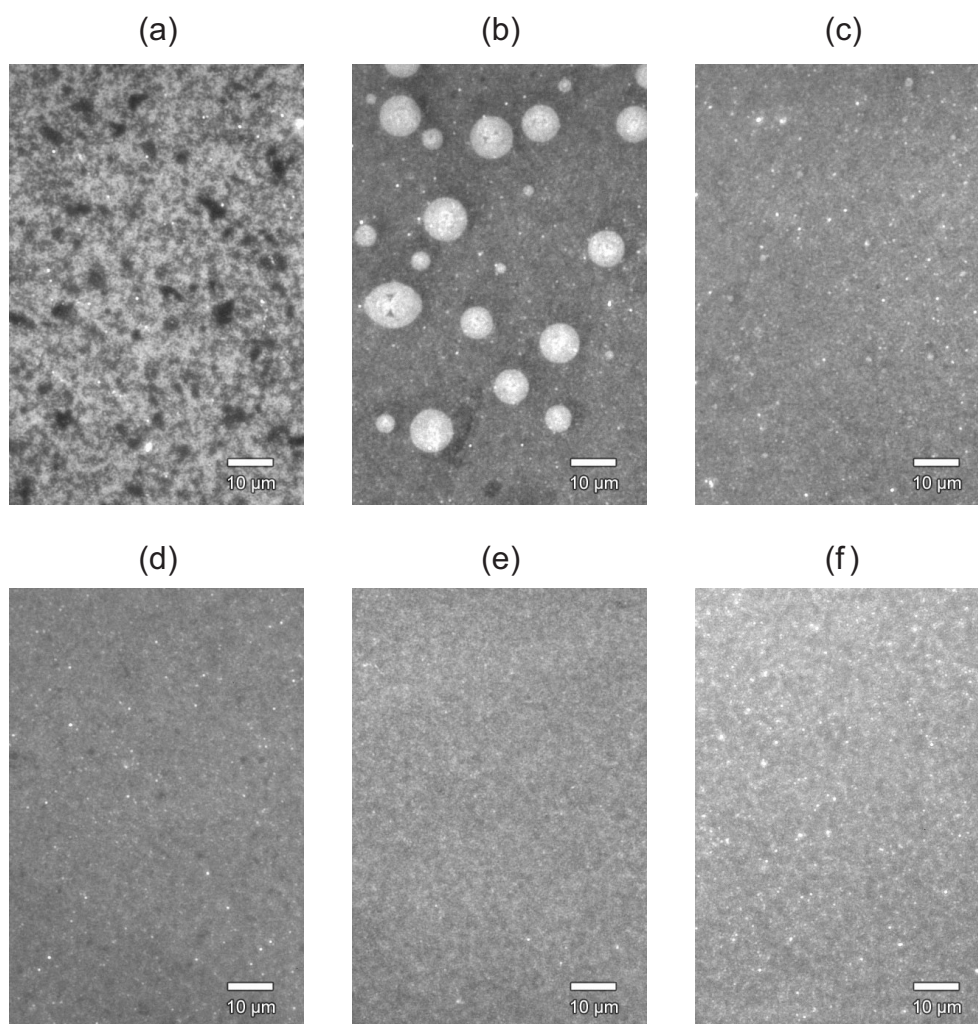


Figure 2.11: Fluorescence image of TAMRA-labelled integrin α_{11b}/β_3 incorporated into lipid membranes. In (a) the proteoliposomes were spread directly onto a bare glass surface, where in (b) to (f), proteoliposomes were spread onto dry LB monolayers containing certain amounts of lipopolymers and SOPS matrix lipids: (b) 5 mol% DS-PMO_{x14}-Si, (c) 5 mol% DS-PMO_{x18}-Si, (d) 5 mol% DS-PMO_{x33}-Si, (e) 0.5 mol% DS-PMO_{x33}-Si, and (f) 0.5 mol% DS-PMO_{x104}-Si.

2.6 Diffusion Measurements in Polymer-Tethered Membranes

2.6.1 Theory of Diffusion

In the fluid mosaic model [Singer & Nicolson, 1972, Jacobson et al., 1995], the cell membrane is described as a “two dimensional oriented solution of integral proteins in the viscous phospholipid bilayer solvent.” The mobility of proteins is influenced by the protein size and concentration, the lipid composition of the membrane, the binding to cytoskeletal or extracellular matrices, and the confinement to domains by the cytoskeleton and tight junctions [Scalettar & Abney, 1991]. Theoretical models can help to understand the complexity of lipid and protein diffusion in membranes.

In the last decades, two theories of diffusion in homogeneous bilayers prevailed, the *continuum hydrodynamic model* for diffusion of particles with a size larger than that of the solvent (= phospholipid), and the *free-volume model*, which takes into account the discreteness of the lipid bilayer. Therefore, the former is best applicable to diffusion of integral membrane proteins in lipid bilayers, where the latter is best suited to describe lipid diffusion. These two models have been used most often and with best results in the interpretation of experimental data. For review of diffusion in membranes, one should consult the work of Vaz et al. [Vaz et al., 1984, Vaz et al., 1985], Scalettar & Abney [Scalettar & Abney, 1991], and Almeida & Vaz [Almeida & Vaz, 1995].

Definition of a Diffusion Coefficient in Two Dimensions

Considering a tracer performing a *random walk* on a two dimensional lattice. The probability density $c(r, t)$ of the tracer at a certain time t with a displacement r is a Gaussian distribution:

$$c(r, t) = \frac{1}{4\pi Dt} \exp\left(-\frac{r^2}{4Dt}\right) , \quad (2.1)$$

which is the solution of the diffusion equation,

$$\frac{\partial c(x, y)}{\partial t} = D\nabla^2 c(r, t) , \quad (2.2)$$

where D is the diffusion coefficient, and ∇^2 the Laplacian operator. Hence, the mean square displacement of the tracer is

$$\langle r^2 \rangle = \int_0^\infty r^2 c(r, t) 2\pi r dr = 4Dt . \quad (2.3)$$

Protein Diffusion: The Continuum Hydrodynamic Model

In this model proposed by Saffman and Delbrück [Saffman & Delbrück, 1975, Saffman, 1976], the lipid bilayer is represented as a two dimensional continuum. The concreteness of the lipid molecular structure is ignored. Motion of proteins is driven by random, fluctuating forces provided by unbalanced collisions with the solvent molecules (= lipids) and is resisted by the frictional forces inherent in a viscous solvent (= lipid bilayer). The diffusing molecule (= protein) is represented as a cylinder of height h and radius R . Its diffusion coefficient D is given by the Einstein relation

$$D = \frac{k_B T}{f} \quad , \quad (2.4)$$

where k_B is the Boltzmann constant, T the temperature, and f is the friction coefficient¹.

In the continuum treatment of Saffman and Delbrück, the lipid bilayer membrane has a very small thickness h_m and a viscosity η_m , bound on both sides by three-dimensional fluids of much smaller viscosities η_1 and η_2 , which are treated as equal, $\eta_1 = \eta_2 = \eta_l$. The resulted friction coefficient, f , is

$$f = 4\pi\eta_m h_m \left(\ln \frac{\eta_m h_m}{\eta_l R} - \gamma \right)^{-1} \quad , \quad (2.5)$$

where $\gamma = 0.5772$ is Euler's constant, and the particle has the same height as the membrane $h = h_m$. The system can be characterized by the dimensionless parameter, ε [Hughes et al., 1981]:

$$\varepsilon = \frac{R}{h} \frac{\eta_1 + \eta_2}{\eta_m} \quad . \quad (2.6)$$

The solution given by Saffman and Delbrück is valid only for $\varepsilon \leq 0.1$. This is appropriate for model membranes bound by water or dilute salt solutions but may not be valid for biological systems, where the bounding solutions (cytoplasm on one side and extracellular glyocalix on the other) are often highly viscous, or membrane model systems, where the bilayers experience weak dynamic coupling to an adjacent solid support (see Figure 2.12).

Considering this effect, Evans and Sackmann [Evans & Sackmann, 1988] obtained

$$f = 4\pi\eta_m h_m \left(\frac{1}{4}\varepsilon'^2 + \frac{\varepsilon' K_1(\varepsilon')}{K_0(\varepsilon')} \right) \quad , \quad (2.7)$$

¹In case of a spherical particle of radius R in a medium of viscosity η , the friction coefficient is $f = 6\pi\eta R$

where K_0 and K_1 are modified Bessel functions of the second kind, orders zero and one, and ε' is a dimensionless parameter defined by

$$\varepsilon' = R \sqrt{\frac{b_s}{\eta_m h_m}} \quad , \quad (2.8)$$

b_s is the friction coefficient between membrane and the support:

$$b_s = \frac{\eta_l}{d} \quad , \quad (2.9)$$

where d is the distance between membrane and substrate, and η_l is the viscosity of the liquid in between. For $\varepsilon \gg 1$, one obtains for the diffusion coefficient

$$D \approx \frac{k_B T d}{\pi \eta_l R^2} \quad . \quad (2.10)$$

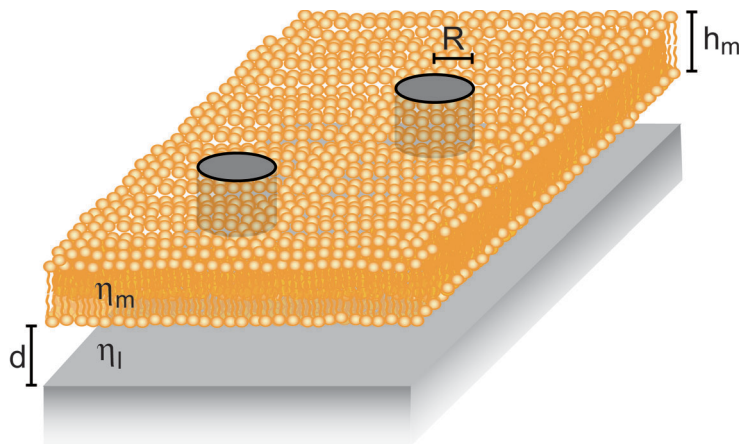


Figure 2.12: Hydrodynamic model, proposed by Evans and Sackmann, of the membrane in close proximity of a substrate, separated by a thin lubricant layer of thickness d and viscosity η_l . Proteins are treated as cylinders with height h and radius R moving in the membrane (viscosity η_m) by Brownian motion.

The Free-Volume Model

On the basis of the free-volume theory of Cohen and Turnbull [Cohen & Turnbull, 1959] for diffusion in fluid, glass-forming materials, Galla et al. [Galla et al., 1979] developed a free-volume model for diffusion in two-dimensional membrane systems.

According to free-volume theory, diffusion of a particle with the size of the molecules that constitute the fluid takes place only when a free volume greater than a certain critical size exists next to the particle. Free volumes smaller than this critical size do not contribute to diffusion, and the problem is reduced to determination of the

distribution of free volume in the system.

In such a system, the diffusion coefficient is defined as

$$D = D(a^*) \exp\left(-\frac{\gamma a^*}{a_f}\right) , \quad (2.11)$$

where a^* is the critical free area (areas below a^* are useless for diffusion), a_f is the average free-area in the system ($a_f = a_t - a^*$, where a_t is the total average area per molecule; note that a^* is a constant, but a_t and therefore a_f are in general functions of temperature). The parameter γ is a geometric factor that corrects for overlap of free-areas; it varies between 0.5 and 1. The pre-exponential factor $D(a^*)$ is related to the gas kinetic velocity.

Macedo and Litovitz [Macedo & Litovitz, 1965] proposed a hybrid equation, which is more general because it includes an energy factor in the diffusion coefficient, and contains the result of Cohen and Turnbull [Cohen & Turnbull, 1959] as a limiting case. That equation, has the general form

$$D = D' \exp\left(-\frac{\gamma a^*}{a_f} - \frac{E_a}{k_B T}\right) , \quad (2.12)$$

where E_a is the activation energy associated with diffusion. The pre-exponential factor D' is the “unhindered” diffusion coefficient, which is identical to $D(a^*)$.

2.6.2 Diffusion of Lipids

Since the fluidity of the lipid membrane strongly influences the function of membrane proteins, lateral diffusion coefficients of lipids in top- and underlayers were measured by FRAP and continuous bleaching (CBL) technique. Since the half time of the flip-flop exchange in fluid lipid bilayers is about 7h to 10 days [Kornberg & McConnell, 1971, Rothman & Dawidowicz, 1975], the exchange of the lipids between inside and outside of the membrane is almost negligible in the experimental time scale.

In the beginning, continuous bleaching experiments were carried out, since they can be performed with a standard fluorescence microscope in addition to the optical characterization. Furthermore, measurements with substrates of non-standard thickness ($\neq 0.17$ mm) can be done (see e.g. [Steinhoff et al., 2003], where sapphire wafers with GaN surfaces were used), since one is not restricted to oil immersion objectives which have only the correction to standard glass cover slides.

As one can see in Figure 1.8(a) (Section 1.5.1), the illumination of the homogeneous membrane and therefore the excitation of fluorescence dye tracers is not homogeneous over the entire aperture. Even careful readjustment of the HBO position could

not avoid this problem. Therefore, the deviation of the bleaching rate B_0 in the center and at the edge of the illuminated area was estimated, yielding a difference of $\approx 20\%$. Since the diffusion coefficient D is linearly dependent on B_0 , all results from CBL experiments were scaled down by this factor.

Table 2.1 summarizes the diffusion coefficients of lipids obtained by CBL experiments. In all cases, the diffusion of lipid in the upper membrane leaflet was slightly higher than in the proximal membrane leaflet.

lipopolymer fraction		diffusion coefficient	
		underlayer [$\mu\text{m}^2\text{s}^{-1}$]	toplayer [$\mu\text{m}^2\text{s}^{-1}$]
5 mol%	DS-PMO _{x14} -Si	2.3 ± 0.7	2.6 ± 0.8
10 mol%	DS-PMO _{x14} -Si	1.6 ± 0.5	2.7 ± 0.8
20 mol%	DS-PMO _{x14} -Si	1.4 ± 0.4	1.6 ± 0.5

Table 2.1: Diffusion coefficients of lipids measured by the CBL technique. The membranes were composed of various fractions of DS-PMO_{x14}-Si (5 - 20 mol%) and SOPC matrix lipids, where either the proximal or distal membrane leaflet was doped with 1 mol% NBD-PC.

Due to the uncertainties in obtaining diffusion coefficients by CBL reported above, and furthermore, the problems of measuring diffusion coefficients in the range of $D < 0.2 \mu\text{m}^2\text{s}^{-1}$, where membrane protein diffusion in supported membranes is reported [Wagner & Tamm, 2000], this technique was stopped to be applied. All further diffusion coefficients were determined by the fluorescence recovery after photobleaching (FRAP) method. To study the influence of lipopolymer spacer length and concentration, diffusion and mobility of lipid dye tracers in the underlayer were studied in detail.

As a control system, pure SOPC membrane prepared by the same methods (LB and subsequent vesicle fusion) were spread directly onto the bare substrate. The obtained diffusion coefficient ($D = 1.4 \mu\text{m}^2\text{s}^{-1}$) is in reasonable agreement with previously reported results [Merkel et al., 1989, Wagner & Tamm, 2000].

As summarized in Table 2.2 (upper panel), the increase in the molar fraction of lipopolymers (DS-PMO_{x14}-Si) does not seem to influence the diffusion coefficients ($D = 0.9 - 1.6 \mu\text{m}^2\text{s}^{-1}$) or the mobile fractions ($> 85\%$) within the lipopolymer fraction between 0 and 20 mol%. This range coincides well to that suggested from the Langmuir isotherms (Figure 2.3 in Section 2.2), where the polymer-polymer interactions are negligible. In fact, when the lipopolymer fraction was increased to 50 mol%, the diffusion constant and mobile fraction decreased to $D = 0.4 \mu\text{m}^2\text{s}^{-1}$ and 10%, respectively. This can be attributed either to the increase in viscosity within interacting polymer chains in the water reservoir, or to the increase in the fraction

of grafted lipopolymer tethers acting as obstacles.

lipopolymer fraction	diffusion constant [$\mu\text{m}^2\text{s}^{-1}$]	mobile fraction [%]
0 mol% -	1.4 ± 0.2	98 ± 3
5 mol% DS-PMO _{x14} -Si	1.6 ± 0.3	98 ± 4
10 mol% DS-PMO _{x14} -Si	0.9 ± 0.4	86 ± 12
20 mol% DS-PMO _{x14} -Si	1.3 ± 0.4	96 ± 2
50 mol% DS-PMO _{x14} -Si	0.4 ± 0.3	10 ± 1
5 mol% DS-PMO _{x18} -Si	1.4 ± 0.1	98 ± 2
5 mol% DS-PMO _{x33} -Si	1.4 ± 0.1	97 ± 3

Table 2.2: Diffusion constants of lipids in the underlayers. Diffusion coefficients of lipids with various fractions of DS-PMO_{x14}-Si (upper panel). Influence of the spacer length was studied for the membranes with 5 mol% of DS-PMO_{x18}-Si and DS-PMO_{x33}-Si (lower panel).

As the next step, the impact of the spacer length was studied by measuring the diffusion coefficients of the membranes with 5 mol% of DS-PMO_{x18}-Si and DS-PMO_{x33}-Si (Table 2.2, lower panel). By choosing the same transfer velocity ($400 \mu\text{ms}^{-1}$), homogeneous monolayers and bilayers were deposited. Here, the increase in the spacer length caused no distinct decrease in the diffusion coefficients or in mobile fractions, suggesting that the higher steric demands of the intermediate polymer chains did not increase the viscosity of the water reservoir. This agrees with Langmuir isotherms, where the spacer length showed almost no influence in the global shape of the isotherms of lipid/lipopolymer monolayers (Figure 2.4 in Section 2.2).

The diffusion coefficients of lipids in the toplayer were found to be almost constant within the experimental errors, $D = 1 - 2 \mu\text{m}^2\text{s}^{-1}$, independent from the underlying monolayers. Since the alkyl chains incorporated in the underlayer were in all cases fluid and homogeneous, it is plausible that the friction between top- and underlayers is almost identical [Evans & Sackmann, 1988].

From long term studies with repeated measurements of the diffusion coefficient of the polymer-tethered membranes, it was found that all supported membranes were thermodynamically and mechanically stable for more than two weeks, showing no decrease in the membrane quality (homogeneity and fluidity) within the experimental error.

In some experiments, the diffusion coefficients of the underlayer were unexpectedly low, in the range of $D = 0.006 - 0.2 \mu\text{m}^2\text{s}^{-1}$. This low diffusion changed after ~ 30 min to the “normal” diffusion reported above, obtained from the same sample. This finding denotes an uncomplete hydration of the previously dry proximal leaflet

of the membrane in the beginning of the experiments, which changed with time.

In Figure 2.13, the results obtained by the FRAP technique and continuous bleaching (CBL) method are compared. The values from CBL method are always higher than that from FRAP, exhibiting ≈ 10 to 80% higher diffusion coefficients. Therefore, if one is aware of this fact and the required corrections of the bleaching rate B_0 , one can apply the continuous bleaching technique as a fast, non-laborious method to preliminary estimate diffusion coefficients of two dimensional membrane systems.

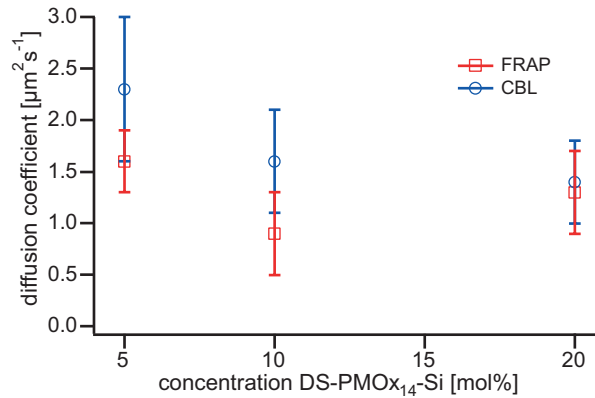


Figure 2.13: Comparison of diffusion coefficients obtained by the FRAP technique and continuous bleaching (CBL) method.

Tamm and co-workers [Wagner & Tamm, 2000] calculated the diffusion coefficient of the underlayer with longer ($n = 77$) poly(ethylene oxide) spacers from bleached patterns (pattern width $\sim 10 \mu\text{m}$). The diffusion coefficient was found to be $D = 0.4 - 1.8 \mu\text{m}^2\text{s}^{-1}$ for lipopolymer fractions of $< 5 \text{ mol}\%$, whereas it decreased to $D = 0.1 - 0.3 \mu\text{m}^2\text{s}^{-1}$ for the membranes with 5-10 mol% of lipopolymers. The mobile fractions they reported seem to be slightly smaller (80-90%) than those we found in this study. The difference in diffusion coefficients and mobile fractions of the underlayer can be related to an increase in the viscosity within the water reservoir.

Naumann et al. [Naumann et al., 2002] bleached a quite large area (diameter: $150 \mu\text{m}$) using a conventional fluorescence microscopy setup. For the underlayer with 5 mol% of lipopolymer ($n = 85$), they found the mobile fraction of 80% that agrees well with those reported by Tamm et al. However, the diffusion constant they measured ($D = 17.4 \mu\text{m}^2\text{s}^{-1}$, at 40°C) seems to be unreasonably large. Such a large discrepancy might be due to a very slow bleaching rate (bleaching time: 10 s) as well as to the very large bleached area (diameter: $150 \mu\text{m}$), which are 50 times longer and 15 times larger than our experimental systems, respectively.

2.6.3 Diffusion of Transmembrane Cell Receptors

After successful incorporation of transmembrane cell receptors integrin $\alpha_{\text{IIb}}\beta_3$ into polymer-tethered membranes (as demonstrated in Section 2.5), their mobility, which is important for protein function, was checked by FRAP.

Two types of integrin containing proteoliposomes were used, one with DMPC/DMPG matrix lipids, the others with SOPC/SOPG matrix lipids (called *D-liposomes* and accordingly *S-liposomes* in the following). Since all measurements were performed at temperatures of around 25 – 28 °C, all lipids were in the fluid state and therefore did not influence the protein diffusion by gel phase². 10% of integrins were labelled with TAMRA in advance to the proteoliposome preparation.

The ratios of proteins to lipids in proteoliposome suspensions were determined to be 1 : 6200 (D-liposomes), and 1 : 2600 (S-liposomes), respectively. The average distances between two incorporated integrins were $d_D \approx 66$ nm (incorporated integrin from D-liposomes), and $d_S \approx 43$ nm (incorporated integrin from S-liposomes), respectively, assuming an average area of $A_l \approx 0.7$ nm² per phospholipid in the fluid state [Marsh, 1990]. Details can be found in the Appendix A.1.

Figure 2.14 illustrates a typical fluorescence intensity recovery curve of a FRAP experiment for the determination of integrin diffusivity and mobility. The line denotes the fit of the data according to the theory of Soumpasis [Soumpasis, 1983].

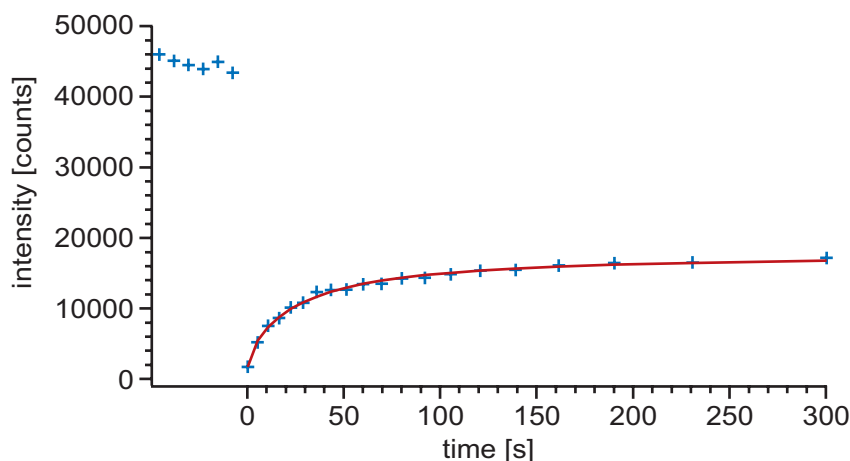


Figure 2.14: Fluorescence intensity recovery curve, the line illustrates the fit of the data. D-liposomes were spread onto a dry LB monolayer composed of 0.5 mol% DS-PMO_{x104}-Si and 99.5 mol% SOPC. The evaluation of this experiment yielded $D = (0.26 \pm 0.01) \mu\text{m}^2\text{s}^{-1}$ and $R = (38 \pm 1) \%$.

²Phase transition temperatures: $T_m = 23$ °C for DMPC and DMPG, $T_m = 6$ °C for SOPC and SOPG [Silvius, 1982]

Since polymer-tethered membranes with longer lipopolymer spacers exhibited higher homogeneity in fluorescence and hence in integrin distribution (see Section 2.5), experiments of protein diffusion were carried out with DS-PMO_{x33}-Si and DS-PMO_{x104}-Si lipopolymer tethers.

In Table 2.3, the results of FRAP experiments are summarized. When spreading D-liposomes with integrins onto polymer-tethered membranes, the diffusivity and mobility of incorporated proteins exhibited a dependence on lipopolymer length and density. Comparing the results on membranes with 5 mol% ($X_p = 0.05$ molar fraction) and 0.5 mol% ($X_p = 0.005$ molar fraction) DS-PMO_{x33}-Si in the underlayer, one could see an increase in the diffusion coefficient D and in the mobile fraction R of integrin, changing from $D = (0.08 \pm 0.05) \mu\text{m}^2\text{s}^{-1}$ and $R = (16 \pm 6) \%$ to $D = (0.11 \pm 0.04) \mu\text{m}^2\text{s}^{-1}$ and $R = (21 \pm 10) \%$.

Increasing the length of the polymer tether, i.e. the degree of polymerization, from $n = 33$ (DS-PMO_{x33}-Si) to $n = 104$ (DS-PMO_{x104}-Si), higher values of D and R were obtained: $D = (0.13 \pm 0.06) \mu\text{m}^2\text{s}^{-1}$ and $R = (24 \pm 8) \%$.

When spreading S-liposomes onto LB monolayers composed of 0.5 mol% DS-PMO_{x33}-Si or DS-PMO_{x104}-Si and 99.5 mol% SOPC, the diffusion coefficients, D , and mobile fractions, R , were $D = (0.51 \pm 0.14) \mu\text{m}^2\text{s}^{-1}$, $R = (17 \pm 1) \%$, and $D = (0.12 \pm 0.03) \mu\text{m}^2\text{s}^{-1}$, $R = (10 \pm 3) \%$, respectively.

lipopolymer fraction		diffusion coefficient [$\mu\text{m}^2\text{s}^{-1}$]	mobile fraction [%]
D-liposomes, $d_D \approx 66$ nm			
5 mol%	DS-PMO _{x33} -Si	0.08 ± 0.05	16 ± 6
0.5 mol%	DS-PMO _{x33} -Si	0.11 ± 0.04	21 ± 10
0.5 mol%	DS-PMO _{x104} -Si	0.13 ± 0.06	24 ± 8
S-liposomes, $d_S \approx 43$ nm			
0.5 mol%	DS-PMO _{x33} -Si	0.51 ± 0.14	17 ± 1
0.5 mol%	DS-PMO _{x104} -Si	0.12 ± 0.03	10 ± 3

Table 2.3: Diffusion coefficients of integrin $\alpha_{\text{IIb}}\beta_3$ incorporated into polymer-tethered membranes with various concentrations of DS-PMO_{x_n}-Si lipopolymers and SOPC matrix lipids in the underlayer.

To understand the origin of the low recovery, two subsequent bleaching experiments at the same spot of the sample were performed. All proteins are irreversibly bleached during the first laser pulse. Only mobile fluorescent proteins can diffuse into the bleached spot and contribute to the fluorescence signal in the second experiment.

Choosing the samples with 0.5 mol% DS-PMO_{x104}-Si in the underlayer and integrins incorporated from D-liposomes and S-liposomes, much higher recovery rates of $R = (87 \pm 13) \%$ (D-liposomes) and $R = (73 \pm 6) \%$ (S-liposomes) were exhibited, while the diffusion coefficients were similar to the value obtained before, $D = (0.10 \pm 0.06) \mu\text{m}^2\text{s}^{-1}$ (D-liposomes), or slightly lower $D = (0.05 \pm 0.02) \mu\text{m}^2\text{s}^{-1}$ (S-liposomes).

The immobile fraction of integrin can be attributed to the following facts:

- Integrins in proteoliposomes are randomly oriented, facing their large extracellular domain to both sides. When spreading these liposomes onto LB monolayers, the orientation stays preserved. Assuming an equal distribution, approximately 50 % of integrins are pointing their large headgroup (~ 10 nm in diameter) to the substrate and are therefore immobilized and likely denatured.
- The remaining $\approx 50 \%$ are facing their small intracellular domain to the substrate, from which the membrane is separated by a thin lubricant film of water, where the membrane-substrate distance is determined by the lipopolymers. These integrins should be mobile.
- But integrins tend to cluster [Schwartz et al., 1995], which can also lead to a decrease in mobile fraction.
- Furthermore, also nonspecific attraction of integrins to lipopolymers or defects within the membrane is possible.

The lower mobile fraction of incorporated integrins from spread S-liposomes could be attributed to a higher density of integrins within the membrane, with an average distance of $d_S \approx 43$ nm. This generates more obstacles for the diffusion of integrins due to more immobilized proteins within the membrane, which was also exhibited in the lower mobile fraction in second bleaching experiments ($R = (73 \pm 10) \%$). Also an increased tendency of integrin clustering might play a role.

The increase in diffusivity and mobile fraction with decreasing density of lipopolymer tethers can be explained by a lower amount of obstacles and a lower frictional coupling due to a lower viscosity of the water layer between membrane and substrate, since $D \propto \eta_l^{-1}$ (see Equation 2.10). Taking the value of $A_l \approx 0.7 \text{ nm}^2$, the average distance between grafting sites of lipopolymers were $d_p = \sqrt{A_l/X_p} \approx 3.8$ nm ($X_p = 0.05$), and $d_p \approx 11.8$ nm ($X_p = 0.005$). Therefore, the larger molar fraction of lipopolymers occupied a larger volume within the water reservoir, which led to an increase in the entire viscosity.

The increase in diffusivity and mobile fraction with increasing length lipopolymer spacers (see Section 2.8) can be dedicated to the enlargement of water reservoir thickness between membrane and substrate, since $D \propto d$ (see Equation 2.10).

The large diffusion coefficient D for integrins moving in 0.5 mol% DS-PMO_{x33}-Si tethered membrane cannot be understood so far. It seems not to keep in line with the other experiments on different lipopolymer length and concentrations, but is presented here for the sake of completeness.

The estimated mobile fraction R of integrins in membranes with 0.5 mol% DS-PMO_{x104}-Si of $R = 24 \pm 8\%$ coincides with the value reported by Gönnerwein et al. [Gönnerwein et al., 2003]. There, a cellulose cushion was used as polymer support instead of lipopolymer tethers. But the reported diffusion coefficient of $D = (0.6 \pm 0.2) \mu\text{m}^2\text{s}^{-1}$ is approximately 4 times larger than the value of $D = (0.13 \pm 0.06) \mu\text{m}^2\text{s}^{-1}$ estimated in this study. The frictional coupling seems to be lower in cellulose supported membranes, which increases the diffusivity.

The only reports on diffusion measurements of proteins incorporated into tethered membranes are from the group of Tamm and coworkers [Wagner & Tamm, 2000, Wagner & Tamm, 2001]. The diffusion coefficients of cytochrome b_5 , annexin V [Wagner & Tamm, 2000], and target SNARE [Wagner & Tamm, 2001] are in the range of 0.3-1.3 $\mu\text{m}^2\text{s}^{-1}$, but in comparison to integrin these proteins exhibit only one single transmembrane part. Integrin $\alpha_{\text{IIb}}\beta_3$ is provided with two α -helical transmembrane domains [González-Rodríguez et al., 1994], which certainly lower the diffusivity in membranes. Therefore, the diffusion of integrin cannot be compared directly to protein diffusion reported by Wagner and Tamm.

2.7 Determination of Frictional Coupling

To estimate the frictional coupling of integrin to the substrate, the theory of Evans and Sackmann [Evans & Sackmann, 1988] was applied. Figure 2.15 illustrates a plot of the dimensionless mobility m ($4\pi\eta_m h_m/f$) versus the dimensionless particle radius ε , calculated from Equation 2.7. The friction coefficient f can be calculated from the obtained diffusion coefficients D with Equation 2.4 ($f = k_B T/D$). For the membrane viscosity, a value of $\eta_m = 0.032 \text{ Nsm}^{-2}$ was chosen [Kühner et al., 1994]³⁴.

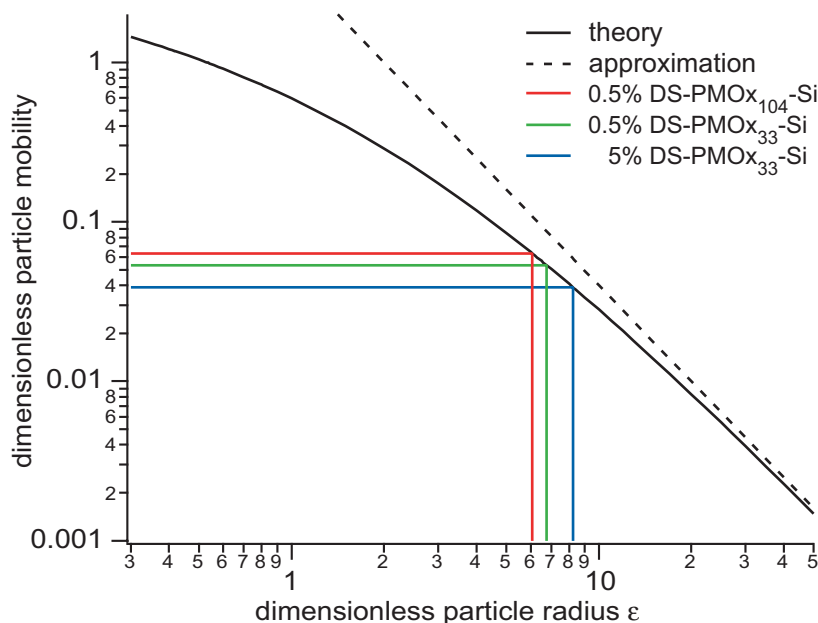


Figure 2.15: Dimensionless particle mobility m ($(4\pi\eta_m h_m D)/(k_B T)$) vs. the dimensionless particle radius ε . The horizontal lines denote the dimensionless particle mobilities evaluated from the diffusion coefficients of integrins, moving in membranes tethered with 5 mol% DS-PMOx₃₃-Si, 0.5 mol% DS-PMOx₃₃-Si, or 0.5 mol% DS-PMOx₁₀₄-Si. The vertical line illustrates the corresponding ε . The dashed line visualizes the approximation of the diffusion theory for $\varepsilon \gg 1$ (Equation 2.10).

The evaluated dimensionless particle mobilities are $m = 0.039$ ($D = 0.08 \mu\text{m}^2\text{s}^{-1}$, 5 mol% DS-PMOx₃₃-Si in the underlayer), $m = 0.053$ ($D = 0.11 \mu\text{m}^2\text{s}^{-1}$, 0.5 mol% DS-PMOx₃₃-Si), and $m = 0.063$ ($D = 0.13 \mu\text{m}^2\text{s}^{-1}$, 0.5 mol% DS-PMOx₁₀₄-Si), respectively.

³Two dimensional viscosity of a DMPC membrane at $T = 26 \text{ }^\circ\text{C}$, $\eta_{2D} = \eta_m h_m = 1.6 \times 10^{-10} \text{ Nsm}^{-1}$, with $h_m = 5 \text{ nm}$.

⁴It should be noted that two dimensional membrane viscosities η_{2D} measured by macroscopic techniques [Vaugh, 1982a, Vaugh, 1982b, Dimova et al., 1999, Dimova et al., 2000] are by a factor of ≈ 10 larger than that resulted from measurements based on diffusion of molecular probes [Vaz et al., 1984, Merkel et al., 1989, Kühner et al., 1994]. But η_{2D} values determined by the latter method appear to be more reliable.

From this, the dimensionless particle radii can be obtained, yielding $\varepsilon = 8.3$ (5 mol% DS-PMO_{x33}-Si), $\varepsilon = 6.8$ (0.5 mol% DS-PMO_{x33}-Si), and accordingly $\varepsilon = 6.1$ (0.5 mol% DS-PMO_{x104}-Si).

Since the values of ε are all $\varepsilon > 1$, the classical Saffman-Delbrück theory does not hold. The approximation for $\varepsilon \gg 1$ (Equation 2.10) was also not applied, since the deviation to the exact theory is quite large for $\varepsilon < 10$ (see Figure 2.15, dashed line).

The friction coefficient b_s can be evaluated according to Equation 2.8

$$b_s = \frac{\varepsilon^2 \eta_m h_m}{R^2} \quad . \quad (2.13)$$

The radius of integrin $\alpha_{\text{IIb}}\beta_3$ can be estimated to $R = 0.64$ nm [González-Rodríguez et al., 1994]⁵. Since the distance d between membrane and substrate is known from FLIC measurements ($d = 2.3$ nm for DS-PMO_{x33}-Si tethered membranes and $d = 4.8$ nm for DS-PMO_{x104}-Si tethered membranes, see Section 2.8), the average viscosity η_l of this water reservoir can be calculated ($\eta_l = b_s d$). The next table summarizes the results (Table 2.4).

lipopolymer fraction		friction coefficient b_s [Nsm ⁻³]	liquid viscosity η_l [Nsm ⁻²]
5 mol%	DS-PMO _{x33} -Si	2.7×10^8	0.63
0.5 mol%	DS-PMO _{x33} -Si	1.8×10^8	0.42
0.5 mol%	DS-PMO _{x104} -Si	1.5×10^8	0.71

Table 2.4: Friction coefficient b_s of integrin $\alpha_{\text{IIb}}\beta_3$ and liquid viscosity η_l of the water reservoir of membranes tethered with DS-PMO_{xn}-Si lipopolymers.

The obtained values of frictional coupling b_s of integrin to the substrate are by a factor of ≈ 10 larger than values for DMPC lipids on polymer supports reported by Kühner et al. [Kühner et al., 1994], and about 100 times larger than that of glass supported DMPC bilayers [Merkel et al., 1989]. The friction coefficient $b_s = 1.8 \times 10^8$ Nsm⁻³ of cytochrome b_5 (α -helical membrane part with $R = 0.6$ nm) reported by Wagner and Tamm [Wagner & Tamm, 2000] coincides with the findings of this thesis, whereas b_s of annexin V was by a factor of ≈ 50 smaller.

The tendencies of b_s can be regarded to the less friction noticed by integrin due to

⁵Integrin $\alpha_{\text{IIb}}\beta_3$ is provided with two α -helical transmembrane parts, each with a radius of 0.45 nm. The total area occupied in the membrane is $2 \times \pi (0.45 \text{ nm})^2 = 1.3 \text{ nm}^2$. From that, an “overall” radius of 0.64 nm can be calculated.

(i) the decrease in tether density (from 5 mol% to 0.5 mol%) and (ii) the further decoupling of the membrane from the substrate (from $d = 2.3$ nm to 4.8 nm) by introduction of longer polymer spacers.

The viscosity η_l of the water reservoir between membrane and substrate was about 500 times larger than the viscosity of bulk water (0.001 Nsm^{-2}). The increase in η_l of about 50% when increasing the tether density from 0.5 mol% to 5 mol% can be attributed to the larger volume occupied by hydrated poly(oxazoline) relative to the “free” water volume without polymers, since the average distance between tethers decreases from 11.8 nm to 3.8 nm.

Keeping a constant tether density (0.5 mol%), the increase in viscosity η_l from DS-PMO_{x33}-Si to DS-PMO_{x104}-Si supported membranes can be understood by the increased volume fraction of polymer within the membrane-substrate cleft.

To summarize, the values for the friction coefficient b_s of integrin $\alpha_{\text{IIb}}\beta_3$ to the substrate demonstrate the potential of the established membrane model, since b_s can be tuned by choosing a certain tether density and length. With this, the extracellular matrix of cell plasma membranes can be mimicked by providing a distinct viscosity to incorporated cell receptors.

2.8 Measurement of Membrane-Substrate Distance by FLIC

To investigate the increase in water reservoir thickness between membrane and substrate by introducing polymer tethers, the method of fluorescence interference contrast microscopy (FLIC) was applied [Lambacher & Fromherz, 1996, Braun & Fromherz, 1997, Lambacher & Fromherz, 2002].

The membrane was deposited by LB transfer and subsequent vesicle fusion onto stepped Si/SiO₂ chips. Figure 2.16 illustrates a fluorescence image of a covered substrate. Over large areas, the coverage with polymer-tethered membranes was homogeneous and defect free within the optical resolution. Even the step difference of ~ 300 nm between lowest and highest oxide did not obstruct the deposition.

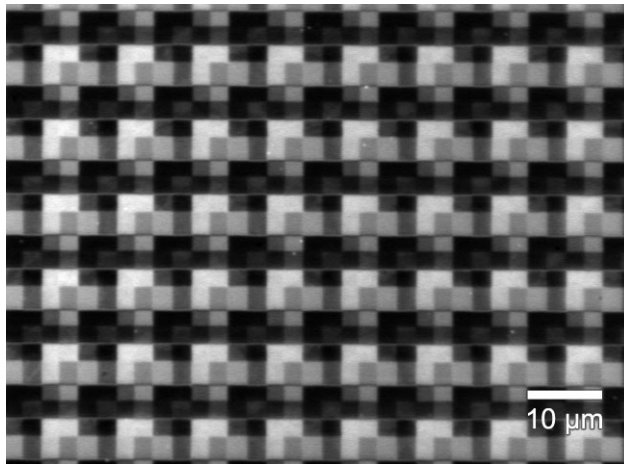


Figure 2.16: Fluorescence image of a FLIC substrate, covered with a polymer-tethered membrane (underlayer: 0.5 mol% DS-PMO_{x104}-Si, 99.0 mol% SOPC, and 0.5 mol% DiI; toplayer: 99.5 mol% SOPC and 0.5 mol% DiI).

The fluorescence intensity of related 16 steps can be evaluated from the image. This can be plotted versus the matching oxide thickness of the step (Figure 2.17). Fitting the FLIC theory to the fluorescence intensity, one obtains the distance between membrane and substrate. For all fits, the inclination angle of the transition dipole of the cyanine dye DiI was assumed to be $\theta = 62^\circ$ with respect to the membrane normal. The fluorescence quantum yield was presumed to be $\Phi_{fl} = 0.38$. Additionally, lifetime and background corrections were applied [Lambacher & Fromherz, 2002].

Table 2.5 summarizes the obtained water reservoir thicknesses in dependence on the spacer length. The fit of the data yielded a distance of $d = (2.9 \pm 0.5)$ nm for the shortest spacer DS-PMO_{x14}-Si, $d = (2.3 \pm 0.7)$ nm for the membrane tethered with DS-PMO_{x33}-Si, and $d = (4.8 \pm 0.6)$ nm for the longest spacer DS-PMO_{x104}-Si. The incorporation of integrin $\alpha_{11b}\beta_3$ led to no increase in distance, but exhibited a larger

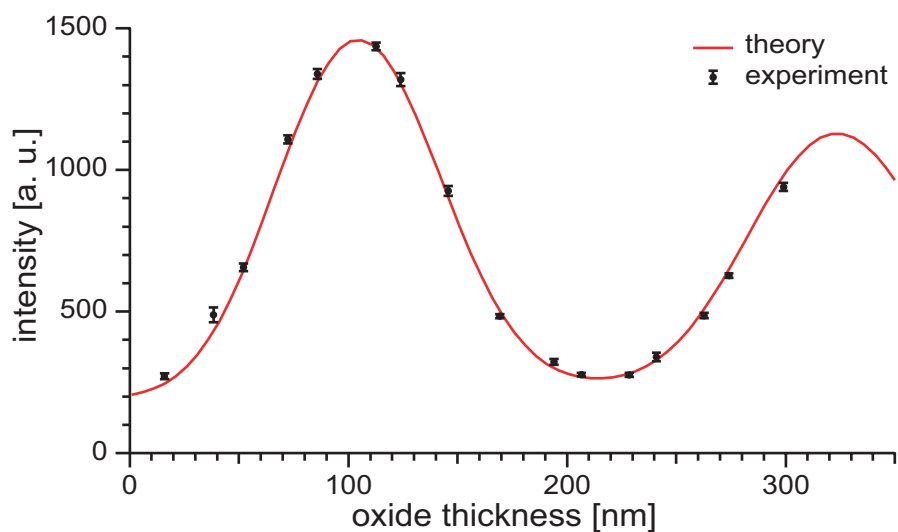


Figure 2.17: The graph illustrates the obtained fluorescence intensity of a deposited membrane (underlayer: 0.5 mol% DS-PMO_{x104}-Si, 99.0 mol% SOPC, and 0.5 mol% DiI; toplayer: 99.5 mol% SOPC and 0.5 mol% DiI) versus the matching oxide thickness. The line denotes the fitted FLIC theory to fluorescence intensity. In this experiment, the determined membrane-substrate distance was $d = (4.8 \pm 2.2)$ nm.

error, $d = (4.8 \pm 1.1)$ nm.

lipopolymer fraction	membrane-substrate distance d [nm]
0.5 mol% DS-PMO _{x14} -Si	2.9 ± 0.5
0.5 mol% DS-PMO _{x33} -Si	2.3 ± 0.7
0.5 mol% DS-PMO _{x104} -Si	4.8 ± 0.6
with incorporated integrins	
0.5 mol% DS-PMO _{x104} -Si	4.8 ± 1.1

Table 2.5: Measurement of membrane-substrate distance of polymer-tethered membranes (underlayers: DS-PMO_{xn}-Si lipopolymers and SOPC matrix lipids) by FLIC. Both membrane leaflets were doped with 0.5 mol% DiI.

The results demonstrate the successful increase in water reservoir thickness by introduction of poly(2-methyl-2-oxazoline) lipopolymer spacers. The distance of (4.8 ± 0.6) nm of a DS-PMO_{x104}-Si tethered membrane is the highest value for tethered membranes reported so far. It is much larger than the distance of (3.9 ± 0.9) nm reported by Kiessling and Tamm [Kiessling & Tamm, 2003], where they used poly(ethylene oxide) lipopolymer spacers.

Furthermore, the applied low tether density of 0.5 mol% (yielding an average distance of 11.8 nm) is sufficient to increase the membrane-substrate distance and therefore overcome the forces that act on the membrane and bring it close to the substrate.

Assuming the lipopolymers as one-side grafted random coil, the size of the polymer follows simple polymer theories. Here, the Flory radius of a polymer with n_p monomers of size a_m is [de Gennes, 1980, de Gennes, 1987, Marsh et al., 2003]

$$R_F = a_m n_p^{3/5} . \quad (2.14)$$

Taking a value of 0.3 nm for the monomer size⁶, one obtains $R_F = 2.4$ nm for DS-PMO_{x33}-Si and $R_F = 4.9$ nm for DS-PMO_{x104}-Si, respectively. These values coincide very well with that from FLIC measurements. Nevertheless, one should be aware of the fact that the used lipopolymers are double tethered with one end to the substrate and the other end to the membrane. Therefore, the situation is different from the assumed case.

The membrane with the shortest lipopolymer spacers ($n_p = 14$, DS-PMO_{x14}-Si) exhibited a higher membrane-substrate distance ($d = (2.9 \pm 0.5)$ nm) than the membrane with longer spacers (DS-PMO_{x33}-Si, $n_p = 33$). This result allows for the fact that this lipopolymer shows oligomeric behavior since with a monomer number of $n_p = 14$ it is too short to be assumed as a random coil. It exhibits a more stretched conformation and it disobeys polymer scaling laws.

Due to the fact that no change in membrane-substrate spacing was obtained by incorporation of integrin $\alpha_{\text{IIb}}\beta_3$, one can conclude that the lipopolymer spacers stabilize the overall distance of the membrane to the substrate. Incorporation of integrins facing their large extracellular matrix to the substrate act as local disturbances in the spacing. This is reflected in the increase in the measuring error. In Figure 2.18, a sketch of the system is drawn to scale. There, the average distance between lipopolymer tethers of $d_p \approx 11.8$ nm (see Section 2.6.3) and integrins $d_D \approx 66$ nm (see Appendix A.1) was adopted.

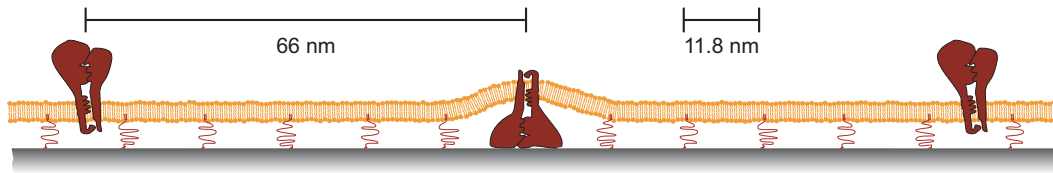


Figure 2.18: Sketch of a polymer-tethered membrane with incorporated integrin. The image is drawn to scale. The average distance between integrins (66 nm) and tethers (11.8 nm) is illustrated.

⁶From molecular mechanics calculations (energy minimization) and re-optimization of the results with molecular dynamics calculations (200 ps), one obtains an equilibrium end-to-end distance of ≈ 3.0 nm for poly(2-ethyl-2-oxazoline) with 10 monomers, which exhibits a zigzag conformation [Jordan, R., personal communication].

2.9 Function of Integrin in Polymer-Tethered Membranes

To verify the functionality of incorporated integrin $\alpha_{\text{IIb}}\beta_3$, the free energy of adhesion Δg_{ad} (also called spreading pressure) to giant vesicles with synthetic ligands was measured quantitatively. The ligand molecule used here was a lipid coupled to a cyclic hexapeptide containing the RGD sequence that is specifically recognized by integrin $\alpha_{\text{IIb}}\beta_3$ [Hu et al., 2000] (Figure 2.19).

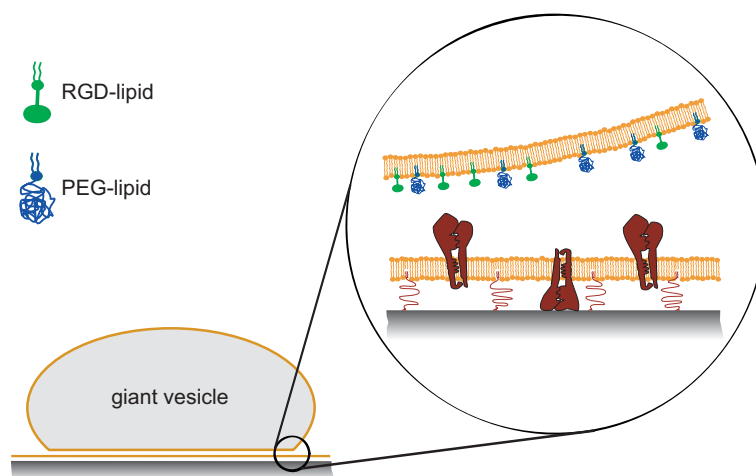


Figure 2.19: Model system of a giant lipid vesicle adhering to a polymer-tethered membrane with integrin $\alpha_{\text{IIb}}\beta_3$. The specific binding is generated by ligands bearing the RGD sequence, whereas the PEG lipids prevent non-specific adhesion.

Using the micro-interferometric technique reflection interference contrast microscopy (RICM) [Albersdörfer et al., 1997], the free energy of adhesion could be determined from the vesicle contour close to the substrate. To avoid non-specific adhesion, lipopolymers with poly(ethylene glycol) headgroups were additionally incorporated into the giant vesicles as steric “repellers” (see Figure 2.19).

Figure 2.20(a) illustrates a RICM image of an adhered vesicle on a polymer-tethered membrane. The white line coincides with the contact line, where the interferogram was analyzed (Figure 2.20(b)). From the intensity profile, the height profile of the vesicle can be calculated (Figure 2.20(c)).

The free energy of adhesion Δg_{ad} can be determined from the mechanical equilibrium between the adhered vesicle and the substrate [Bruinsma, 1995]. This can be described by the classical Young-Dupré law [Bell et al., 1984, Bruinsma et al., 2000, Sackmann & Bruinsma, 2002]:

$$\Delta g_{ad} = \gamma(1 - \cos \alpha) \quad (2.15)$$

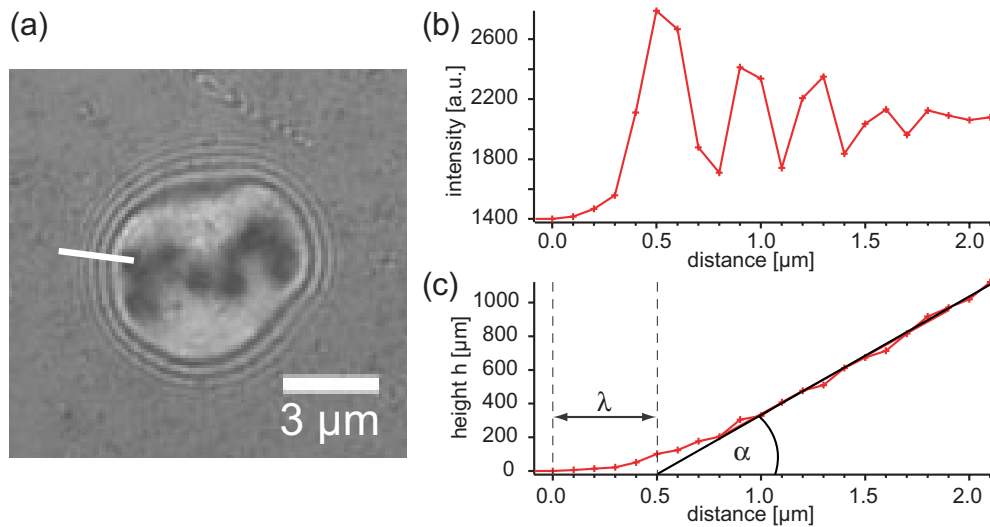


Figure 2.20: (a) Reflection interference contrast microscopy (RICM) image (averaged over 20 images corresponding to ≈ 2 s) of a giant vesicle containing 1% RGD lipid and 1% PEG lipid adhering to a membrane with 0.5 mol% DS-PMO_{x104}-Si in the underlayer and incorporated integrin $\alpha_{\text{IIb}}\beta_3$. The dark areas indicate strongly adhered patches. Newton fringes around the contact area show lines of equal height of the membrane above the surface. (b) The intensity profile along the straight line indicated in the interferogram. (c) The local height profile can be reconstructed from the intensity profile. The contact angle, α , and the characteristic capillary length, λ , are defined in the height profile. The zero point of the x-axis ($x=0$) is determined by the onset of the upward deflection of the membrane from the substrate.

where α is the contact angle defined in Figure 2.20(c), and γ is the lateral membrane tension. Here, the tension of the fluid membrane is assumed to be constant.

However, the quantitative determination of the effective contact angle α is often found to be difficult experimentally (Figure 2.20(c)). To overcome this problem, another length scale λ was introduced to analyze the height profile of the vesicle in the vicinity of the contact line [Bruinsma, 1995]:

$$h(x) = \alpha(x - \lambda) + \alpha\lambda \exp\left(-\frac{x}{\lambda}\right) \quad (2.16)$$

where x is defined in Figure 2.20(c), α is the macroscopic contact angle between the membrane and the substrate, and λ is the capillary length

$$\lambda = \sqrt{\frac{\kappa}{\gamma}} \quad (2.17)$$

λ is a measure for the length over which the height profile of the membrane is dominated by the bending elasticity of the membrane. Namely, the vesicle shape is dominated only by tension when $x > \lambda$. The geometric parameters α and λ can be determined from the RICM image for each location along the rim of the adhesion disc [Albersdörfer et al., 1997].

The capillary length λ is determined by the distance between $x = 0$ and the intersection of the straight line fitted to the contour of the vesicle for $x \gg \lambda$ and the x-axis. The zero point of the axis ($x = 0$) is determined by the onset of the deflection of the membrane (Figure 2.20(c)). The bending stiffness κ is assumed to be $100 k_B T$ for the vesicles containing 50 mol% DMPC and 50 mol% cholesterol [Gennis, 1989].

According to the Young equation (Equation 2.15), the local adhesion energy Δg_{ad} could be determined at every position of the rim. However, the values of λ can not be easily estimated for regions of tight adhesion, thus more accurate results are obtained by measuring the tension γ at sites of weak adhesion, which exhibit many Newton rings. Repeller molecules were incorporated into the vesicle to decrease the free energy of adhesion Δg_{ad} due to the osmotic pressure difference $\Delta\pi_R$ between the adhering and non-adhering parts of the vesicle membrane by [Bruinsma et al., 2000, Guttenberg et al., 2000]

$$\Delta g_{ad} = W_{ad} - \Delta\pi_R \quad (2.18)$$

where W_{ad} is the specific adhesion energy per unit area of the receptor-ligand pairs, and $\Delta\pi_R = k_B T \Delta c_R$ is the osmotic pressure difference including the difference in repeller concentration Δc_R following the van't Hoff's law.

In Figure 2.21, histograms of measured values of Δg_{ad} of vesicles containing 1 and 2 mol% of repeller lipids (PEG lipids) are presented. By extrapolating the measured Δg_{ad} to zero repeller concentration, the specific binding energy W_{ad} could be determined to be $W_{ad} \approx 1.4 \cdot 10^{-6} \text{ Jm}^{-2}$ (Figure 2.22).

From the ratio of integrin : phospholipid in D-liposomes of 1 : 6200 (see Appendix A.1), one can estimate the surface density of integrin to be $2.3 \times 10^{14} \text{ m}^{-2}$. By assuming that about 50 % of integrin are facing their extracellular domain to the bulk electrolyte, this density decreases to $1.65 \times 10^{14} \text{ m}^{-2}$. From the specific adhesion energy per unit area calculated in Figure 2.22, $W_{ad} \approx 1.4 \cdot 10^{-6} \text{ Jm}^{-2}$, one can estimate the specific interaction energy of a integrin-RGD pair to be $w_{ad} \approx 1.22 \times 10^{-20} \text{ J} = 3 k_B T$. This value shows a reasonable agreement with the value reported previously for the supported membrane on ultrathin films of cellulose [Gönnenwein et al., 2003]⁷.

This free energy of adhesion is approximately 30 times larger than the correspond-

⁷Careful recalculation of the integrin density denoted $2.04 \times 10^{14} \text{ m}^{-2}$. From free energy of adhesion per unit area of $W_{ad} \approx 2.5 \times 10^{-6} \text{ Jm}^{-2}$, one derives a binding energy of $w_{ad} \approx 1.23 \times 10^{-20} \text{ J} = 3 k_B T$.

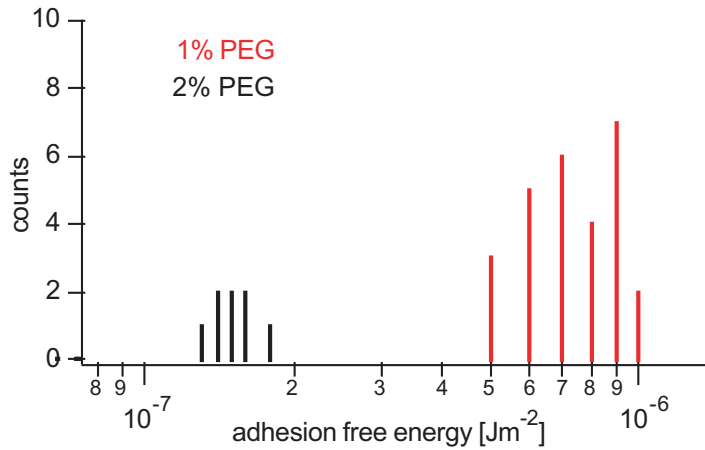


Figure 2.21: Histograms of measured free energies of adhesion of vesicles containing 1 and 2 mol% of repeller lipids (PEG lipids). The largest values correspond to regions of tight adhesion, whereas the lowest values correspond to the spreading pressures of regions of weak adhesion.

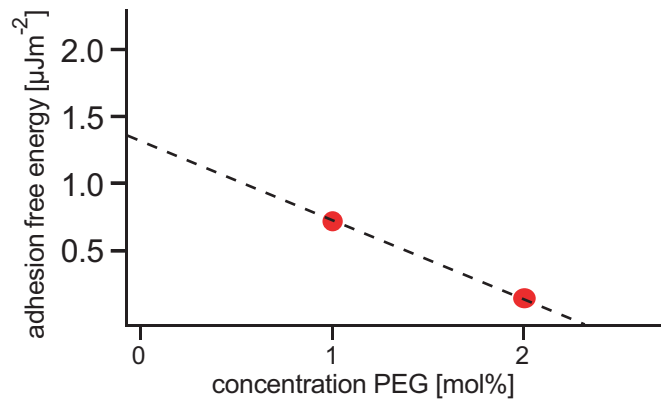


Figure 2.22: Free energy of adhesion as a function of repeller concentration. The specific adhesion energy can be estimated from an extrapolation of the data to the repeller concentration of zero.

ing value on solid supported membranes. In fact, the binding energy on polymer cushions/tethers is in the same order of magnitude as the binding energy of integrin-RGD pairs, $\sim 10 k_B T$, estimated from the dissociation constant $k_D \approx 1.1 \times 10^{-6} \text{ M}$ [Hu et al., 2000].

Thus, the obtained results clearly demonstrate that the soft polymer spacers significantly improve the homogeneity, the lateral mobility (by reduction in the frictional coupling between proteins and the surface), and the biological functionality of trans-membrane cell receptors.

2.10 Limitations of the Membrane Model

Throughout this study, it turned out that the hydrophilic/lipophilic balance (HLB) between polymer headgroup and lipid moiety of lipopolymers plays an important role for the stability of lipid/lipopolymer monolayers at the air/water interface. Since the compression of these Langmuir films was carried out very slowly ($50 \mu\text{ms}^{-1}$), one would lose a large amount of lipopolymers to the subphase if the HLB gets an hydrophilic overweight. This would wreck the advantage of the Langmuir-Blodgett technique of precise control of molar composition of the monolayer.

This finding was obtained in the beginning of the study when lipopolymers with single chain lipid moieties (Ph-PMOx_n-Si) were applied. There, the problems arose when in monomer units were increased from $n = 12$ to $n = 21$. Therefore, lipopolymers with double chain lipid moiety were synthesized, which exhibited an excellent stability at the air/water interface even without phospholipids in the monolayer.

The used DS-PMOx₁₀₄-Si lipopolymer with $n = 104$ monomer units also seems to be a limiting case. By applying a pressure constant mode at the LB film balance, the total surface area was decreasing slightly for very long experiment times indicating a loss in material, namely lipopolymers, to the water subphase. Within the period of time necessary for compression of the film and deposition to a solid substrate, this finding can be neglected.

One should be aware of the fact that one cannot simply extend the monomer unit number to larger values. Assuming a lipopolymer with $n = 200$, the membrane-substrate distance would be increased to $d \sim 7$ nm since this distance seems to follow polymer scaling laws. But this lipopolymer would not form a stable monolayer at the air/water interface, which would impede the successful LB transfer. Furthermore, the applied “living cationic ring-opening polymerization” of 2-alkyl-2-oxazolines is very time consuming. The synthesis of the longest lipopolymer used ($n = 104$) required 15 days. Therefore, also from the polymer chemistry side a limit seems to be reached.

2.11 Conclusion

The established membrane model with poly(2-methyl-2-oxazoline) lipopolymers as membrane tethers exhibits a large potential towards functional immobilization of various transmembrane proteins on solid surfaces.

Supported membranes were prepared in two steps. First, the proximal leaflet of the membrane was deposited by Langmuir-Blodgett transfer of a suitable lipid/lipopolymer mixture onto solid substrates. The distal leaflet was prepared by vesicle fusion onto the dry LB monolayer. Careful optimization of both preparation steps resulted in the formation of stable and defect-free membranes over large areas in cm^2 range.

Impacts of the spacer length and the lipopolymer fraction upon the lateral diffusivity of lipids were systematically compared by fluorescence recovery after photobleaching (FRAP). At 5 mol% of lipopolymers of various length, the lipids in the underlayer exhibited a diffusion coefficient of $D = 1.4 - 1.6 \mu\text{m}^2\text{s}^{-1}$ and a mobile fraction of $R \sim 98\%$. These values coincide with results on other polymer-supported membranes. The diffusion and mobile fraction was reduced to $D = 0.4 \mu\text{m}^2\text{s}^{-1}$ and $R = 10\%$, respectively, by introducing of 50 mol% of DS-PMOx₁₄-Si in the underlayer. This denotes the strong influence of tether concentration on the mobility of membrane components.

With the method of fluorescence interference contrast microscopy (FLIC), it was proven that the membrane-substrate distance d was increased to $d = (4.8 \pm 0.6) \text{ nm}$ by introducing of the longest lipopolymer tethers used (DS-PMOx₁₀₄-Si). Hence, the water reservoir thickness between membrane and substrate was significantly enlarged compared to solid supported membranes. Furthermore, this is the largest membrane-substrate distance of polymer-tethered membranes reported so far. The shorter lipopolymer DS-PMOx₃₃-Si exhibited a membrane separation of $d = (2.3 \pm 0.7) \text{ nm}$, which coincides with the Flory radius of polymer scaling laws. Therefore, the distance between membrane and substrate can be adjusted by the length of the polymer spacer.

The functionality and the feasibility of the membrane model was tested with the transmembrane cell receptor integrin $\alpha_{IIb}\beta_3$. It could be demonstrated that the successful incorporation of integrin is dependent on the length of the lipopolymer spacer. Measuring the diffusivity and mobile fraction of integrins by FRAP, the obtained results by fluorescence microscopy were supported. The diffusion coefficients D and mobile fraction R of integrins increase with decreasing tether density

and with increasing membrane-substrate distance. Decreasing the DS-PMOx₃₃-Si tether concentration from 5 mol% to 0.5 mol%, D increased from (0.08 ± 0.05) to $(0.11 \pm 0.04) \mu\text{m}^2\text{s}^{-1}$, where R increased from (16 ± 6) to $(21 \pm 10) \%$. Taken the same molar fraction but increasing the distance between membrane and substrate by using DS-PMOx₁₀₄-Si lipopolymers, the diffusion coefficient and mobile fraction increase to $D = (0.13 \pm 0.06) \mu\text{m}^2\text{s}^{-1}$ and $R = (24 \pm 8) \%$. This demonstrates that the diffusion of integrins can be tuned by changing the lipopolymer tether concentration and length.

The frictional coupling b_s of integrins to the substrate was estimated to be $b_s = 1.5 - 2.7 \times 10^8 \text{ Nsm}^{-3}$ dependent on the tether length and concentration, whereby the viscosity of the water reservoir between membrane and substrate was in the range of $\sim 400 - 700 \text{ Nsm}^{-2}$. Therefore, the viscous environment of incorporated proteins can be tuned, mimicking the extracellular matrix of cell plasma membranes.

The functionality of incorporated cell receptors was evaluated by quantitative measurements of the free energy of adhesion of giant vesicles with synthetic ligands. Hereby, a lipid coupled cyclic hexapeptide containing the RGD sequence was used as ligand which is specifically recognized by integrin $\alpha_{\text{IIb}}\beta_3$. The free energy of adhesion was approximately 30 times larger than the corresponding value on solid supported membranes without tethers and coincides with the value reported on integrin incorporated into membranes supported by a cellulose cushion. The estimated specific binding energy of integrin-RGD pairs was $w_{ad} \approx 3 k_b T$. This clearly denotes the functional incorporation of integrin into polymer-tethered membranes.

The obtained results demonstrate that the soft polymer spacers significantly improve the homogeneity, the lateral mobility, and the biological functionality of incorporated integrin. Therefore, the strategy of tethering membranes with soft poly(2-methyl-2-oxazoline) lipopolymers exhibits a large potential in functional confinement of transmembrane proteins into planar geometries for biotechnological applications.

2.12 Outlook

The next approaches to enlarge the feasibilities of polymer-tethered membranes will be the further increase of membrane-substrate distance by longer poly(2-methyl-2-oxazoline) lipopolymer spacers. The necessary stability at the air/water interface can probably be achieved by introducing membrane spanning lipid moieties known from archaea [Mathai et al., 2001] instead of distearoyl alkyl chains (Figure 2.23).

This will be a hard challenge for both the polymer chemist and the experimentalist. But the experiments performed in this work proofed the principle of the underlying ideas and makes a further proceeding worthwhile to follow.

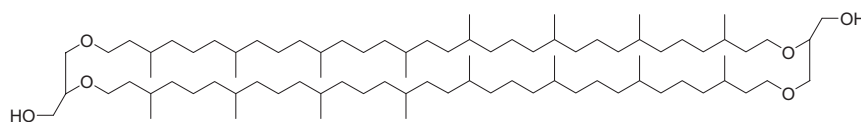


Figure 2.23: Chemical structure of caldarchaeol, the predominant lipid of archaea.

To increase the mobile fraction of $\alpha_{\text{IIb}}\beta_3$ integrins, the incorporation into proteoliposomes need further control. Since integrins are randomly oriented in liposomes, a fraction of $\approx 50\%$ faces their extracellular domains to the substrate and denature. Therefore, using a different preparation technique, integrins might be incorporated side-selectively into proteoliposomes and hence into the polymer-tethered membrane, facing their cytoplasmic domain to the substrate (Figure 2.24).

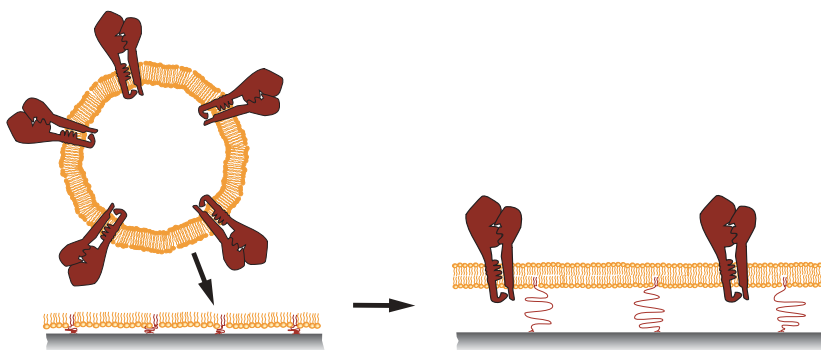


Figure 2.24: Spreading of proteoliposomes onto dry LB monolayers.

With the achievement of this thesis, a new membrane model system was established. This can now serve as a general platform for protein immobilization without denaturing and loss of their native function into planar geometries. This bears a large potential for the pharmaceutical industry, enabling separation, purification, and diagnostic tests against drugs.

3. Dissipative Striped Structures in Lipid/Lipopolymer Langmuir-Blodgett Monolayers

3.1 Introduction

During the preparation of lipid/lipopolymer LB monolayers, stripe micropatterns were obtained, which were aligned parallel to the transfer direction, and whose width and spacing were tunable by the velocity of the film transfer onto a solid substrate. All individual stripes, with a spatial distance in the μm range, were found to be continuous up to cm length scale, and covered the entire substrate without notable defects (Figure 3.1). In this chapter, the origins of pattern formation are tackled to get some insight into its mechanisms, since theoretical predictions are still missing so far .

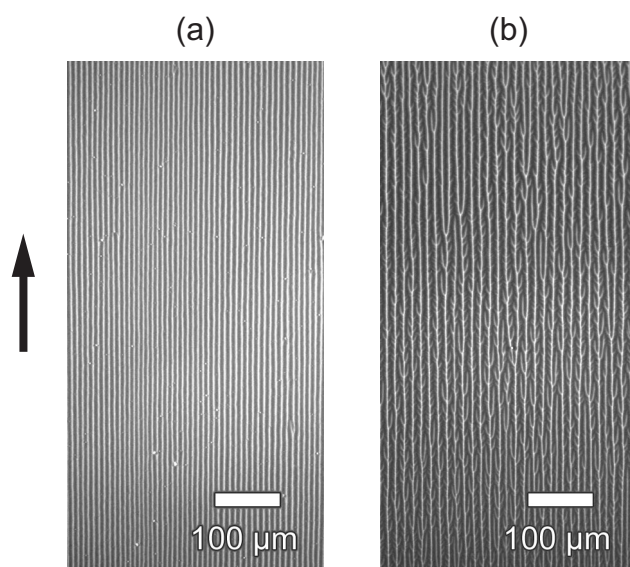


Figure 3.1: Fluorescence image of LB monolayers composed of 94.8 mol% SOPC, 0.2 mol% Texas Red-PE and 5 mol% DS-PMO_{x14}-Si (a), or DS-PMO_{x33}-Si (b). The films were deposited at $T = 20^\circ\text{C}$, $\Pi = 30\text{ mNm}^{-1}$, and at a velocity of $v \sim 50\ \mu\text{ms}^{-1}$.

Since dissipative molecular aggregates in organic materials are drawing increasing attentions as mesoscopic (or nanoscopic) compartments for the confinement of chemical functionalities [Gleiche et al., 2000, Shimomura & Sawadaishi, 2001,

Lenhert et al., 2004], these findings are of relevance for the future.

Along this line, many studies have demonstrated the formation of dissipative structures (e.g. dewetting, fingering instability, etc.) in free-standing and solid-supported polymer thin films [Reiter, 1992, Koneripalli et al., 1996, Herminghaus et al., 1998], as well as in surfactant films [Spratte et al., 1994, Solletti et al., 1996, Yaminski et al., 1997, Gleiche et al., 2000, Moraille & Badia, 2002, Pignataro et al., 2002, Kovalchuk et al., 2003, Lenhert et al., 2004]. So far, micropatterns formed by self-assembly are used predominantly for lithographic processes as masks to micro-/nanostructure surfaces, or to deposit molecules or particles [Shimomura & Sawadaishi, 2001, Lu et al., 2002, Lenhert et al., 2004], but biological applications are still missing. Most of the other known systems for bringing biological function in confinements onto surfaces deal with structuring methods using microcontact printing [Groves & Boxer, 2002] or lithography [Tanaka et al., 2004]. Here, a new method based on self-assembly is presented.

3.2 Lipid/Lipopolymer Monolayers at the Air/Water Interface

To verify that the micropattern formation is not induced by demixing of lipids and lipopolymers at the air/water interface before the LB transfer, experiments with a fluorescence film balance were performed to visualize possible domains and defects. Hereby, the monolayer was doped simultaneously with NBD lipid labels and TRITC polymer labels and observed with suitable filter sets for each dye (Figure 3.2).

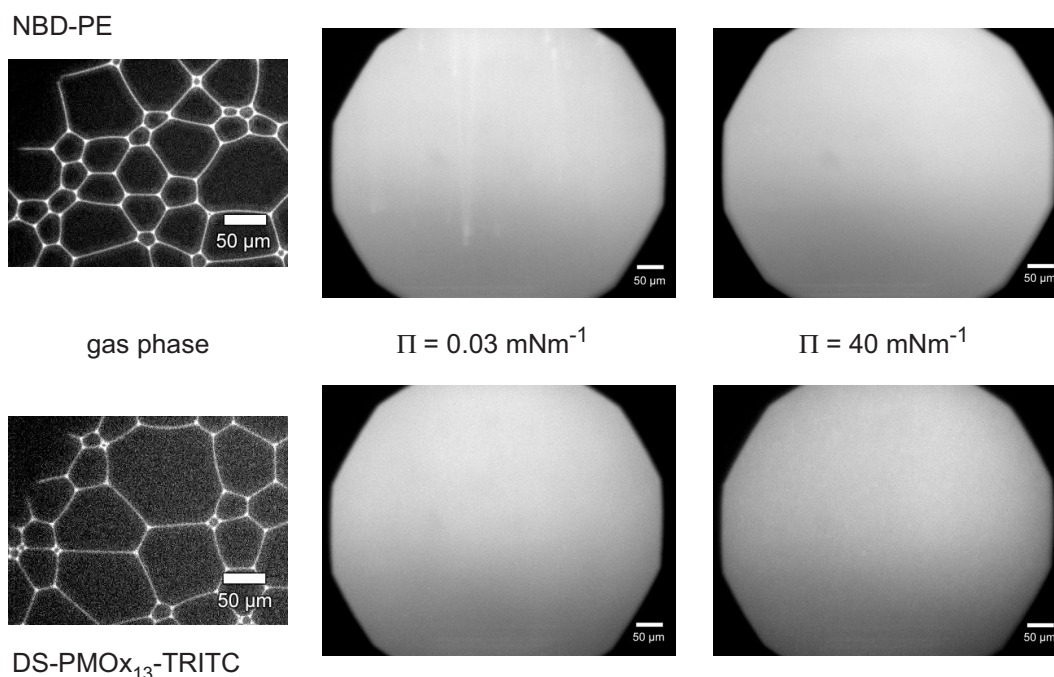


Figure 3.2: Fluorescence images of lipid/lipopolymer monolayers at the air/water interface of a fluorescence film balance. The film was composed of 0.2 mol% DS-PMO_{x13}-TRITC, 4.8 mol% DS-PMO_{x18}-Si, 94 mol% SOPC, and 1 mol% NBD-PE. The film was visualized by using suitable filter sets for each dye. The upper row denotes images of the NBD lipid label, where in the lower row the labelled lipopolymer was visible. The images were taken at $T = 20^\circ\text{C}$ and various surface pressures: gas phase ($\Pi \approx 0$), left), $\Pi = 0.03 \text{ mNm}^{-1}$ (middle), and $\Pi = 40 \text{ mNm}^{-1}$ (right). To compress the film, the barrier was moved with a velocity of $50 \mu\text{ms}^{-1}$.

In the upper row, the lipid labels within the monolayer are illustrated, where the lower row denotes the polymer label within the film. In the gas phase ($\Pi \approx 0$, left images), lipids and lipopolymers are accumulated in random netlike structures. Also bubble-like and other patterns were visible (data not shown), which is quite usual for monolayers in the gas phase [Gaines, 1966]. At surface pressures $\Pi > 0$, the monolayer appeared homogeneous, independent on the kind of dye, up to high pressures ($\Pi = 40 \text{ mNm}^{-1}$, right images).

Therefore, lipid/lipopolymer monolayers exhibited no phase separation at the air/water interface. At the conditions of film transfer ($T = 20^\circ\text{C}$, $\Pi = 30 \text{ mNm}^{-1}$), the monolayer appeared to be in a fluid state.

Thus, the lipid/lipopolymer monolayer is not demixed at the air/water interface [Spratte & Riegler, 1994], and the origin of pattern formation has to be addressed to the Langmuir-Blodgett transfer.

3.3 Influence of Monolayer Constituents on Pattern Formation

3.3.1 Influence of Hydrophobic Mismatch

Since most of the previous works claimed that packing fluctuation and phase separation of alkyl chains are responsible for the pattern formation [Spratte et al., 1994, Solletti et al., 1996, Moraille & Badia, 2002], a monolayer consisting of phospholipids and lipopolymers with diphytanoyl alkyl chains (DPhPC and DPh-PMO_x₂₁-Si, see Appendix A.4). As phytanoyl chains are known to have no chain melting transition between $T = -120^{\circ}\text{C}$ and $+80^{\circ}\text{C}$ [Lindsey et al., 1979], the possibility for local crystallization of alkyl chains can be excluded. As shown in Figure 3.3, the monolayer transferred at “standard” conditions (i.e., a transfer velocity of $50\ \mu\text{ms}^{-1}$, a transfer pressure of $30\ \text{mNm}^{-1}$, and a temperature of 20°C) forms almost an identical stripe micropattern as those presented in Figure 3.9 of Section 3.4.1. There, a mixture of the same molar ratio of lipopolymers with distearoyl alkyl chains and SOPC phospholipid was used.

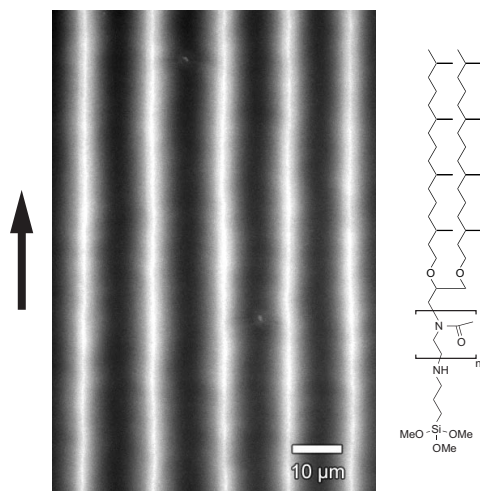


Figure 3.3: Fluorescence image of a lipid/lipopolymer monolayer containing 94.8 mol% DPhPC, 0.2 mol% Texas Red-PE, and 5 mol% DPh-PMO_x₂₁-Si. The monolayer was prepared at the same conditions as those in Figure 3.9. The arrow denotes the direction of film transfer.

Although the contrast in fluorescence intensity and the branching of the stripes seem slightly different, the characteristic distance between the neighboring stripes was $13.5\ \mu\text{m}$, which is in the same order of that in Figure 3.9.

Therefore, one can conclude that the pattern formation is not caused by local condensation of alkyl chains, but is dominated by the dissipation of polymer head groups during the transfer.

3.3.2 Influence of the Polymer Chain

Another component of the LB monolayer is the lipopolymer itself. Therefore, the influence of the “standard” polymer DS-PMO_{x_n}-Si was investigated. Here, different targets were approached:

- Changing the degree of polymerization n of DS-PMO_{x_n}-Si to see the influence of the size of the polymer. This should lead to an increased viscosity with increasing n within the vicinity of the three phase contact line between substrate and Langmuir monolayer.
- Using lipopolymers with different polymer side chains. For this, the lipopolymer was exchanged to poly(2-ethyl-2-oxazoline) (DS-PEO_{x_n}-Si).
- To see the influence of the surface coupling group, lipopolymers with piperidin termination instead of trimethoxysilane were applied.
- Also experiments with poly(ethylene glycol) (PEG) lipopolymers as substitute to DS-PMO_{x_n}-Si were performed.

This work will be presented in the following parts.

Polymer Chain Length

First, the influence of the polymer chain length on the stripe pattern formation was studied. Figure 3.4 presents the fluorescence images of transferred monolayers containing 5 mol% of lipopolymers with different degrees of polymerization, $n = 14, 33,$ and $104,$ respectively. Since the other preparation conditions are set constant (i.e., the transfer velocity of $50 \mu\text{ms}^{-1}$ and the transfer pressure of 30mNm^{-1}), the dynamics of film dissipation is supposed to be dominated by the frictional coupling between the film and the substrate. As seen in the figures, the increase in the polymer chain length leads to the transformation of individually separated “stripes“ (DS-PMO_{x₁₄}-Si, Figure 3.4(a)) into branched stripes (DS-PMO_{x₃₃}-Si, Figure 3.4(b)), which further results in the reduced contrast in the fluorescence intensity (DS-PMO_{x₁₀₄}-Si, Figure 3.4(c)). Nevertheless, it should be noted that the mean distance between the fluorescent patterns does not show a clear dependence on polymer chain length, but remains the same within the experimental error ($d_{space} = 13.7 \mu\text{m}$ for DS-PMO_{x₁₄}-Si, $15.1 \mu\text{m}$ for DS-PMO_{x₃₃}-Si, and $14.9 \mu\text{m}$ for DS-PMO_{x₁₀₄}-Si). The observed tendency thus denotes that the increase in the apparent chain viscosity due to the elongation of polymer chains causes the branching of the stripes and reduces the contrast in phase separation; however, it does not influence the spacing between the

neighboring stripes.

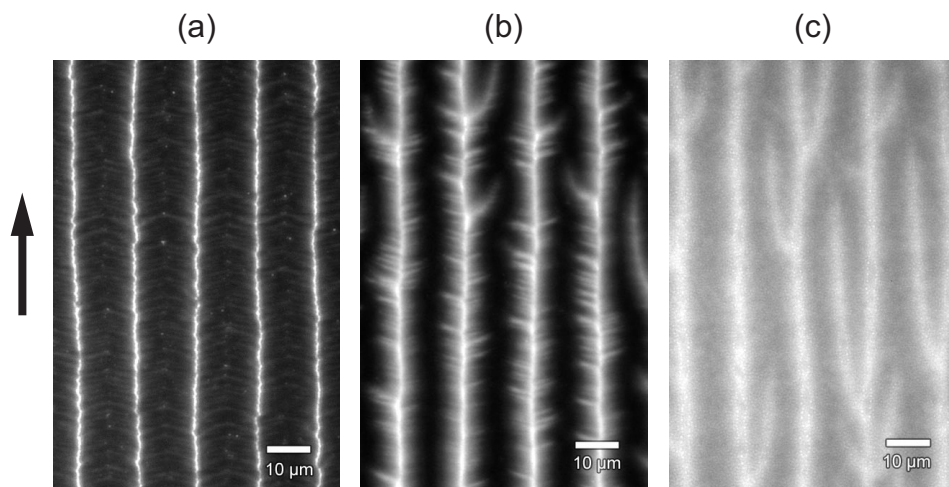


Figure 3.4: Fluorescence images of mixed monolayers containing lipopolymers with different monomer numbers, (a) $n = 14$ (DS-PMO_{x14}-Si), (b) $n = 33$ (DS-PMO_{x33}-Si), and (c) $n = 104$ (DS-PMO_{x104}-Si). The molar fraction of lipopolymer (5 mol%), the transfer pressure (30 mNm^{-1}), and the transfer velocity ($50 \mu\text{ms}^{-1}$) are set constant in order to highlight the influence of the length of polymer chains on the stripe micropatterns. The arrow denotes the direction of film transfer.

Polymer Side Chain

To exclude the origin of pattern formation by polymer crystallization, experiments with poly(2-ethyl-2-oxazoline) instead of poly(2-methyl-2-oxazoline) lipopolymers were performed. It is known that ethyl-oxazoline is the only 2-alkyl-2-oxazoline that exhibits no crystalline phase but is just amorphous [Bassiri et al., 1967, Litt et al., 1969]. Therefore, experiments with poly(2-ethyl-2-oxazoline) lipopolymers were performed (Figure 3.5). LB monolayers prepared at the same conditions than before exhibited similar stripe micropatterns compared to findings with DS-PMO_{xn}-Si lipopolymers. Also the increased tendency for branching of stripes with increased length of the lipopolymer can be observed, when increasing n from 10 to 19 (Figure 3.5(b)). Due to this fact, pattern formation on the basis of polymer crystallization can be excluded.

Surface Coupling Group

To see the influence of the lipopolymer surface coupling group on pattern formation, the trimethoxysilane end termination was exchanged by piperidin. This has no binding group for covalent coupling to surfaces. In Figure 3.6, a LB monolayer composed of 10 mol% Ph-PMO_{x12}-Pip, 89.8 mol% DPhPC, and 0.2 mol% Texas Red-PE

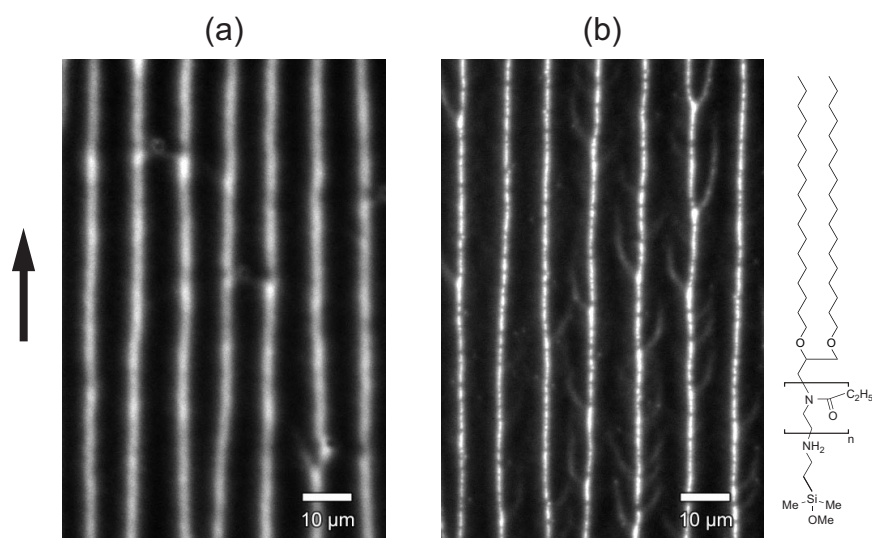


Figure 3.5: Representative fluorescence images of lipid/lipopolymer monolayers, containing 94.8 mol% SOPC, 0.2 mol% Texas Red-PE, and (a) 5 mol% DS-PEO_{x10}-Si or (b) 5 mol% DS-PEO_{x19}-Si. The monolayers were transferred at a velocity of $50 \mu\text{ms}^{-1}$, a surface pressure of 30mNm^{-1} , and at $T = 20^\circ\text{C}$.

is illustrated. It is clearly visible that even without a covalent fixation micropatterns are obtained similar to that of DS-PMO_{xn}-Si containing monolayers. Therefore, the surface coupling group, i.e. the end termination of the polymer, plays no dominant role in the pattern formation process.

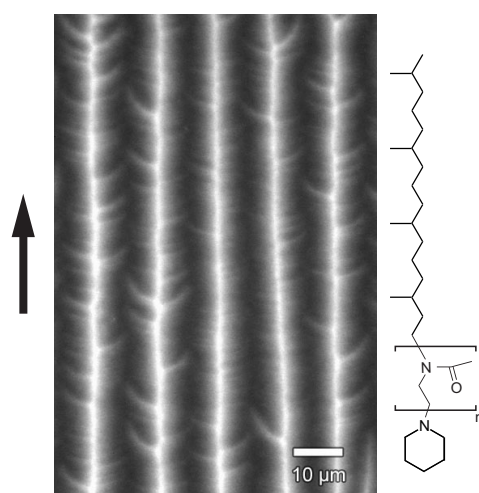


Figure 3.6: Fluorescence image of a LB monolayer composed of 10 mol% Ph-PMO_{x12}-Pip, 89.8 mol% DPhPC, and 0.2 mol% Texas Red-PE. The monolayer was transferred at a velocity of $50 \mu\text{ms}^{-1}$, a surface pressure of 30mNm^{-1} , and at $T = 20^\circ\text{C}$.

Poly(Ethylene Glycol)

To test the effect of the polymer part of the lipopolymer on pattern formation, poly(ethylene glycol) (PEG) lipopolymers purchased from Avanti Polar Lipids (Alabaster, USA) were used. They bear a dioleoyl lipid moiety and a methyl group as end termination (DOPE-PEG2000). Figure 3.7 illustrates a LB monolayer composed of 5 mol% DOPE-PEG2000, 94.8 mol% SOPC, and 0.2 mol% Texas Red-PE. The transfer conditions were the same as before. This image exhibits also some patterns, aligned roughly parallel to the transfer direction. Nevertheless, distinct stripe patterns are not visible. Assuming the lipopolymer as one side grafted random coil, the Flory radius of DOPE-PEG2000 is $R_F = 3.8$ nm [Marsh et al., 2003]. This is quite close to the Flory radius of DS-PMOx₁₀₄-Si of $R_F = 4.8$ nm (see Section 2.8). Since also with this poly(oxazoline) lipopolymer the fluorescence appeared rather “smeared out” (see Section 3.3.2), the increased frictional coupling to the substrate in comparison to the shorter lipopolymers seems to play a dominant role. But parallel stripe pattern formation can be assumed to be special for poly(oxazoline)/lipid LB monolayers.

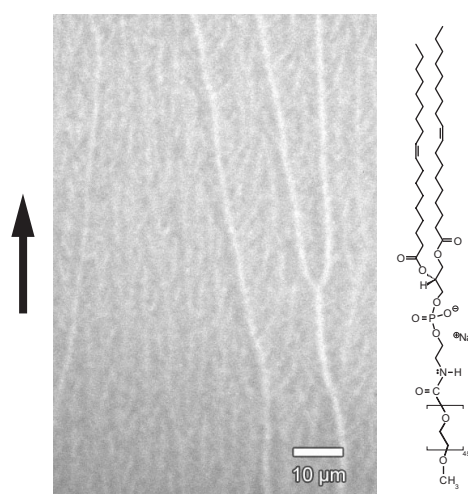


Figure 3.7: Fluorescence image of a LB monolayer composed of 5 mol% DOPE-PEG2000, 94.8 mol% SOPC, and 0.2 mol% Texas Red-PE. The transfer was carried out at a velocity of $50 \mu\text{ms}^{-1}$, a surface pressure of 30 mNm^{-1} , and at $T = 20^\circ\text{C}$.

3.4 Influence of Preparation Conditions on Pattern Formation

3.4.1 Influence of Transfer Velocity

Figure 3.9 represents the fluorescence images (upper row) and the normalized fluorescence intensity (lower row) of stripe micropatterns formed in lipid (SOPC)/lipopolymer (DS-PMO_{x14}-Si) monolayers doped with 0.2 mol% of Texas Red-PE, deposited at 50, 80, 180, and 500 μms^{-1} . The mixed monolayer, which was initially homogeneous at the air/water interface without phase separation at $\Pi > 0 \text{ mNm}^{-1}$ (see Section 3.2), formed stripe micropatterns parallel to the transfer direction (as indicated by an arrow). By increasing the transfer velocity from 50 μms^{-1} (Figure 3.9(a)) to 80 μms^{-1} (Figure 3.9(b)), the mean distance between individual stripes decreased: $d_{\text{space}} = 13.7 \mu\text{m}$ (50 μms^{-1}), and 7.2 μm (80 μms^{-1}). Further increase in the transfer velocity (180 μms^{-1} , Figure 3.9(c)) led to a branching of stripe patterns and the decrease in the mean distance between the stripes ($d_{\text{space}} = 3.4 \mu\text{m}$), followed by a reduced contrast in fluorescence intensity. At the maximum transfer velocity of the setup (500 μms^{-1} , Figure 3.9(d)), the structures totally vanish up to optical resolution, resulting in a homogeneous fluorescence image. Figure 3.8 illustrates the obtained mean distance d_{space} versus the corresponding transfer velocity v . The dependency seems to obey a power law $\sim v^{-1}$, but further data have to be evaluated.

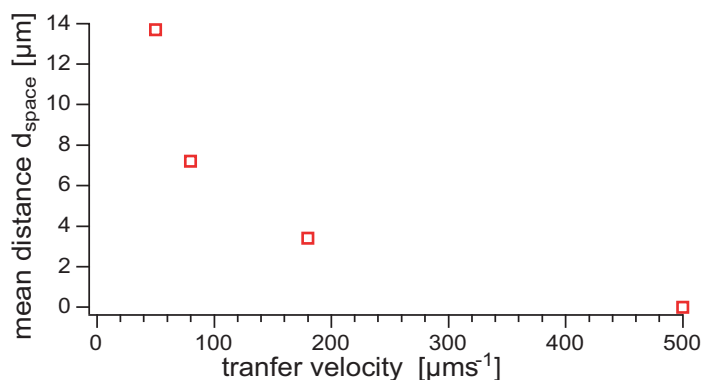


Figure 3.8: Mean distance d_{space} plotted versus the transfer velocity.

It should be noted that the transfer ratio of the film, i.e., the decrease in the subphase area divided by the area of the substrate, remains 100% within the experimental error ($\pm 5\%$), confirming that there is no loss of material through the transfer. Thus, the clear tendency observed here denotes that the hydrodynamic flow of water near the meniscus significantly influences the formation of stripe micropatterns.

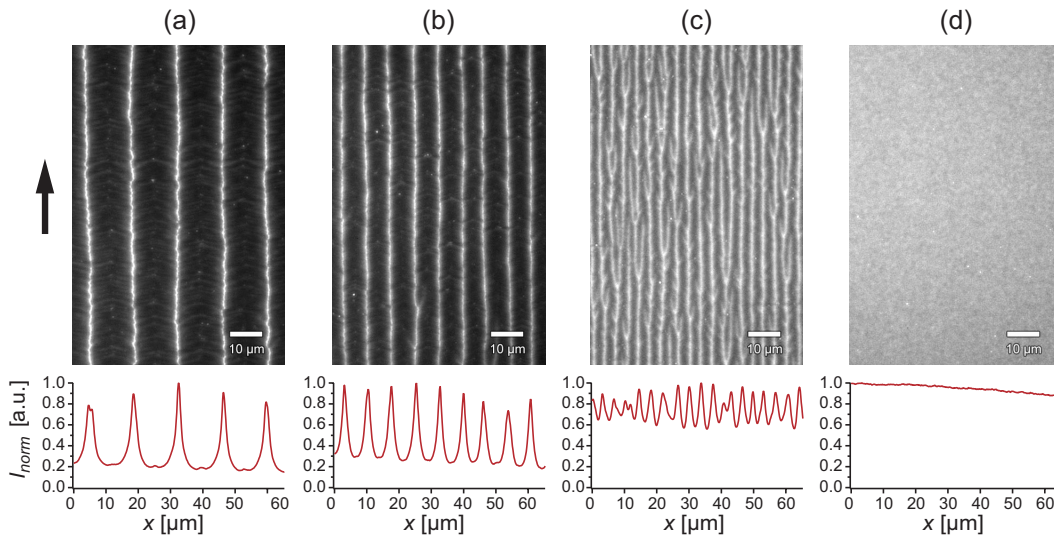


Figure 3.9: Upper row: Representative fluorescence images of lipid/lipopolymer monolayers on an arbitrary position, containing 94.8 mol% SOPC, 5 mol% DS-PMO_{x14}-Si, and 0.2 mol% Texas Red-PE. The monolayers were transferred at velocities of (a) $50 \mu\text{ms}^{-1}$, (b) $80 \mu\text{ms}^{-1}$, (c) $180 \mu\text{ms}^{-1}$, and (d) $500 \mu\text{ms}^{-1}$. The arrow denotes the direction of film transfer. Lower row: Plots of the normalized fluorescence intensity I_{norm} of the horizontal cross section, averaged vertically over the whole image.

3.4.2 Influence of Subphase Viscosity

Another parameter to tune the dissipation of the film is the viscosity within the vicinity of the three phase contact line between substrate and Langmuir monolayer. This can be achieved by increasing the viscosity by exchanging the water subphase with a glycerol/water mixture.

The subphase viscosity was raised by addition of glycerol to the water. Here, the viscosity was changed from 1 mPa s (pure water) to 6.0 mPa s for a 50 wt% glycerol, 50 wt% water mixture [Wohlfarth & Wohlfarth, 2001]. Taking the same conditions as in Figure 3.9(a) but changing the subphase viscosity as mentioned before, stripe micropatterns vanished nearly totally (Figure 3.10(a)). Going to higher transfer velocities ($v = 180 \mu\text{ms}^{-1}$), as in Figure 3.9(c), a homogeneous fluorescence appeared, where no stripe micropatterns were visible within the optical resolution (Figure 3.10(b)). Both results demonstrate that the frictional coupling between substrate and LB monolayer plays a dominant role on the pattern formation process, which requires further investigations to get more insight into the mechanisms acting in the vicinity of the meniscus.

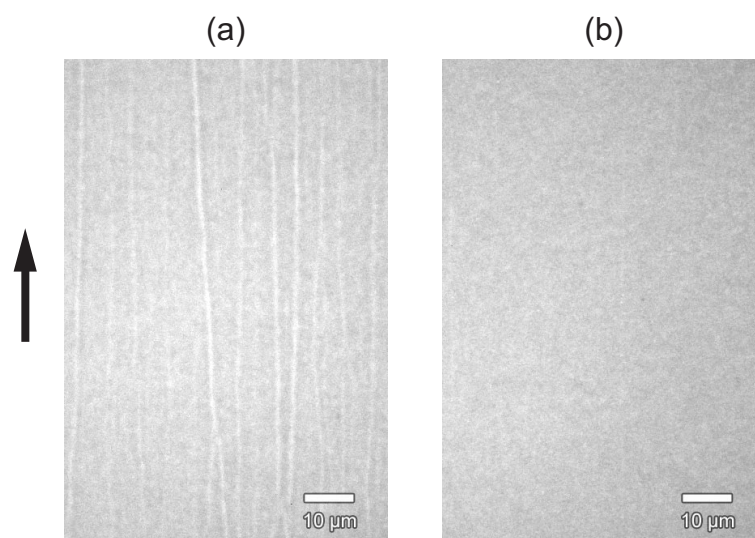


Figure 3.10: Representative fluorescence images of lipid/lipopolymer monolayers, containing 94.8 mol% SOPC, 5 mol% DS-PMO_{x14}-Si, and 0.2 mol% Texas Red-PE. The monolayers were transferred at a velocity of (a) $50 \mu\text{ms}^{-1}$ and (b) $180 \mu\text{ms}^{-1}$, a surface pressure of 30 mNm^{-1} , and at $T = 20^\circ\text{C}$. As subphase, a 50 wt% glycerol, 50 wt% water mixture with a viscosity of 6.0 mPas was used.

3.5 Confirmation of Demixing of Lipid/Lipopolymer LB Monolayers

To verify that stripe micropatterns are formed due to demixing of lipids and lipopolymers but not due to the segregation of fluorescence lipids, a monolayer doped with NBD labelled lipids (NBD-PE) and TRITC labelled lipopolymers (DS-PMO_{x13}-TRITC) was prepared. By using suitable filter sets, the fluorescence signals from each label could be monitored individually at the same region of the mixed monolayer.

As presented in Figure 3.11 (upper left and right panels), stripe-like patterns can be observed for both labels. The overlay of two images at the same region (Figure 3.11, upper middle panel, in false color) exhibits the alternative stripes of lipids and lipopolymers, suggesting the demixing of two species. Actually, in the averaged cross-sectional intensity profiles (Figure 3.11, lower panel), the maximum intensity of one label clearly matches to the minimum of the other dye. Although the fluorescence labelling experiments carried out here do not allow to determine whether the lipids and lipopolymers are completely demixed or not, the selective labelling of two components postulates that the dynamic phase separation of lipids and lipopolymers results in the formation of dissipative micropatterns of alternating lipopolymer-rich and lipid-rich domains.

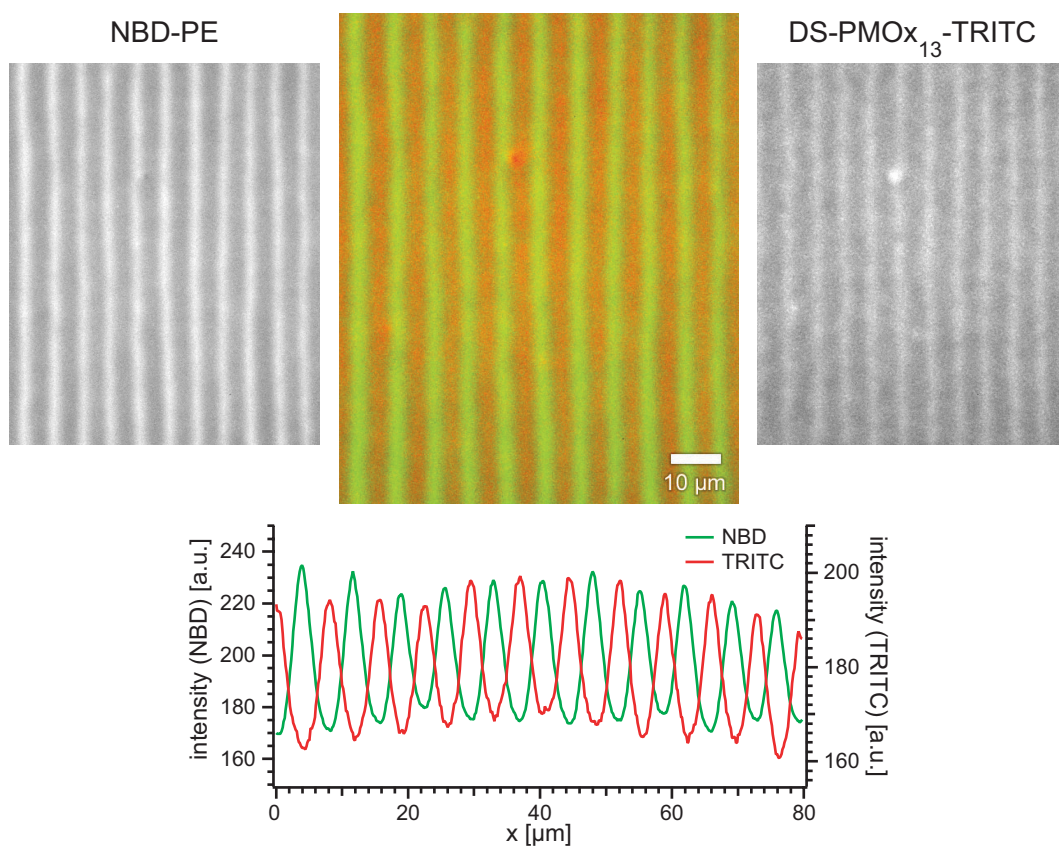


Figure 3.11: Fluorescence images of a mixed monolayer containing 0.2 mol% DS-PMO_{x13}-TRITC, 4.8 mol% DS-PMO_{x18}-Si, 94 mol% SOPC, and 1 mol% NBD-PE. The images from the NBD filter (upper left) and from the TRITC filter (upper right) were taken at the same region of the monolayer. The overlay of these two images in false color (upper middle) suggests the demixing of two species, which is confirmed by the horizontal cross section of fluorescence intensities, averaged vertically over the whole images taken with NBD or TRITC filters (lower panel).

3.6 Mechanisms of Micropattern Formation

The stripe patterns with periodicities of μm range are continuous up to cm length scale, coating the entire substrate without topographic defects (Figure 3.1, Section 3.1). As demonstrated in Figure 3.11 (Section 3.5), the stripes coincide with the demixing of lipids and lipopolymers during the film deposition. All of them are aligned perpendicular to the meniscus, whose spacing can flexibly be tuned by the transfer velocity (Figure 3.9, Section 3.4.1). This tendency suggests that the dominant role of the speed of water drainage in determination of stripe periodicity.

To adjust the frictional coupling between the surfactant head groups (i.e, phosphocholine head groups and polymer chains) and the solid substrate, two physical parameters are altered. The increase in the polymer viscosity as a result of chain elongation leads to the branching of the stripes and reduction in the pattern contrast (Figure 3.4, Section 3.3.2). On the other hand, the stripe patterns almost disappeared at an increased subphase viscosity (Figure 3.10, Section 3.4.2). The experimental results obtained here suggest a different mechanism of the pattern formation from the other stripe defects/patterns reported previously. For example, the striped defects aligned parallel to the meniscus in a single component lipid monolayer are found when films are transferred at the coexistence of the liquid-expanded (LE) and liquid-condensed (LC) phase [Spratte et al., 1994, Yaminski et al., 1997, Gleiche et al., 2000, Kovalchuk et al., 2003]. The mechanism of pattern formation has been attributed to the fluctuation of the meniscus during the fast film transfer.

Recently, Lenhert et al. [Lenhert et al., 2004] reported that the stripes aligned perpendicular to the meniscus can be formed when a phospholipid monolayer was transferred at a certain surface pressure ($\Pi = 5 \text{ mNm}^{-1}$). However, the mechanism of pattern formation is hardly understood, although a transition from the parallel aligned stripes to the perpendicularly oriented ones could be observed at around $\Pi = 3.5 \text{ mNm}^{-1}$. On the contrary, the mixed monolayers studied here are transferred at a high surface pressure ($\Pi = 30 \text{ mNm}^{-1}$), corresponding to the mean area per molecule of about 55 \AA^2 . This value suggests that the fluid alkyl chains have no free voids to create defects. In fact, the tapping mode AFM experiments show no sign of topographic defects [Förtig, T., personal communication], which agrees very well with the obtained transfer ratio of $\sim 100\%$.

It should be noted that the pattern formation does not depend upon the crystallization of alkyl chains. The result presented in Figure 3.3 (Section 3.3.1) clearly excludes the possible contribution of phase separation due to hydrophobic mismatch,

since the diphytanoyl chains of DPh-PMOx₂₁-Si and DPhPC have no chain melting transition between $T = -120^\circ\text{C}$ and $+80^\circ\text{C}$. This is in clear contrast to the recent paper by Pignataro et al. [Pignataro et al., 2002], reporting the formation of perpendicularly aligned stripe defects in a “frozen” DMPC monolayer transferred at 10°C and $\Pi = 30 \text{ mNm}^{-1}$. On the other hand, the other types of stripe nanopatterns were found in lipid monolayers with clear hydrophobic mismatches, i.e. the alkyl chains of two lipids are immiscible [Solletti et al., 1996, Moraille & Badia, 2002]. Here, the formation of the stripes aligned parallel to the meniscus are interpreted in terms of the fluctuation in molecular packing at the coexistence of lipids in LE and LC phases. This scenario does not seem to hold in our experimental systems, because the mixed monolayers of lipids and lipopolymers show no sign of phase separation at the air/water interface up to $\Pi = 40 \text{ mNm}^{-1}$ (Section 3.2). Moreover, the experiments with diphytanoyl lipid anchors (Figure 3.3) clearly exclude this scenario.

Furthermore, the origin of pattern formation by polymer crystallization can also be excluded, since experiments with poly(2-ethyl-2-oxazoline) instead of poly(2-methyl-2-oxazoline) lipopolymers exhibited similar stripe micropatterns. Therefore, even the amorphous phase of poly(2-ethyl-2-oxazoline) [Bassiri et al., 1967, Litt et al., 1969] does not prevent pattern formation. Also the influence of the surface coupling group of the lipopolymer was tested (Figure 3.6). There, the used trimethoxysilane was exchanged by a piperidin group. Similar dissipative structures were observed. Hence, the covalent fixation of the monolayer plays no dominant role in the pattern formation process.

At present, the exact mechanism of the pattern formation still remains unclear. The instabilities in mixtures of liquids with different viscosities and surface tensions are formed according to the concentration gradient created by evaporation of one component [Vuilleumier et al., 1995, Fanton & Cazabat, 1998], or by chemical reactions [Dalle Vedove & Sanfeld, 1981], which can be referred as *solutal Marangoni* effects. However, the concentration of lipids and lipopolymers should be constant, since the average area per molecule and therefore, the surface tension are kept constant. This enables us to conclude that our experimental systems cannot be treated within the Marangoni-Bénard instability.

On the other hand, the successful deposition of all the films (transfer ratio of $\sim 100\%$) confirms that the transfer velocities chosen in this study remain smaller than the maximum transfer velocity v_{max} predicted by the lubrication theorem

[de Gennes, 1986],

$$v_{max} \propto \frac{\gamma\theta^3}{\eta} . \quad (3.1)$$

θ is the contact angle at the meniscus, η is the dynamic viscosity of the subphase liquid. γ is the surface tension ($\gamma = \gamma_0 - \Pi$), corresponding to the difference between the surface tension of solvent γ and the surface pressure Π at which the deposition takes place. As experimentally demonstrated by Petrov et al. [Petrov et al., 1980], v_{max} depends upon the short range intermolecular forces. The cooperative substrate-monolayer attraction can be referred as a “surface reactivity”, where the “binding energy” between the substrate and the transferred film corresponds to the energy of head group hydration. As the poly(oxazoline) chains are highly hygroscopic [Rehfeldt et al., 2002], one can assume a contrast in hydration forces operated within the polymer head groups and those within phospholipids head groups.

3.7 Confinement of Transmembrane Cell Receptors into Micropatterns

Natural plasma membranes do not only possess intrinsically asymmetric distribution of lipids in their cytoplasmic and extracellular leaflets, but also form laterally organized functional micro-domains enriched with certain types of lipids and proteins. These domains, such as well known “lipid rafts” [Simons & Ikonen, 1997], are postulated to govern complex cellular functions like endocytic traffic, signal transduction, and apoptosis. Furthermore, dynamic accumulation of ligand-receptor pairs plays an important role in cell adhesion (such as extravasations of leukocytes into tissues at inflammation sites) in order to establish a firm adhesion [Springer, 1995].

In contrast to the geometric control of cellular activities achieved by soft lithography [Chen et al., 1997], the tunable stripe patterns were utilized here as self-assembled templates to confine cell receptor proteins. Owing to the covalent coupling of silane groups to a glass surface, the transferred lipid/lipopolymer monolayer studied here can be used as a spacer to separate a lipid membrane and a substrate. Here, a spacer length of $n=33$ was chosen to selectively accommodate integrins. When

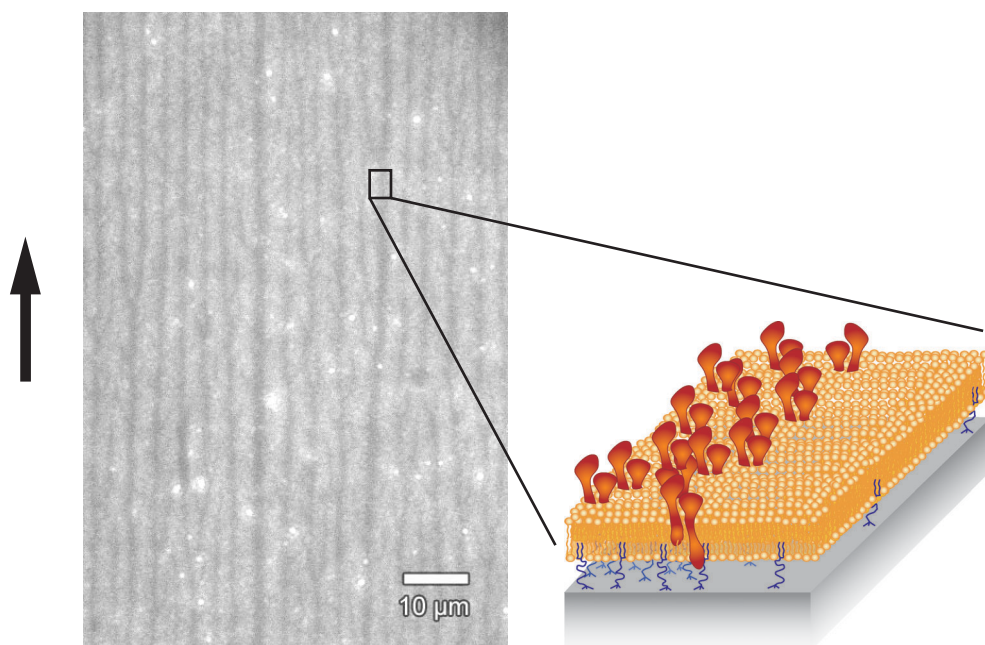


Figure 3.12: Fluorescence image of a lipid membrane containing fluorescently labelled transmembrane cell receptors integrin $\alpha_{\text{IIb}}\beta_3$. The proximal LB monolayer was composed of 10 mol% DS-PMO_{x33}-Si and 90 mol% SOPC, which was prepared at $v = 50 \mu\text{ms}^{-1}$, $\Pi = 30 \text{ mNm}^{-1}$, and $T = 20^\circ\text{C}$. The distal monolayer was prepared by fusion of proteoliposomes containing labelled integrin $\alpha_{\text{IIb}}\beta_3$ and SOPC/SOPG matrix lipids.

proteoliposomes with fluorescently labelled integrin $\alpha_{\text{IIb}}\beta_3$ were incubated on a patterned monolayer consisting of 10 mol% DS-PMO_{x33}-Si and 90 mol% SOPC (analog to Section 2.5), proteins are preferably incorporated into the lipopolymer-rich region (Figure 3.12). As demonstrated in Section 3.4.1, the periodicity of the stripe patterns can be adjusted in the range of 1 - 15 μm , suggesting a large potential of the tunable stripes of receptors for the control of cellular functions via geometry of protein patterns.

3.8 Conclusion

In this chapter, a new class of stripe micropatterns formed in transferred lipid/lipopolymer monolayers is reported, whose width and spacing was tunable by physical parameters. In contrast to the other stripe-like patterns of lipid monolayers, the isolated stripes with the spacing in the μm range are found to be always parallel to the transfer direction in a macroscopic length scale (cm scale), exhibiting no remarkable defects. Fluorescence labelling of lipopolymer headgroups further confirmed the separation of lipids and lipopolymers through the transfer. The observed results systematically demonstrate that the stripe micropatterns are formed by the dissipation of polymer chains in the vicinity of the three phase contact line. Since the spacing between the neighboring stripes shows a clear dependence on the transfer velocity, such a structure formation seems to be determined by the forces exerted from the thinning of the “swollen“ headgroup region (e.g. capillary forces, tension induced by distortion of polymer chains, etc.) [Debrégeas et al., 1995, Reiter, 2002].

In contrast to other stripe-like patterns of surfactants [Moraille & Badia, 2003, Lenhart et al., 2004], the structures are not physisorbed but covalently bound to the substrate through a silane anchoring group. After fusion of liposomes with the preformed LB monolayer, these microstripes are stable under water and can therefore serve as a lipid membrane platform with biological interest. Transmembrane cell receptors integrin $\alpha_{\text{IIb}}\beta_3$ were selectively incorporated into the lipopolymer-rich region, which includes a large potential towards the confinement of various transmembrane proteins in quasi two-dimensional stripe micropatterns with thickness in the nm range.

3.9 Outlook

One of the possible experimental approaches to quantify the forces within the thin surfactant films would be the measurement of the local film thickness near the meniscus [Elender & Sackmann, 1994, Langevin, 1998] to determine the “critical thickness” [Debrégeas et al., 1995] at which the film dissipation (or dewetting) takes place. This can be achieved by coupling a Langmuir film balance to an imaging ellipsometer, which realizes nm accuracy in thickness and μm resolution in lateral dimensions (Figure 3.13).

The lipid/lipopolymer monolayer can be transferred onto a solid substrate and the local thickness distribution can be monitored in parallel.

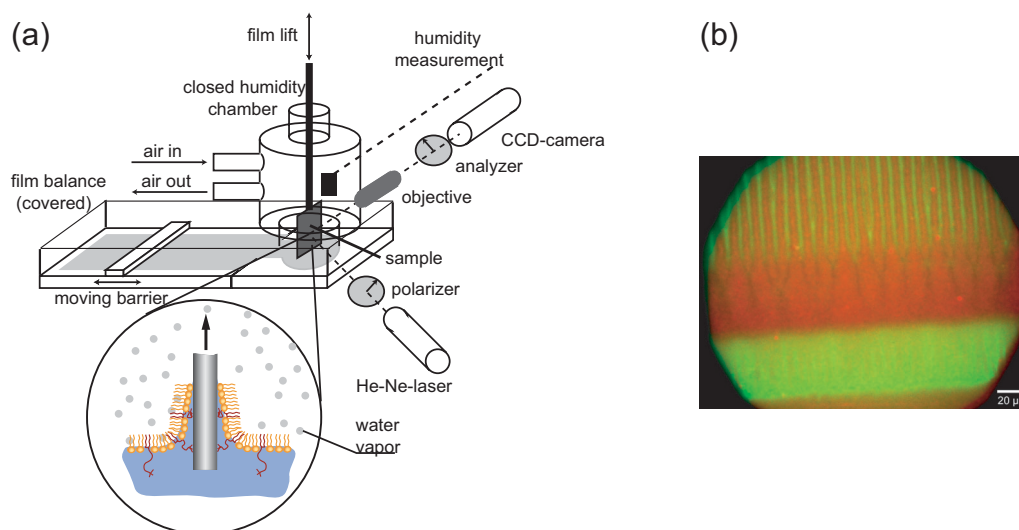


Figure 3.13: (a) Sketch of a Langmuir film balance coupled to an imaging ellipsometer. With this setup, the local film thickness near the meniscus can be evaluated. (b) Fluorescence images of a LB monolayer containing 0.2 mol% DS-PMO_{x13}-TRITC, 4.8 mol% DS-PMO_{x18}-Si, 94 mol% SOPC, and 1 mol% NBD-PE. The images from NBD and TRITC filters were overlaid and presented in false color. In the middle of the illustrated substrate region, the constant film transfer was stopped. By lowering the meniscus to its equilibrium state, lipids were accumulated at the bottom region (green label), where lipopolymers were fixed to the substrate (red label).

Another task is the application of the micropatterns in 2D electrophoresis of transmembrane proteins. By using an electric field, incorporated proteins can be transported in the direction along the isolated μ -channels, but are prohibited to move across the channels (Figure 3.14).

Therefore, various incorporated proteins can be separated due to their isoelectric points. The proteins are in their native membrane environment, separated by the

lipopolymer tethers from the solid substrate. Hence, misfolding and denaturing is prohibited.

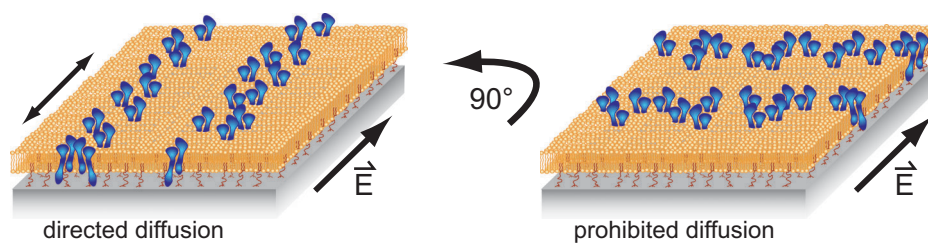


Figure 3.14: Sketch of transmembrane cell receptors confined into tuneable micropatterns. By applying an electrical field, the proteins can be driven along the stripes, but movement is prohibited perpendicular to the stripes.

A. Appendix

A.1 Estimation of Protein/Lipid Ratio in Proteoliposomes

For characterization of the membrane model system, the ratio between phospholipids and incorporated integrin $\alpha_{\text{IIB}}\beta_3$ in polymer-tethered membranes was estimated. This can be performed by measuring the lipid and protein concentration of proteoliposomes suspensions separately. Since these liposomes were spread onto LB monolayers of lipids and lipopolymers, the ratio of proteins/lipids within the supported membrane is the half of that estimated by the following procedure.

Two proteoliposome suspensions were characterized, one with DMPC/DMPG matrix lipids (called *D-liposomes* further one), and one with SOPC/SOPG matrix lipids (called *S-liposomes* in the following).

Quantitative Determination of the Integrin Concentration

Following the method reported by Bradford [Bradford, 1976], the concentration of proteins was determined with an adsorption technique. By binding a specific dye to proteins, here Coomassie Brilliant Blue G-250 (Sigma-Aldrich, Munich, Germany), the absorption maximum of the dye shifts from 465 to 595 nm.

20 μl of the sample volume was added to 980 μl of the protein reagent solution (0.01 % (w/v) dye, 4.7 % (w/v) ethanol and 8.5 % (w/v) phosphoric acid). The absorbance was measured at 595 nm in an UV-spectroscope and compared to a control sample (pure buffer with protein reagent), yielding an absolute protein concentration of ~ 41 nM (D-liposome suspension) and ~ 46 nM (S-liposome suspension), respectively.

Quantitative Determination of the Phosphate Concentration

Since each phospholipid has one phosphate group, the molar content of phosphate in the sample can be determined and equated with the molar lipid content. The phosphate content of proteins is negligibly small. The determination is done

according to the method reported by Fiske and Subbarow [Fiske & Subbarow, 1925] and Bartlett [Bartlett, 1958].

Ammonium-molybdate is reduced by phosphate and leads to an increase in light absorption at 797 nm. The adsorption is linearly dependent on the amount of reduced ammonium-molybdate, which is proportional to the amount of phosphate present in the sample. The method is shown to be reliable for concentrations of phosphate from 0.02 μM to 1 mM.

The phosphate analysis was performed with reference solutions in order to calibrate the measured absorbance to molar contents, with a dilution series of a 1 mM KH_2PO_4 to 0 mM, 0.05 mM, 0.1 mM, 0.2 mM, 0.6 mM, and 1 mM of phosphate. The different liquids were pipetted into test tubes and heated to 180 °C for 5 min to evaporate the liquid. Successively 0.3 ml perchloric acid (HClO_4 , 70%, Sigma-Aldrich, Munich, Germany) was added to each tube. All tubes - closed with a marble to prevent evaporation - were kept at 180 °C for 2 h. After the samples have cooled to room temperature, 1.4 ml H_2O and 0.2 ml NH_4 -molybdate of a 2.5 % stock solution was added (0.3 wt.% NH_4 -molybdate in total). The solutions were then well mixed and 0.2 ml ascorbic acid solution of a freshly prepared 10 wt.% solution was added (1 wt.% ascorbic acid in total). By heating the test tubes to 100 °C for 6 min, a clear blue solution appears in the tubes where phosphate was present.

The absorbance for the different dilutions was measured in a 1 cm cuvette in an UV-spectroscopy (797 nm), which is proportional to the concentration of phosphate, as shown in Figure A.1. From this linear dependence, the phosphate concentration of the studied sample can be calculated. For the integrin vesicle solutions phosphate concentrations of $\sim 250 \mu\text{M}$ (D-liposome suspension) and $\sim 120 \mu\text{M}$ (S-liposome suspension) were determined.

In summary, *D-liposome* suspensions exhibited an integrin concentration of $\sim 41 \text{ nM}$ and a lipid concentration of $\sim 250 \mu\text{M}$, resulting in a molar ratio of integrin : lipids of **$\sim 1 : 6200$** .

The *S-liposome* suspensions exhibited an integrin concentration of $\sim 46 \text{ nM}$ and a lipid concentration of $\sim 120 \mu\text{M}$, resulting in a molar ratio of integrin : lipids of **$\sim 1 : 2600$** .

Since these proteoliposomes were spread onto LB monolayers of lipids and small fractions of lipopolymers, the amount of lipids per incorporated integrin double. Therefore, the ratio of incorporated proteins : lipids per area are $X_D = 1.61 \times 10^{-4}$ (from D-liposome suspensions) and accordingly $X_S = 3.85 \times 10^{-4}$ (from S-liposome

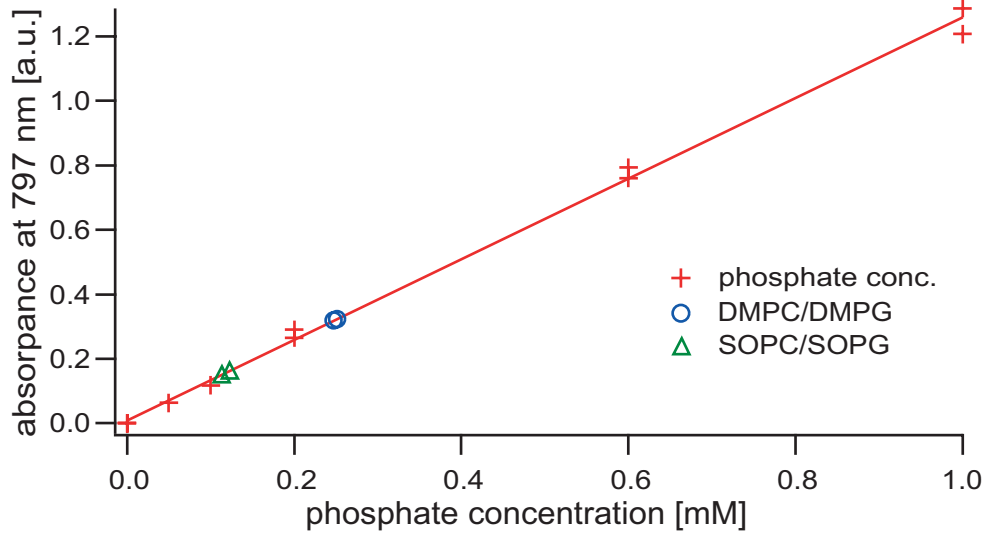


Figure A.1: The linear dependence of the light absorption at 797 nm to the phosphorus content is shown in the calibration curve. The circle markers are the absorbance of two DMPC/DMPG/intergrin proteoliposome samples, the triangle markers are the absorbance of two SOPC/SOPG/intergrin proteoliposomes samples.

suspensions).

The average distances between two incorporated integrins are $\mathbf{d_D} = \sqrt{A_l/X_D} \approx \mathbf{66\text{ nm}}$ (incorporated integrin from D-liposomes), and $\mathbf{d_S} = \sqrt{A_l/X_S} \approx \mathbf{43\text{ nm}}$ (incorporated integrin from S-liposomes), respectively, assuming an average area of $A_l \approx 0.7\text{ nm}^2$ per phospholipid in the fluid state [Marsh, 1990].

A.2 X-ray Scattering of Lipid/Lipopolymer Dispersions

To get more insight into the phase behavior of binary mixtures of lipids and poly(2-oxazoline) lipopolymers, small-angle and wide-angle X-ray scattering (SAXS, WAXS) measurements were carried out for dispersions of poly(2-methyl-2-oxazoline) lipopolymers with different degrees of polymerization (DS-PMO_{x14}-Si, DS-PMO_{x18}-Si, DS-PMO_{x33}-Si) and DSPC lipids in various molar ratios.

Figure A.2 illustrates SAXS/WAXS results of mixtures of 90 mol% DSPC and 10 mol% DS-PMO_{x14}-Si, DS-PMO_{x18}-Si, or DS-PMO_{x33}-Si, recorded at different temperatures.

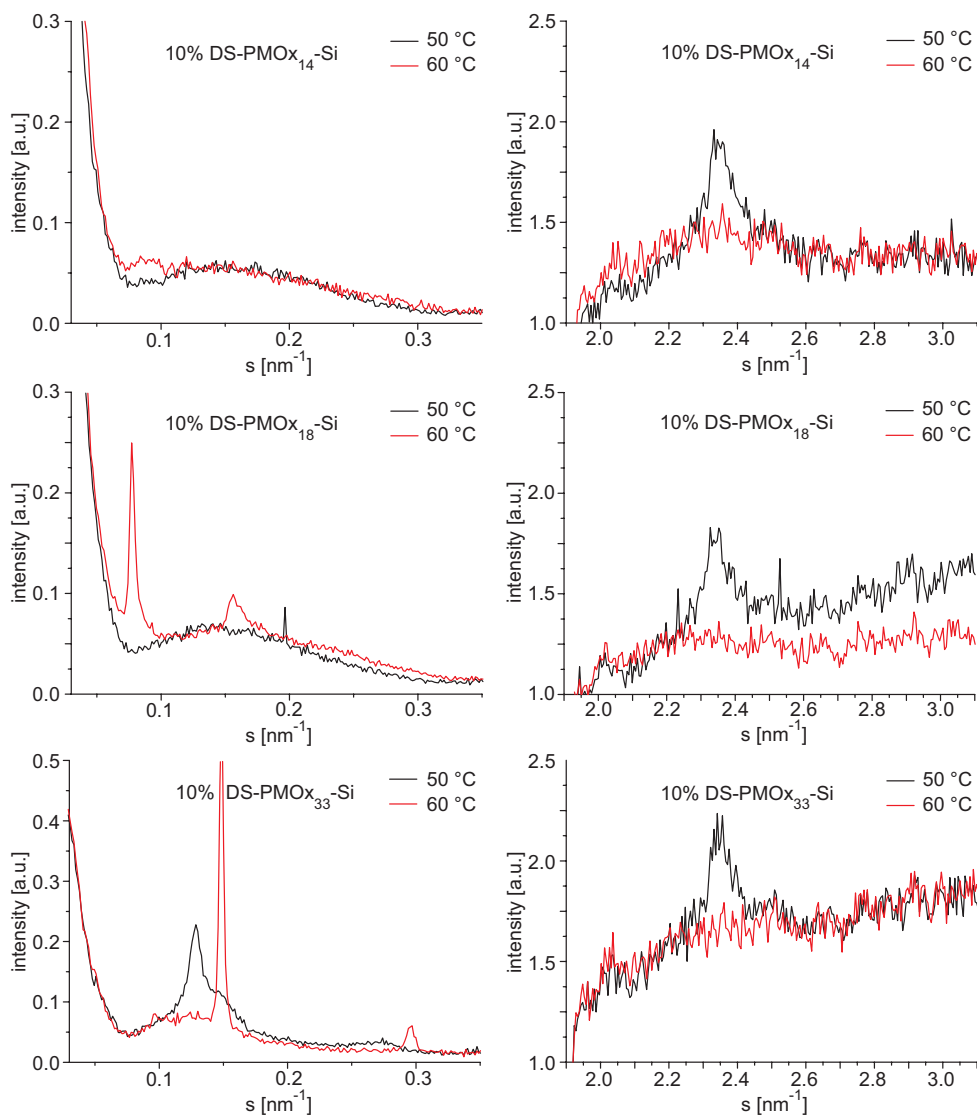


Figure A.2: SAXS (left side) and WAXS (right side) measurements of dispersions containing 90 mol% DSPC and 10 mol% DS-PMO_{x14}-Si, DS-PMO_{x18}-Si, or DS-PMO_{x33}-Si.

In the WAXS region, all samples exhibited a L_β to L_α phase transition at $T_m \sim 55^\circ\text{C}$, which is indicated by the disappearance of peaks ($s \sim 2.35 \text{ nm}^{-1}$, corresponding to $d \sim 0.43 \text{ nm}$)(see right side graphs of Figure A.2).

In the SAXS region, no long-range order of the phase could be determined for the shortest lipopolymer (DS-PMO_{x14}-Si), neither for temperatures below T_m , nor above. Only broad humps were present, with a maximum at $s \sim 0.152 \text{ nm}^{-1}$ (corresponding to $d \sim 6.6 \text{ nm}$ in real space) at temperatures below T_m .

For mixtures with slightly larger lipopolymers, DS-PMO_{x18}-Si (middle panels of Figure A.2), a similar hump for temperatures below chain melting was observed ($s \sim 0.147 \text{ nm}^{-1}$, corresponding to $d \sim 6.8 \text{ nm}$) At 60°C , two peaks were exhibited: $s_1 = 0.081 \text{ nm}^{-1}$, and $s_2 = 0.164 \text{ nm}^{-1}$ (corresponding to $d_1 = 12.3 \text{ nm}$, and $d_2 = 6.1 \text{ nm}$, respectively).

For lower temperatures (20°C to 40°C) and higher temperatures (70°C to 80°C), the results for DS-PMO_{x14}-Si and DS-PMO_{x18}-Si were similar to that obtained at 50°C , or accordingly 60°C .

The Dispersion of 10 mol% DS-PMO_{x33}-Si and 90 mol% DS-PC revealed a different behavior. For temperatures below chain melting, two Bragg peaks in close proximity were present in the SAXS spectra. Deconvolution of these Lorentzian peaks yielded the following values for s and d : $s_1 = 0.128 \text{ nm}^{-1}$, and $s_2 = 0.149 \text{ nm}^{-1}$, corresponding to $d_1 = 7.8 \text{ nm}$, and $d_2 = 6.7 \text{ nm}$, respectively. Increasing the temperature to 60°C , the peak at $s_1 = 0.128 \text{ nm}^{-1}$ disappeared, and a sharp peak at $s_1 = 0.148 \text{ nm}^{-1}$ ($d_1 = 6.7 \text{ nm}$) and a smaller at $s_2 = 0.300 \text{ nm}^{-1}$ ($d_2 = 3.4 \text{ nm}$) were visible.

To get some information about pure lipopolymer dispersion, measurements with 100 mol% DS-PMO_{x14}-Si, DS-PMO_{x18}-Si, and DS-PMO_{x33}-Si were carried out (Figure A.3). All samples exhibited no short-range order visible in the WAXS region, no melting of the alkyl chains could be observed.

Similar to the samples with 10 mol% lipopolymers, dispersions of 100 mol% DS-PMO_{x14}-Si showed just a broad hump at all temperatures, denoting also no long-range order for these kind of dispersions.

From the sample with 100 mol% DS-PMO_{x18}-Si, one distinct peak at $s_1 = 0.082 \text{ nm}^{-1}$ ($d_1 = 12.2 \text{ nm}$, 50°C), and at $s_1 = 0.083 \text{ nm}^{-1}$ ($d_1 = 12.1 \text{ nm}$, 60°C) was observable. The corresponding small humps were located at $s_2 \sim 0.141 \text{ nm}^{-1}$ ($d_2 = 7.1 \text{ nm}$, or $s_2 \sim 0.144 \text{ nm}^{-1}$ ($d_2 = 7.0 \text{ nm}$), respectively.

The dispersion of 100 mol% DS-PMO_{x33}-Si exhibited a similar behavior to DS-

PMO_x₁₈-Si, with one sharp peak at $s_1 = 0.084 \text{ nm}^{-1}$ ($d_1 = 11.9 \text{ nm}$, 50°C), and at $s_1 = 0.087 \text{ nm}^{-1}$ ($d_1 = 11.5 \text{ nm}$, 60°C), respectively. The small humps are located at $s_2 \sim 0.146 \text{ nm}^{-1}$ ($d_2 = 6.8 \text{ nm}$), or $s_2 \sim 0.150 \text{ nm}^{-1}$ ($d_2 = 6.7 \text{ nm}$) (60°C).

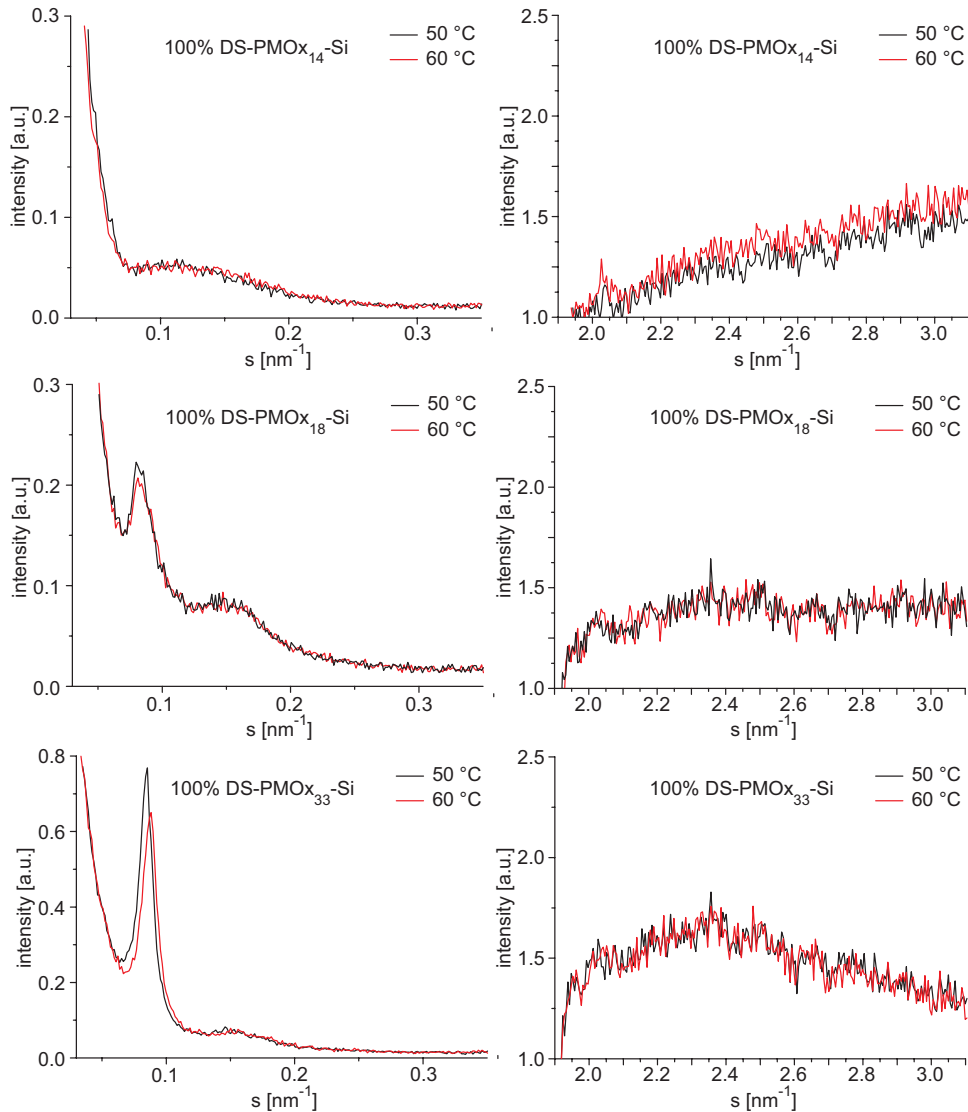


Figure A.3: SAXS (left side) and WAXS (right side) measurements of dispersions containing 100 mol% of DS-PMO_x₁₄-Si, DS-PMO_x₁₈-Si, or DS-PMO_x₃₃-Si.

Since the obtained results of the lipopolymer DS-PMO_x₁₄-Si exhibit no long-range order at any of the investigated temperatures, and DS-PMO_x₁₈-Si samples only show some distinct peaks above the chain melting temperature T_m , the focus will lie on dispersions with DS-PMO_x₃₃-Si lipopolymers.

In Figure A.4, SAXS results of lipid/lipopolymer dispersions are presented, where the ratio of DS-PMO_x₃₃-Si was varied between 0 and 100 mol%. Starting from the sample of pure DSPC lipid dispersion (left upper graph), one can observe two

distinct peaks $s_1 = 0.145 \text{ nm}^{-1}$ ($d_1 = 6.9 \text{ nm}$) and $s_2 = 0.290 \text{ nm}^{-1}$ ($d_2 = 3.4 \text{ nm}$) at 50°C , which change to sharp peaks at 60°C : $s_1 = 0.145 \text{ nm}^{-1}$ ($d_1 = 6.9 \text{ nm}$) and $s_2 = 0.288 \text{ nm}^{-1}$ ($d_2 = 3.4 \text{ nm}$). This results denote the lamellar L_β and L_α phase of DSPC lipid dispersions, where the peaks at s_2 are second order peaks of the lamellar stacks. The estimated distances between lamellae coincide with previous reports [Mattai et al., 1987, Cunningham et al., 1998].

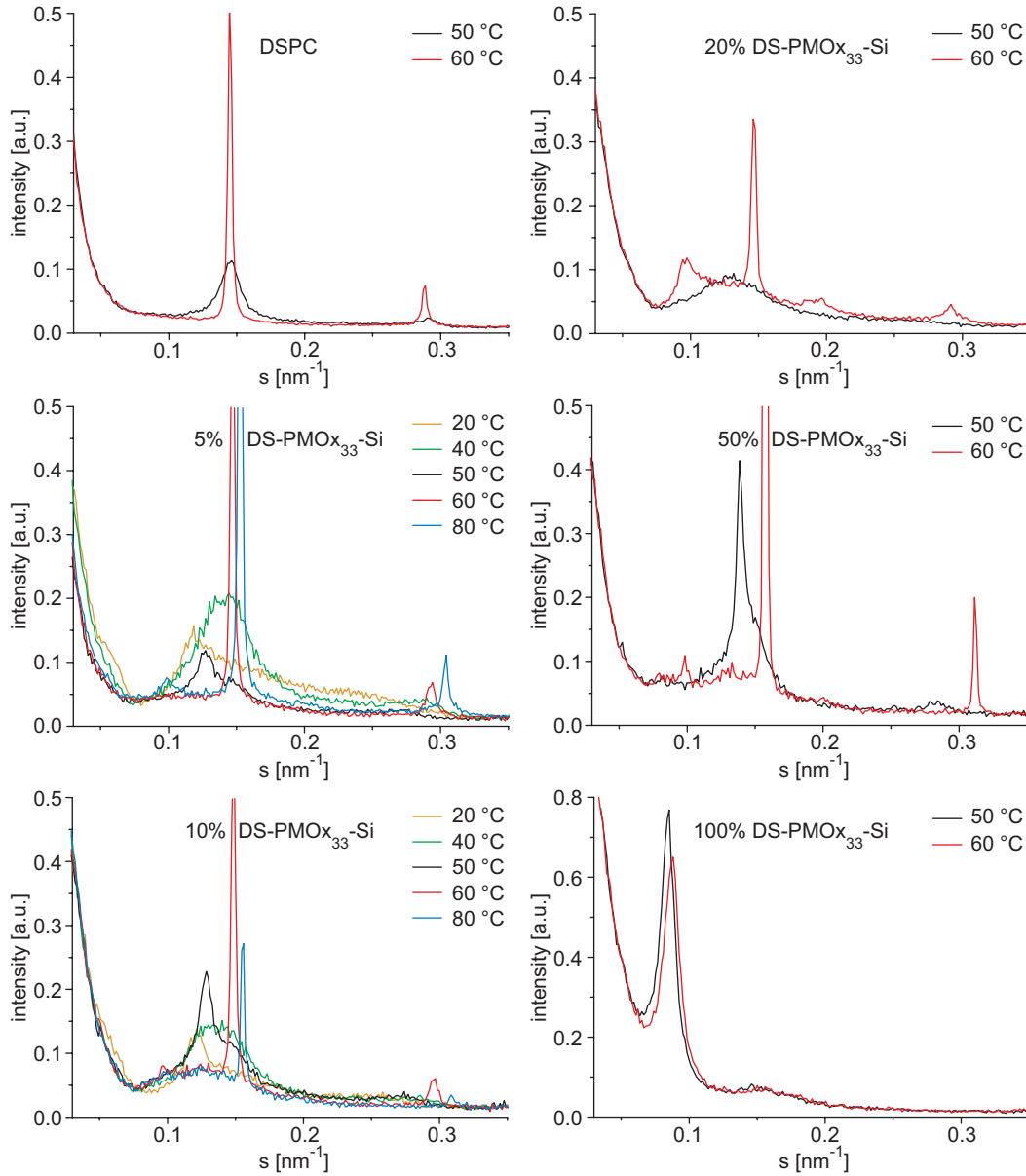


Figure A.4: SAXS results of lipid/lipopolymer dispersions, where the ratio of DS-PMO₃₃-Si was varied between 0 and 100 mol%.

After adding a certain amount of lipopolymers, two Bragg peaks in close proximity were present for temperatures below chain melting. The intensity of the two peaks varies with temperature, which can be seen in the graphs of 5 mol% and

10 mol% DS-PMO_{x33}-Si. At high temperatures above T_m , always a very distinct peak at $s \sim 0.15 \text{ nm}^{-1}$ is present. Furthermore, two small peaks are visible, one at $s \sim 0.29 \text{ nm}^{-1}$ and one around $s \sim 0.1 \text{ nm}^{-1}$, which holds for all measured mixing ratios of 5 to 50 mol% lipopolymer.

Table A.1 summarizes the evaluated distances d in real space from lipid/lipopolymer dispersions with DS-PMO_{x33}-Si:

Dispersion	d [nm]						
	20 °C	30 °C	40 °C	50 °C	60 °C	70 °C	80 °C
100 % DSPC	7.0	6.9	6.9	6.9	6.9	6.8	6.8
	-	3.5	3.5	3.4	3.5	3.4	3.4
5 % DS-PMO _{x33} -Si 95 % DSPC	8.4	8.2	7.7	7.9	-	-	-
	6.4	6.7	6.8	6.7	6.8	6.6	6.5
	-	-	3.6	3.7	3.4	3.3	3.3
	-	-	-	-	-	10.1	10.0
10 % DS-PMO _{x33} -Si 90 % DSPC	8.3	n.m.	8.0	7.8	-	n.m.	-
	6.9	n.m.	6.8	6.7	6.7	n.m.	6.4
	-	n.m.	-	3.8	3.4	n.m.	3.2
	-	n.m.	-	-	10.2	n.m.	10.1
20 % DS-PMO _{x33} -Si 80 % DSPC	8.3	8.3	7.6	7.8	-	-	-
	7.0	6.7	6.8	-	6.8	6.6	6.3
	-	-	-	-	5.2	5.0	-
	-	-	-	-	3.4	3.3	-
	-	-	-	-	10.3	9.8	8.0
50 % DS-PMO _{x33} -Si 50 % DSPC	7.5	7.4	7.0	7.2	-	-	-
	6.6	6.6	-	6.7	6.4	6.2	6.1
	3.8	3.6	3.5	3.5	3.2	3.1	3.1
	-	-	-	-	10.2	10.1	10.2
100 % DS-PMO _{x33} -Si	13.0 (7.7)	12.7 (7.3)	12.5 (7.1)	11.9 (6.8)	11.5 (6.7)	11.3 (6.4)	11.3 (6.3)

Table A.1: Distances d in real space evaluated from lipid/lipopolymer dispersions with DS-PMO_{x33}-Si. Bold numbers denote the most intensive peak at the particular temperature, distances in brackets are values obtained from hump-like peaks. “n.m.” stands for ‘not measured’ SAXS data at certain temperatures.

To interpret the data, one can consult previous reports on lipid/lipopolymer dispersions composed of phospholipids and lipid-anchored poly(ethylene glycol) [Warriner et al., 1996, Safinya, 1997, Warriner et al., 1998, Montesano et al., 2001, Hansen et al., 2003].

Below the chain melting temperature T_m , one obtains two average distances, d_1 and d_2 , where the smaller distance, d_1 , reflects the lamellar L_β spacing in DSPC lipid stacks of about $\sim 6.9 \text{ nm}$. The increased spacing d_2 results from the undulation

of the membrane induced by larger headgroup of poly(2-oxazoline) lipopolymers in comparison to the small phospholipid headgroup (see Figure A.5). The system might undergo an in-plane phase separation, where lipopolymers are creating regions of high spontaneous curvature and defects, in which the lipopolymers accumulate at the monolayer with higher curvature, and simultaneously they stabilize these kind of defects [Warriner et al., 1998].

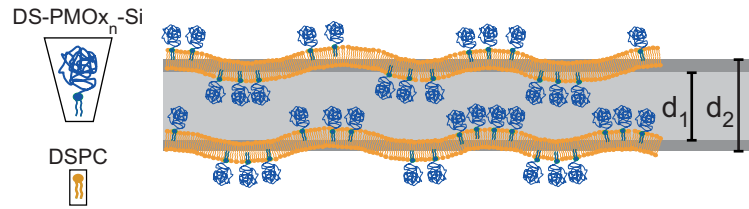


Figure A.5: Sketch of membrane stack of lipid/lipopolymer dispersion at temperatures below T_m . The lipid-anchored poly(2-oxazolines) induce undulations of the membranes, which results in two distances of the lamellar stacks, d_1 and d_2 . The figures at the left side illustrate the headgroup influence on molecule shape.

At temperatures above chain melting, all samples with molar fractions of 5 to 50% exhibited highly ordered lamellar stacks with similar repeat distances like pure DSPC lipid dispersions. The lipopolymers seem to be excluded from the lipid phase and arranged into a hexagonal phase of micellar tubes with lattice distances of about ~ 10 nm.

In summary, one can derive a crude phase diagram for DSPC/DS-PMOx₃₃-Si dispersions, visualized in Figure A.6.

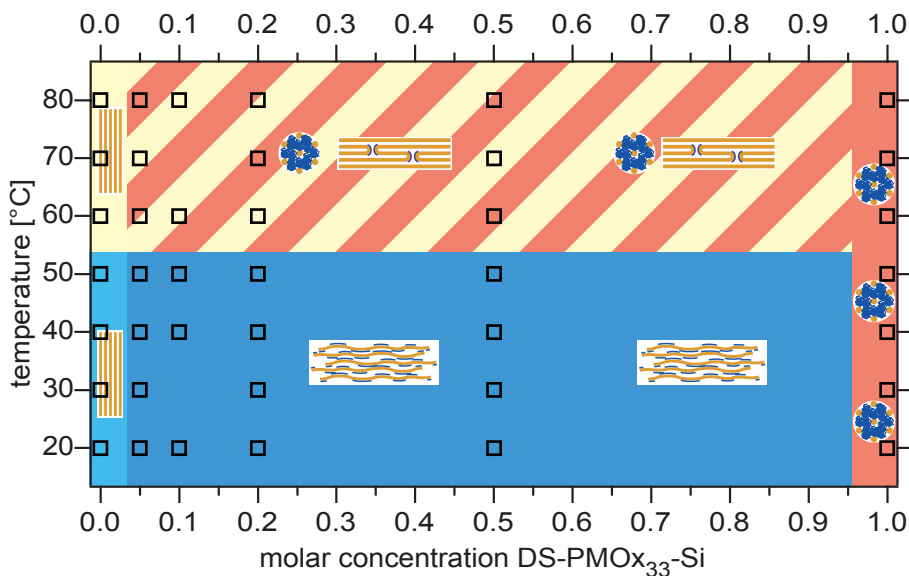


Figure A.6: Phase diagram of DSPC/DS-PMOx₃₃-Si dispersions, derived from SAXS/WAXS measurements. The boxes denote the measured data points, where the inserted sketches illustrate the different phases.

A.3 Lipids

The chemical structures of the used lipid and fluorescence dye tracers are presented in Figure A.7. For further details, see Section 1.1.2.

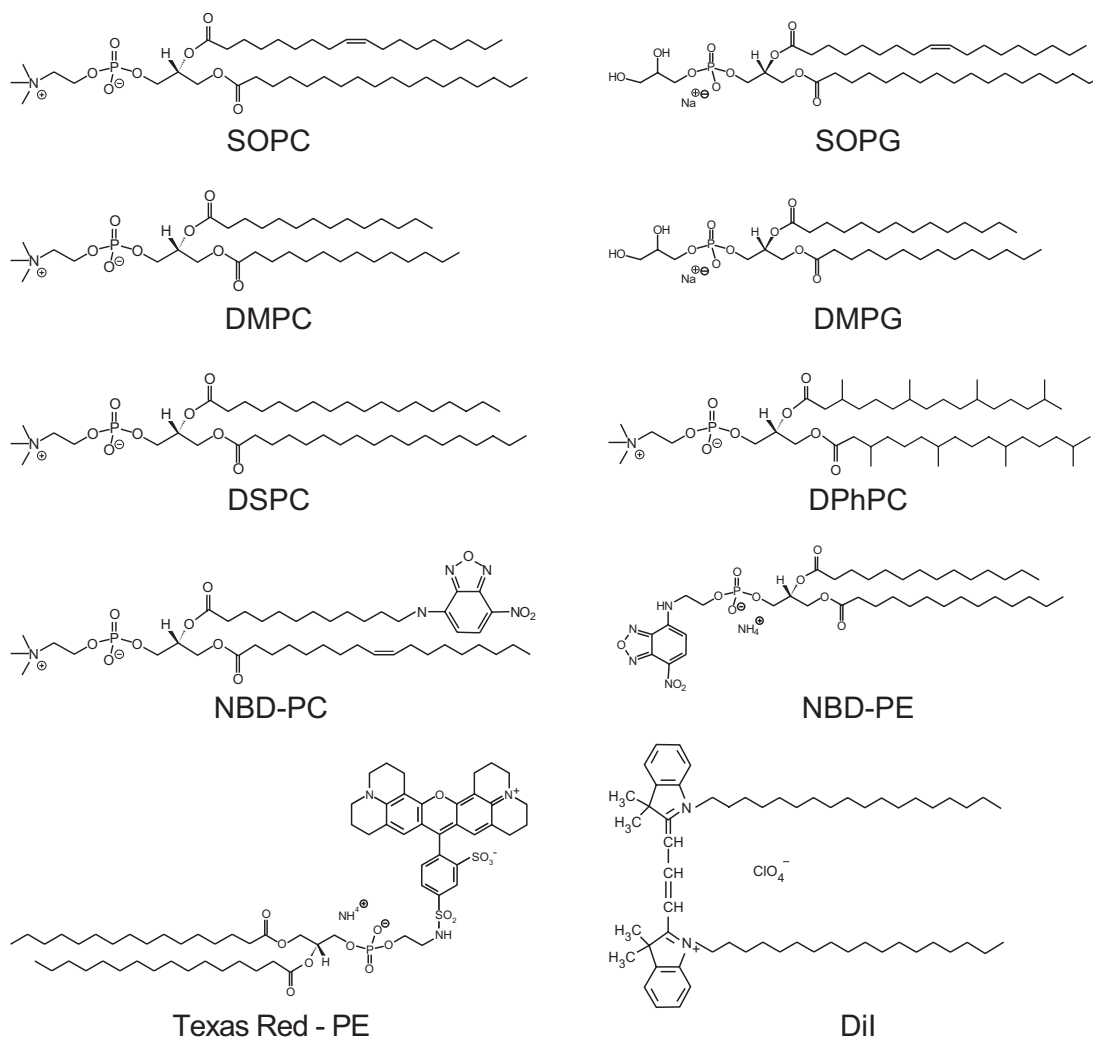


Figure A.7: Chemical structures of the used lipids and fluorescence dye tracers.

A.4 Poly(2-oxazoline) Lipopolymers

In Figure A.8, the chemical structures of the used lipopolymers are illustrated. These lipopolymers were synthesized by Anton Förtig (Lehrstuhl für Makromolekulare Stoffe, Technische Universität München, Germany)¹. For further details, see Section 1.1.1.

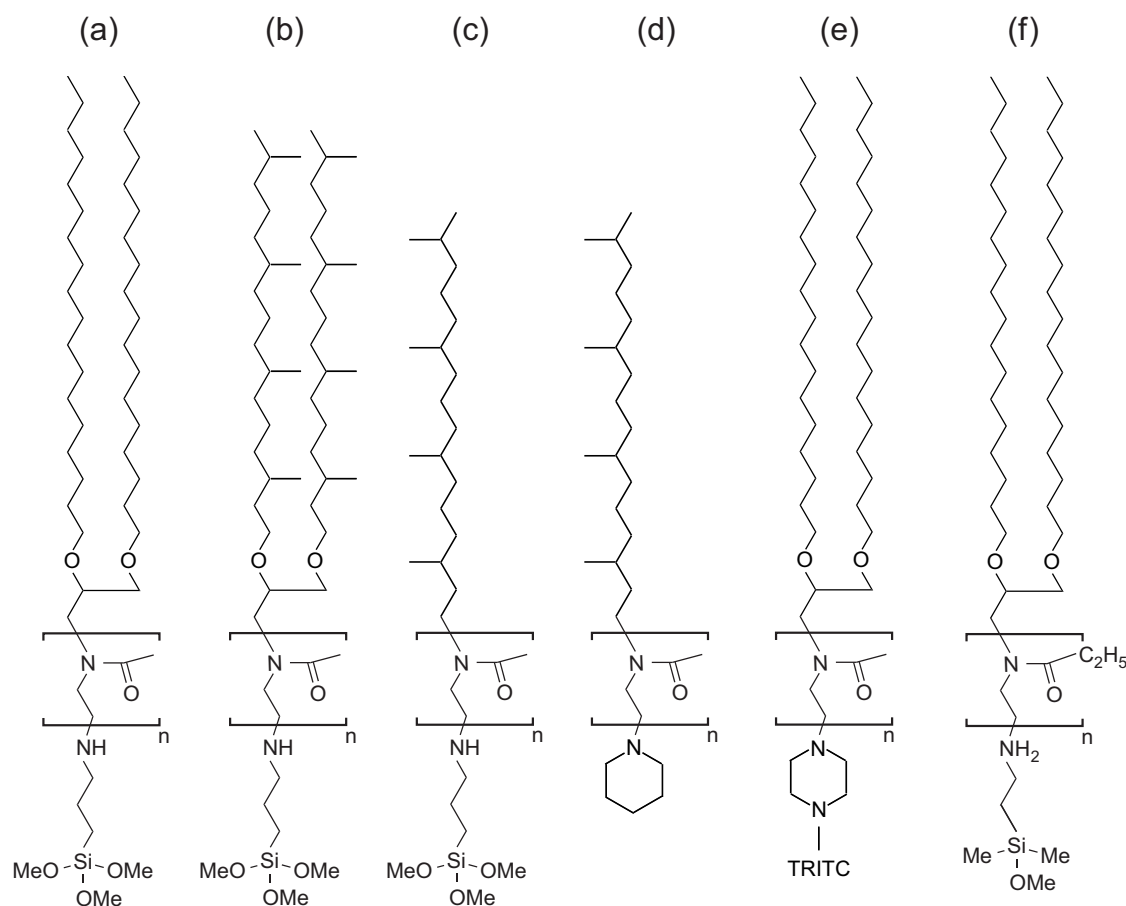


Figure A.8: Chemical structures of the used poly(2-oxazolines). (a) Poly(2-methyl-2-oxazoline) with distearoyl lipid moiety and a trimethoxysilane coupling group (DS-PMO_{x_n}-Si). (b) Poly(2-methyl-2-oxazoline) with diphytanoyl lipid moiety and a trimethoxysilane coupling group (DPh-PMO_{x_n}-Si). (c) Poly(2-methyl-2-oxazoline) with single phytanoyl lipid moiety and a trimethoxysilane coupling group (Ph-PMO_{x_n}-Si). (d) Poly(2-methyl-2-oxazoline) with single phytanoyl lipid moiety and a piperidin termination (Ph-PMO_{x_n}-Pip). (e) Poly(2-methyl-2-oxazoline) with distearoyl lipid moiety and a TRITC fluorescence tracer coupled via a piperazine group (DS-PMO_{x_n}-TRITC). (f) Poly(2-ethyl-2-oxazoline) with distearoyl lipid moiety and a trimethoxysilane coupling group (DS-PEO_{x_n}-Si).

¹DS-PMO_{x_n}-TRITC was synthesized by Karin Lüdtke, Lehrstuhl für Makromolekulare Stoffe, Technische Universität München, Germany

The following table summarizes the properties of the used poly(2-oxazolines):

Poly(2-oxazoline)	lipid moiety	end functionalization	DP ²	MW [g mol ⁻¹]	PDI ³
DS-PMO _{x14} -Si	distearoyl	trimethoxysilane	14	1950	1.09
DS-PMO _{x18} -Si	distearoyl	trimethoxysilane	18	2290	1.33
DS-PMO _{x33} -Si	distearoyl	trimethoxysilane	33	3567	1.30
DS-PMO _{x104} -Si	distearoyl	trimethoxysilane	104	9609	1.30
DS-PMO _{x13} -TRITC	distearoyl	piperazin-TRITC	13	2214	
DPh-PMO _{x21} -Si	diphytanoyl	trimethoxysilane	21	2517	1.07
Ph-PMO _{x12} -Si	phytanoyl	trimethoxysilane	12	1481	1.12
Ph-PMO _{x21} -Si	phytanoyl	trimethoxysilane	21	2247	1.16
Ph-PMO _{x12} -Pip	phytanoyl	piperidin	12	1387	1.16
DS-PEO _{x10} -Si	distearoyl	dimethylmethoxysilane	10	1896	1.16
DS-PEO _{x19} -Si	distearoyl	dimethylmethoxysilane	19	2807	1.31

²degree of polymerization, estimated from ¹H-NMR measurements

³polydispersity index, estimated with gel permeation chromatography (GPC)

A.5 Abbreviations

AFM	atomic force microscope
BLM	black lipid membrane
DiI	1,1'-dioctadecyl-3,3,3',3'-tetramethylindocarbocyanine perchlorate
DMPC	1,2-dimyristoyl- <i>sn</i> -glycero-3-phosphocholine
DMPG	1,2-dimyristoyl- <i>sn</i> -glycero-3-[phospho- <i>rac</i> -(1-glycerol)]
DPh	diphytanoyl
DPhPC	1,2-diphytanoyl- <i>sn</i> -glycero-3-phosphocholine
DS	distearoyl
DSPC	1,2-distearoyl- <i>sn</i> -glycero-3-phosphocholine
ELISA	enzyme-linked immunosorbent assay
FLIC	fluorescence interference contrast microscopy
FRAP	fluorescence recovery after photobleaching
Hepes	4-(2-hydroxyethyl) piperazine-1-ethanesulfonic acid
LB	Langmuir-Blodgett
NBD	7-nitro-2-1,3-benzoxadiazol-4-yl
NBD-PC	1-oleoyl-2-[12-[(7-nitro-2-1,3-benzoxadiazol-4-yl)amino]dodecanoyl]- <i>sn</i> -glycero-3-phosphocholine
NBD-PE	1,2-dimyristoyl- <i>sn</i> -Glycero-3-Phosphoethanolamine-N-(7-nitro-1-1,3-benzoxadiazol-4-yl)
PEG	poly(ethylene glycol)
PEOx	poly(2-ethyl-2-oxazoline)
Ph	phytanoyl
PMOx	poly(2-methyl-2-oxazoline)
RICM	reflection interference contrast microscopy
SAXS	small-angle X-ray scattering
SOPC	1-stearoyl-2-oleoyl- <i>sn</i> -glycero-3-phosphocholine
SOPG	1-stearoyl-2-oleoyl- <i>sn</i> -glycero-3-[phospho- <i>rac</i> -(1-glycerol)]
TAMRA	5-(and-6)-carboxytetramethylrhodamine (5(6)-TAMRA)
Texas Red-PE	1,2-dihexadecanoyl- <i>sn</i> -glycero-3-phosphoethanolamine, triethylammonium salt
TRIS	tris-(hydroxymethyl)-aminomethane
TRITC	tetramethylrhodamineisothiocyanate
Triton X-100	4-(1,1,3,3-Tetramethylbutyl)phenyl-polyethylene glycol
WAXS	wide-angle X-ray scattering

A.6 Symbols

A	area per molecule
A_l	lipid area
a_m	monomer size
B_0	bleaching rate
b_s	friction coefficient
c	concentration
d	distance
D	diffusion coefficient
ε	dimensionless particle radius
η	liquid viscosity of the cleft between membrane and substrate
η_m	membrane viscosity (3D)
f	friction coefficient
γ	membrane tension
Δg_{ad}	adhesion free energy
h_m	membrane thickness
I_0, I_1	spherical bessel functions, 1st and 2nd order
κ	membrane bending stiffness
K_0, K_1	modified bessel functions of the second kind, orders zero and one
λ	characteristic decay length
m	dimensionless particle mobility
n_p	monomer number
Π	surface pressure
r	radius
R	fluorescence recovery
ρ	density
t	time
τ	characteristic time constant
w_{ad}	specific binding energy per integrin-RGD pair
W_{ad}	specific adhesion energy per unit area

Bibliography

- [Albersdörfer et al., 1997] Albersdörfer, A., Feder, T., & Sackmann, E. (1997). Adhesion-induced domain formation by interplay of long-range repulsion and short-range attraction force: A model membrane study. *Biophysical Journal*, 73(1), 245–257. Article.
- [Albrecht et al., 1978] Albrecht, O., Gruler, H., & Sackmann, E. (1978). Polymorphism of phospholipid monolayers. *Journal de Physique I*, 39, 301–313.
- [Albrecht et al., 1981] Albrecht, O., Gruler, H., & Sackmann, E. (1981). Pressure-composition phase diagrams of cholesterol/lecithin, cholesterol/phosphatidic acid, and lecithin/phosphatidic acid mixed monolayers: A langmuir film balance study. *Journal of Colloid and Interface Science*, 79(2), 319–338.
- [Almeida & Vaz, 1995] Almeida, P. F. F. & Vaz, W. L. C. (1995). 'Lateral Diffusion in Membranes' in 'Handbook of Biological Physics', volume 1, (pp. 305–357). Elsevier Science B. V.: Amsterdam.
- [Axelrod et al., 1976] Axelrod, D., Koppel, D., Schlessinger, J., Elson, E., & Webb, W. (1976). Mobility measurement by analysis of fluorescence photobleaching recovery kinetics. *Biophysical Journal*, 16, 1055–1069.
- [Baekmark et al., 1998] Baekmark, T. R., Sprenger, I., Ruile, M., Nuyken, O., & Merkel, R. (1998). Compression-induced formation of surface micelles in monolayers of a poly(2-oxazoline) diblock copolymer at the air-water interface: A combined film balance and electron microscopy study. *Langmuir*, 14, 4222–4226.
- [Baekmark et al., 1997] Baekmark, T. R., Wiesenthal, T., Kuhn, P., Bayerl, T. M., Nuyken, O., & Merkel, R. (1997). New insights into the phase behavior of lipopolymer monolayers at the air/water interface. IRRAS study of a polyoxazoline lipopolymer. *Langmuir*, 13, 5521–5523.
- [Bartlett, 1958] Bartlett, G. (1958). Phosphorus assay in column chromatography. *Journal of Biological Chemistry*, 234(3), 466–468.
- [Bassiri et al., 1967] Bassiri, T. G., Levy, A., & Litt, M. (1967). Polymerization of cyclic imino ethers .I. Oxazolines. *Journal of Polymer Science Part B-Polymer Letters*, 5(9PB), 871.
- [Bell et al., 1984] Bell, G. I., Dembo, M., & Bongrand, P. (1984). Cell adhesion - competition between nonspecific repulsion and specific bonding. *Biophysical Journal*, 45, 1051–1064.
- [Blaurock, 1982] Blaurock, A. E. (1982). Evidence of bilayer structure and of membrane interactions from X-ray diffraction analysis. *Biochimica et Biophysica Acta*, 650, 167–184.
- [Blodgett, 1934] Blodgett, K. B. (1934). Monomolecular films of fatty acids on glass. *Journal of the American Chemical Society*, 56, 495.

- [Blodgett, 1935] Blodgett, K. B. (1935). Films built by depositing successive monomolecular layers on a solid surface. *Journal of the American Chemical Society*, 57, 1007–1022.
- [Blodgett & Langmuir, 1937] Blodgett, K. B. & Langmuir, I. (1937). Built-up films of barium stearate and their optical properties. *Physical Review*, 51, 964–982.
- [Bradford, 1976] Bradford, M. (1976). A rapid and sensitive method for the quantitation of microgram quantities of protein utilizing the principle of protein-dye binding. *Analytical Biochemistry*, 72, 248–254.
- [Braun & Fromherz, 1997] Braun, D. & Fromherz, P. (1997). Fluorescence interference-contrast microscopy of cell adhesion on oxidized silicon. *Applied Physics A*, 65, 341–348.
- [Brochard-Wyart & de Gennes, 1992] Brochard-Wyart, F. & de Gennes, P. (1992). Dynamics of partial wetting. *Advances in Colloid and Interface Science*, 39, 1–11.
- [Bruinsma, 1995] Bruinsma, R. (1995). 'Adhesion an Rolling of Leukocytes. A Physical Model' in 'Proceedings of the NATO Advanced Institute of Physics and Biomaterials, NATO Advanced Study Institute Series B: Physics', (pp. 611). Kluwer: London.
- [Bruinsma et al., 2000] Bruinsma, R., Behrisch, A., & Sackmann, E. (2000). Adhesive switching of membranes: Experiment and theory. *Physical Review E*, 61(4), 4253–4267.
- [Bunjes et al., 1997] Bunjes, N., Schmidt, E., Jonczyk, A., Rippmann, F., Beyer, D., Ringsdorf, H., P., G., Knoll, W., & Naumann, R. (1997). Thiopeptide-supported lipid layers on solid substrates. *Langmuir*, 13, 6188–6194.
- [Campbell et al., 1999] Campbell, N., Reece, J., & Mitchell, L. (1999). *Biology*. Benjamin Cummings, 5th edition. <http://omega.dawsoncollege.qc.ca/ray/401course.htm>.
- [Chen et al., 1997] Chen, C. S., Mrksich, M., Huang, S., Whitesides, G. M., & Ingber, D. E. (1997). Geometric control of cell life and death. *Science*, 276, 1425–1428.
- [Chen et al., 1990] Chen, F. P., Ames, A. E., & Taylor, L. D. (1990). Aqueous solutions of poly(ethyloxazoline) and its lower consolute phase transition. *Macromolecules*, 23, 4688–4695.
- [Cohen & Turnbull, 1959] Cohen, M. H. & Turnbull, D. (1959). Molecular transport in liquids and glasses. *Journal of Chemical Physics*, 31, 1164–1169.
- [Cornell et al., 1997] Cornell, B. A., Braach-Maksvytis, V., King, L. G., Osman, P. D. J., Raguse, B., Wiczorek, L., & Pace, R. J. (1997). A biosensor that uses ion-channel switches. *Nature*, 387, 580–583.
- [Cunningham et al., 1994] Cunningham, B. A., Bras, W., Lis, L. J., & Quinn, P. J. (1994). Synchrotron X-ray studies of lipids and membranes: a critique. *Journal of Biochemical and Biophysical Methods*, 29, 87–111.
- [Cunningham et al., 1998] Cunningham, B. A., Brown, A.-D., Wolfe, D. H., Williams, W. P., & Brain, A. (1998). Ripple phase formation in phosphatidylcholine: Effect of acyl chain relative length, position, and unsaturation. *Physical Review E*, 58(3), 3662–3672.

- [Dalle Vedove & Sanfeld, 1981] Dalle Vedove, W. & Sanfeld, A. (1981). Hydrodynamic and chemical stability of fluidfluid reacting interfaces : I. Gfeneral theory for aperiodic regimes. *Journal of Colloid and Interface Science*, 84, 318–327.
- [de Gennes, 1980] de Gennes, P. G. (1980). Conformations of polymers attached to an interface. *Macromolecules*, 13, 1069–1075.
- [de Gennes, 1986] de Gennes, P. G. (1986). Deposition of Langmuir-Blodgett layers. *Colloid and Polymer Science*, 264(5), 463–465.
- [de Gennes, 1987] de Gennes, P. G. (1987). Polymers at an interface; a simplified view. *Advances in Colloid and Interface Science*, 27, 189–209.
- [Debrégeas et al., 1995] Debrégeas, G., Martin, P., & Brochard-Wyart, F. (1995). Viscous bursting of suspended films. *Physical Review Letters*, 75(21), 3886–3889.
- [Dietrich et al., 1997] Dietrich, C., Merkel, R., & Tampe, R. (1997). Diffusion measurement of fluorescence-labeled amphiphilic molecules with a standard fluorescence microscope. *Biophysical Journal*, 72, 1701–1710.
- [Dietrich & Tampe, 1995] Dietrich, C. & Tampe, R. (1995). Charge determination of membrane molecules in polymer-supported lipid layers. *Biochimica et Biophysica Acta*, 1238, 183–191.
- [Dimova et al., 1999] Dimova, R., Dietrich, C., Hadjiisky, A., Danov, K., & Pouligny, B. (1999). Falling ball viscosimetry of giant vesicle membrane: Finite-size effects. *European Physical Journal B*, 12, 589–598.
- [Dimova et al., 2000] Dimova, R., Pouligny, B., & Dietrich, C. (2000). Pretransitional effects in dimyristoylphosphatidylcholine vesicle membranes: Optical dynamometry study. *Biophysical Journal*, 79, 340–356.
- [Elender et al., 1996] Elender, G., Kühner, M., & Sackmann, E. (1996). Functionalisation of Si/SiO₂ and glass surfaces with ultrathin dextran films and deposition of lipid bilayers. *Biosensors & Bioelectronics*, 11, 565.
- [Elender & Sackmann, 1994] Elender, G. & Sackmann, E. (1994). Wetting and dewetting of Si/SiO₂-wafers by free and lipid-monolayer covered aqueous solutions under controlled humidity. *Journal de Physique II*, 4, 455–479.
- [Erb et al., 1997] Erb, E.-M., Tangemann, K., Bohrmann, B., Müller, B., & Engel, J. (1997). Integrin $\alpha_{IIb}\beta_3$ reconstituted into lipid bilayers is nonclustered in its activated state but clusters after fibrinogen binding. *Biochemistry*, 36, 7395–7402.
- [Erdelen et al., 1994] Erdelen, C., Häussling, L., Naumann, R., Ringsdorf, H., Wolf, H., & Yang, J. (1994). Self-assembled disulfide-functionalized amphiphilic copolymers on gold. *Langmuir*, 10, 1246–1250.
- [Evans & Sackmann, 1988] Evans, E. & Sackmann, E. (1988). Translational and rotational drag coefficients for a disk moving in a liquid membrane associated with a rigid substrate. *Journal of Fluid Mechanics*, 194, 553–561.
- [Fanton & Cazabat, 1998] Fanton, X. & Cazabat, A. (1998). Spreading and instabilities induced by a solutal Marangoni flow. *Langmuir*, 14, 2554–2561.

- [Fiske & Subbarow, 1925] Fiske, C. H. & Subbarow, Y. (1925). The colorimetric determination of phosphorus. *Journal of Biological Chemistry*, 66, 375–400.
- [Fitzgerald et al., 1985] Fitzgerald, L., Leung, B., & Phillips, D. (1985). A method for purifying the platelet membrane glycoprotein IIB-IIIa complex. *Analytical Biochemistry*, 151(1), 169–177.
- [Foreman et al., 2003] Foreman, M. B., Coffmann, J. P., Murcia, M. J., Cesana, S., Jordan, R., Smith, G. S., & Naumann, C. (2003). Gelation of amphiphilic lipopolymers at the air-water interface: 2D analogue to 3D gelation of colloidal systems with grafted polymer chains? *Langmuir*, 19, 326–332.
- [Förtig et al., 2004] Förtig, A., Jordan, R., Graf, K., Schiavon, G., Purucker, O., & Tanaka, M. (2004). Solid-supported biomimetic membranes with tailored lipopolymer tethers. *Macromolecular Symposia*, 210, 329–338.
- [Förtig et al., 2003] Förtig, A., Jordan, R., Purucker, O., & Tanaka, M. (2003). 2-alkyl-2-oxazoline lipopolymers for the construction of polymer tethered lipid bilayers. *Polymer Preprints*, 44, 850–851.
- [Gaines, 1966] Gaines, G. L. (1966). *Insoluble Monolayers at Liquid-Gas Interfaces*. New York: Wiley - Interscience.
- [Galla et al., 1979] Galla, H.-J., Hartmann, W., Theilen, U., & Sackmann, E. (1979). On two-dimensional passive random walk in lipid bilayers and fluid pathways in biomembranes. *Journal of Membrane Biology*, 48, 215–236.
- [Gennis, 1989] Gennis, R. B. (1989). *Biomembranes - Molecular Structure and Function*. New York: Springer, 1st edition.
- [Gleiche et al., 2000] Gleiche, M., Chi, L., & Fuchs, H. (2000). Nanoscopic channel lattices with controlled anisotropic wetting. *Nature*, 403, 173–175.
- [Gönnenwein et al., 2003] Gönnenwein, S., Tanaka, M., Hu, B., Moroder, L., & Sackmann, E. (2003). Functional incorporation of integrins into solid supported membranes on ultrathin films of cellulose - impact on adhesion. *Biophysical Journal*, 48, 646–655.
- [González-Rodríguez et al., 1994] González-Rodríguez, J., Acuña, A. U., Alvarez, M. V., & Jovin, T. M. (1994). Rotational mobility of the fibrinogen receptor glycoprotein IIb/IIIa or integrin $\alpha_{IIb}\beta_3$ in the plasma membrane of human platelets. *Biochemistry*, 33, 266–274.
- [Groves & Boxer, 2002] Groves, J. & Boxer, S. (2002). Micropattern formation in supported lipid membranes. *Accounts of Chemical Research*, 35, 149–157.
- [Guttenberg et al., 2000] Guttenberg, Z., Bausch, A. R., Hu, B., Bruinsma, R., Moroder, L., & Sackmann, E. (2000). Measuring ligand-receptor unbinding forces with magnetic beads: Molecular leverage. *Langmuir*, 16(23), 8984–8993.
- [Hansen et al., 2003] Hansen, P. L., Cohen, J. A., Podgornik, R., & Parsegian, V. A. (2003). Osmotic properties of poly(ethylene glycols): Quantitative features of brush and bulk scaling laws. *Biophys. J.*, 84(1), 350–355.

- [Häussling et al., 1991] Häussling, R., Knoll, W., Ringsdorf, H., Schmitt, F.-J., & Yang, J. (1991). Surface functionalization and surface recognition: Plasmon optical detection of molecular recognition at self assembled monolayers. *Makromolekulare Chemie - Macromolecular Symposia*, 46, 145–155.
- [Heibel et al., 1998] Heibel, C., Maus, S., Knoll, W., & Rühle, J. (1998). *Polymer-Supported Biomembrane Models*, volume 695, (pp. 104). American Chemical Society: Washington (DC).
- [Herminghaus et al., 1998] Herminghaus, S., Jacobs, K., Mecke, K., Bischof, J., Fery, A., Ibn-Elhaj, M., & Schlogowski, S. (1998). Spinodal dewetting in liquid crystal and liquid metal films. *Science*, 282, 916–919.
- [Heyse et al., 1995] Heyse, S., Vogel, H., Sanger, M., & Sigrist, H. (1995). Covalent attachment of functionalized lipid bilayers to planar waveguides for measuring protein binding to biomimetic membranes. *Protein Science*, 4(12), 2532–2544.
- [Hillebrandt et al., 1999] Hillebrandt, H., Wiegand, G., Tanaka, M., & Sackmann, E. (1999). High electric resistance thin polymer/lipid composite systems on indium-tin-oxide (ITO) electrode-arrays. *Langmuir*, 15(24), 8451–8459.
- [Hu et al., 2000] Hu, B., Finsinger, D., Peter, K., Guttenberg, Z., Bärmann, M., Kessler, H., Escherich, A., Moroder, L., Böhm, J., Baumeister, W., Sui, S., & Sackmann, E. (2000). Intervesicle cross-linking with integrin $\alpha_{IIb}\beta_3$ and cyclic-RGD-lipopeptide. A model of cell-adhesion processes. *Biochemistry*, 39, 12284–12294.
- [Hughes et al., 1981] Hughes, B. D., A., P. B., & White, L. R. (1981). The translational and rotational drag on a cylinder moving in a membrane. *Journal of Fluid Mechanics*, 110, 349–372.
- [Hynes, 1992] Hynes, R. O. (1992). Integrins - versatility, modulation, and signaling in cell-adhesion. *Cell*, 69(1), 11–25.
- [Israelachvili, 1997] Israelachvili, J. N. (1997). The different phases of poly(ethylene glycol). *Proceedings of the National Academy of Sciences of the United States of America*, 94, 8378–8379.
- [Jacobson et al., 1995] Jacobson, K., Sheets, D. S., & Simson, R. (1995). Revisiting the fluid mosaic model of membranes. *Science*, 268, 1441–1442.
- [Johnson et al., 1991] Johnson, S. J., Bayerl, T. M., McDermott, D. C., Adam, G. W., Rennie, A. R., Thomas, R. K., & Sackmann, E. (1991). Structure of an adsorbed dimyristoylphosphatidylcholine bilayer measured with specular reflection of neutrons. *Biophysical Journal*, 59(2), 289–294. Article.
- [Jordan et al., 1996] Jordan, R., Graf, K., Riegler, H., & Unger, K. K. (1996). Polymer-supported alkyl monolayers on silica: Synthesis and self-assembly of terminal functionalized poly(N-propionylethylenimine)s. *Chemical Communications*, 9, 1025–1026.
- [Jordan et al., 2001a] Jordan, R., Martin, K., Rader, H. J., & Unger, K. K. (2001a). Lipopolymers for surface functionalizations: I. Synthesis and characterization of terminal functionalized poly(N-propionylethylenimine)s. *Macromolecules*, 34, 8858–8865.

- [Jordan & Ulman, 1998] Jordan, R. & Ulman, A. (1998). Surface initiated living cationic polymerization of 2-oxazolines. *Journal of the American Chemical Society*, 120(2), 243–247.
- [Jordan et al., 2001b] Jordan, R., West, N., Ulman, A., Chou, Y.-M., & Nuyken, O. (2001b). Nanocomposites by surface-initiated living cationic polymerization of 2-oxazolines on functionalized gold nanoparticles. *Macromolecules*, 34, 1606–1611.
- [Kalb et al., 1992] Kalb, E., Frey, S., & Tamm, L. (1992). Formation of supported planar bilayers by fusion of vesicles to supported phospholipid monolayers. *Biochimica et Biophysica Acta*, 1103, 307–316.
- [Keller et al., 2001] Keller, M., Schilling, J., & Sackmann, E. (2001). Oscillatory magnetic bead rheometer for complex fluid microrheometry. *Review in Scientific Instruments*, 72, 3626–3634.
- [Kern & Puotinen, 1970] Kern, W. & Puotinen, D. (1970). Cleaning solutions based on hydrogen peroxide for use in silicon semiconductor technology. *RCA Review*, 31, 187–206.
- [Kiessling & Tamm, 2003] Kiessling, V. & Tamm, L. (2003). Measuring distances in supported bilayers by fluorescence interference-contrast microscopy: Polymer supports and SNARE proteins. *Biophys. J.*, 84, 408–418.
- [Kjellander & Florin, 1981] Kjellander, R. & Florin, E. (1981). Water-structure and changes in thermal-stability of the system poly(ethylene oxide)-water. *Journal of the Chemical Society-Faraday Transactions I*, 77(9), 2053–2077. Part 9.
- [Knoll et al., 2000] Knoll, W., Frank, C., Heibel, C., Naumann, R., Offenhäuser, A., Rühle, J., Schmidt, E., Shen, W., & Sinner, A. (2000). Functional tethered lipid bilayers. *Review in Molecular Biotechnology*, 74, 137–158.
- [Koenig et al., 1996] Koenig, B. W., Krueger, S., Orts, W. J., Majkrzak, C. F., Berk, N. F., Silverton, J., & Gawrisch, K. (1996). Neutron reflectivity and atomic force microscopy studies of a lipid bilayer in water adsorbed to the surface of a silicon single crystal. *Langmuir*, 12, 1343–1350.
- [Koneripalli et al., 1996] Koneripalli, N., Levicky, R., Bates, F. S., Ankner, J., Kaiser, H., & Satija, S. K. (1996). Confinement-induced morphological changes in diblock copolymer films. *Langmuir*, 12(26), 6681–6690. DEC 25.
- [Kornberg & McConnell, 1971] Kornberg, R. D. & McConnell, H. (1971). Inside-outside transitions of phospholipids in vesicle membranes. *Biochemistry*, 10(7), 1111–1120.
- [Kovalchuk et al., 2003] Kovalchuk, V., Bondarenko, M. P., Zholkovskiy, E., & Vollhardt, D. (2003). Mechanism of meniscus oscillations and stripe pattern formation in Langmuir-Blodgett films. *Journal of Physical Chemistry B*, 107, 3486–3495.
- [Kühner & Sackmann, 1996] Kühner, M. & Sackmann, E. (1996). Ultrathin hydrated dextran films grafted on glass: preparation and characterization of structural, viscous, and elastic properties by quantitative microinterferometry. *Langmuir*, 12, 4866–4876.

- [Kühner et al., 1994] Kühner, M., Tampe, R., & Sackmann, E. (1994). Lipid mono- and bilayer supported on polymer films: Composite polymer-lipid films on solid substrates. *Biophysical Journal*, 67, 217–226.
- [Lambacher & Fromherz, 1996] Lambacher, A. & Fromherz, P. (1996). Fluorescence interference-contrast microscopy on oxidized silicon using a monomolecular dye layer. *Applied Physics A*, 63, 207–216.
- [Lambacher & Fromherz, 2002] Lambacher, A. & Fromherz, P. (2002). Luminescence of dye molecules on oxidized silicon and fluorescence interference contrast microscopy of biomembranes. *Journal of the Optical Society of America B*, 19(6), 1435–1453.
- [Lang et al., 1994] Lang, H., Duschl, C., & Vogel, H. (1994). A new class of thiolipid for the attachment of lipid bilayers on gold surfaces. *Langmuir*, 10, 197–210.
- [Langevin, 1998] Langevin, D. (1998). Dynamics of surfactant layers. *Current Opinion in Colloid and Interface Science*, 3(6), 600–607. DEC.
- [Lasic & Needham, 1995] Lasic, D. & Needham, D. (1995). The “stealth” liposome: A prototypical biomaterial. *Chemical Reviews*, 95(8), 2601–2628.
- [Lehmann & Rühle, 1999] Lehmann, T. & Rühle, J. (1999). Polyethyloxazoline monolayers for polymer supported biomembrane models. *Macromolecular Symposia*, 142, 1–12.
- [Lenhart et al., 2004] Lenhart, S., Zhang, L., Mueller, J., Wiesmann, H. P., G., E., Fuchs, H., & Chi, L. (2004). Self-organized complex patterning: Langmuir-Blodgett lithography. *Advanced Materials*, 16(7), 619–624.
- [Lindsey et al., 1979] Lindsey, H., Petersen, N., & Chan, S. (1979). Physicochemical characterization of 1,2-diphytanoyl-*sn*-glycero-3-phosphocholine in model membrane systems. *Biochimica et Biophysica Acta*, 555(1), 147–167.
- [Litt et al., 1969] Litt, M., Rahl, F., & Roldan, L. G. (1969). Polymerization of cyclic imino ethers .6. X-ray study of some polyaziridines. *Journal of Polymer Science Part A-2-Polymer Physics*, 7(3PA2), 463.
- [Lu et al., 2002] Lu, N., Gleiche, M., Zheng, J., Lenhart, S., Xu, B., Chi, L., & Fuchs, H. (2002). Fabrication of chemically patterned surfaces based on template-directed self-assembly. *Advanced Materials*, 14(24), 1812–1815.
- [Luzzati, 1968] Luzzati, V. (1968). ‘X-ray diffraction studies of lipid-water systems’ in ‘*Biological Membranes*’, volume 1, (pp. 71–123). Academic Press: London.
- [Macedo & Litovitz, 1965] Macedo, P. B. & Litovitz, T. A. (1965). On the relative roles of free volume and activation energy in the viscosity of liquids. *Journal of Chemical Physics*, 42, 245–256.
- [Majewski et al., 1998] Majewski, J., Wong, J. Y., Park, K., Seitz, M., Israelachvili, J. N., & Smith, G. S. (1998). Structural studies of polymer-cushioned lipid bilayers. *Biophysical Journal*, 75, 2363.
- [Marsh, 1990] Marsh, D. (1990). *Handbook of Lipid Bilayers*. Boca Raton, FL: CRC Press.

- [Marsh et al., 2003] Marsh, D., Bartucci, R., & Sportelli, L. (2003). Lipid membranes with grafted polymers: Physicochemical aspects. *Biochimica et Biophysica Acta*, 1615, 33–59.
- [Mathai et al., 2001] Mathai, J. C., Sprott, G. D., & Zeidel, M. L. (2001). Molecular mechanisms of water and solute transport across archaebacterial lipid membranes. *Journal of Biological Chemistry*, 276(29), 27266–27271.
- [Mattai et al., 1987] Mattai, J., Sripada, P. K., & Shipley, G. G. (1987). Mixed-chain phosphatidylcholine bilayers: structure and properties. *Biochemistry*, 26(12), 3287–3297.
- [Merkel et al., 1989] Merkel, R., Sackmann, E., & Evans, E. (1989). Molecular friction and epitactic coupling between monolayers in supported bilayers. *Journal de Physique II*, 50, 1535–1555.
- [Möhwald, 1990] Möhwald, H. (1990). Phospholipid and phospholipid-protein monolayers at the air/water interface. *Annual Reviews of Physical Chemistry*, 41, 441–476.
- [Möhwald, 1995] Möhwald, H. (1995). 'Phospholipid Monolayers' in 'Handbook of Biological Physics', volume 1, (pp. 161–211). Elsevier Science B. V.: Amsterdam.
- [Montesano et al., 2001] Montesano, G., Bartucci, R., Belsito, S., Marsh, D., & Sportelli, L. (2001). Lipid membrane expansion and micelle formation by polymer-grafted lipids: Scaling with polymer length studied by spin-label electron spin resonance. *Biophys. J.*, 80(3), 1372–1383.
- [Moraille & Badia, 2002] Moraille, P. & Badia, A. (2002). High parallel, nanoscale stripe morphology in mixed phospholipid monolayers formed by Langmuir-Blodgett transfer. *Langmuir*, 18(11), 4414–4419.
- [Moraille & Badia, 2003] Moraille, P. & Badia, A. (2003). Nanoscale stripe patterns in phospholipid bilayers formed by the Langmuir-Blodgett technique. *Langmuir*, 19(19), 8041–8049.
- [Müller et al., 1993] Müller, B., Zerwes, H.-G., Tangemann, K., Peter, J., & Engel, J. (1993). Two-step binding mechanism of fibrinogen to α IIb β 3 integrin reconstituted into planar lipid bilayers. *Journal of Biological Chemistry*, 268(9), 6800–6808.
- [Müller & Rudin, 1968] Müller, P. & Rudin, D. (1968). Action potentials induce in bimolecular lipid membranes. *Nature*, 217, 713–719.
- [Müller et al., 1962] Müller, P., Rudin, D., Tien, H., & Wescott, W. (1962). Reconstitution of cell membrane structure in vitro and its transformation into an excitable system. *Nature*, 194, 976–980.
- [Naumann et al., 2002] Naumann, C., Prucker, O., Lehmann, T., Rühle, J., Knoll, W., & Frank, C. (2002). The polymer-supported phospholipid bilayer: Tethering as a new approach to substrate-membrane stabilization. *Biomacromolecules*, 3, 27–35.
- [Naumann et al., 1999] Naumann, R., Schmid, E. K., Jonczyk, A., Fendler, K., Kadenbach, B., Liebermann, T., Offenhäuser, A., & Knoll, W. (1999). The peptide-tethered lipid membrane as a biomimetic system to incorporate cytochrome c oxidase in a functionally active form. *Biosensors & Bioelectronics*, 14, 651–662.

- [Petrov et al., 1980] Petrov, J. G., Kuhn, H., & Möbius, D. (1980). 3-phase contact line motion in the deposition of spread monolayers. *Journal of Colloid and Interface Science*, 73(1), 66–75.
- [Phillips & Chapman, 1968] Phillips, M. C. & Chapman, D. (1968). Monolayer characteristics of saturated 1,2-diacyl phosphatidylcholines (lecithins) and phosphatidylethanolamines at the air-water interface. *Biochimica et Biophysica Acta*, 163, 301–313.
- [Pignataro et al., 2002] Pignataro, B., Sardone, L., & Marletta, G. (2002). From micro- to nanometric scale patterning by Langmuir-Blodgett technique. *Materials Science and Engineering C*, 22, 177–181.
- [Plant, 1993] Plant, A. (1993). Self-assembled phospholipid/alkanethiol biomimetic bilayers on gold. *Langmuir*, 9, 2764–2767.
- [Purrucker et al., 2004a] Purrucker, O., Förtig, A., Jordan, R., & Tanaka, M. (2004a). Supported membranes with well-defined polymer tethers - incorporation of cell receptors. *ChemPhysChem*, 5, 327–335.
- [Purrucker et al., 2004b] Purrucker, O., Förtig, A., Lüdtke, K., Jordan, R., & Tanaka, M. (2004b). Confinement of transmembrane cell receptors in tunable stripe micropatterns. *Journal of the American Chemical Society*, submitted.
- [Raguse et al., 1998] Raguse, B., Braach-Maksvytis, V., Cornell, B., King, L., Osman, P., Pace, R., & Wiczorek, L. (1998). Tethered lipid bilayer membranes: Formation and ionic reservoir characterization. *Langmuir*, 14(3), 648–659.
- [Rehfeldt et al., 2002] Rehfeldt, F., Tanaka, M., Pagnoni, L., & Jordan, R. (2002). Static and dynamic swelling of grafted poly(2-alkyl-2-oxazoline)s. *Langmuir*, 18, 4908–4914.
- [Reiter, 1992] Reiter, G. (1992). Dewetting of thin polymer-films. *Physical Review Letters*, 68(1), 75–78.
- [Reiter, 2002] Reiter, G. (2002). Are changes in morphology clear indicators for the glass transition in thin polymer films? Tentative ideas. *European Physical Journal E*, 8(2), 251–255.
- [Rothman & Dawidowicz, 1975] Rothman, J. & Dawidowicz, E. (1975). Asymmetric exchange of vesicle phospholipids catalyzed by the phosphatidylcholine exchange protein. measurement of inside-outside transitions. *Biochemistry*, 14(13), 2809–2816.
- [Ruoslahti, 1996] Ruoslahti, E. (1996). RGD and other recognition sequences for integrins. *Annual Review of Cell Developmental Biology*, 12, 697–715.
- [Sackmann, 1995] Sackmann, E. (1995). 'Physical Basis of Self-Organization and Function of Membranes: Physics of Vesicles' in 'Handbook of Biological Physics', volume 1, (pp. 213–305). Elsevier Science B. V.: Amsterdam.
- [Sackmann, 1996] Sackmann, E. (1996). Supported membranes. *Science*, 271, 43–48.
- [Sackmann & Bruinsma, 2002] Sackmann, E. & Bruinsma, R. (2002). Cell adhesion as wetting transition? *ChemPhysChem*, 3, 262–269.

- [Sackmann & Tanaka, 2000] Sackmann, E. & Tanaka, M. (2000). Supported membranes on soft polymer cushions: Fabrication, characterization and applications. *Trends in Biotechnology*, 18, 58–64.
- [Saffman, 1976] Saffman, P. G. (1976). Brownian motion in thin sheets of viscous fluid. *Journal of Fluid Mechanics*, 73, 593–602.
- [Saffman & Delbrück, 1975] Saffman, P. G. & Delbrück, M. (1975). Brownian motion in biological membranes. *Proceedings of the National Academy of Sciences of the United States of America*, 72, 3111–3113.
- [Safinya, 1997] Safinya, C. R. (1997). Biomolecular materials: Structure, interactions and higher order self-assembly. *Colloids and Surfaces, A: Physicochemical and Engineering Aspects*, 128, 183–195.
- [Scalettar & Abney, 1991] Scalettar, B. A. & Abney, J. R. (1991). Molecular crowding and protein diffusion in biological membranes. *Comments on Molecular and Cell Biophysics*, 7(2), 79–107.
- [Schaub et al., 1993] Schaub, M., Wenz, G., Wegner, G., Stein, A., & Klemm, D. (1993). Ultrathin films of cellulose on silicon wafers. *Advanced Materials*, 5, 919–922.
- [Schiller et al., 2003] Schiller, S., Naumann, R., Lovejoy, K., Kunz, H., & Knoll, W. (2003). Archaea analogue thiolipids for tethered bilayer lipid membranes on ultra-smooth gold surfaces. *Angewandte Chemie International Edition*, 42, 208–211.
- [Schilling, 2004] Schilling, J. (2004). *Entwicklung einer schnellen digitalen Bildverarbeitungstechnik und einer interferometrischen 2λ - Mikroskopietechnik: Anwendung in der Zell-Biophysik*. PhD Thesis, Technische Universität München, Germany.
- [Schmidt et al., 1998] Schmidt, E., Liebermann, T., Kreiter, M., Jonczyk, A., Naumann, R., & Offenhäuser, A. (1998). *Biosensors & Bioelectronics*, 14, 585.
- [Schwartz et al., 1995] Schwartz, M. A., Schaller, M. D., & Ginsberg, M. H. (1995). Integrins: Emerging paradigms of signal transduction. *Annual Review of Cell Developmental Biology*, 11, 549–599.
- [Seddon & Templer, 1995] Seddon, J. M. & Templer, R. H. (1995). 'Polymorphism of Lipid-Water Systems' in 'Handbook of Biological Physics', volume 1, (pp. 97–160). Elsevier Science B. V.: Amsterdam.
- [Seitz et al., 2000] Seitz, M., Ter-Ovanesyan, E., Hausch, M., Park, C. K., Zasadzinski, J. A., Zentel, R., & Israelachvili, J. N. (2000). Formation of tethered supported bilayers by vesicle fusion onto lipopolymer monolayers promoted by osmotic stress. *Langmuir*, 16, 6067–6070.
- [Shen et al., 2001] Shen, W., Boxer, S., Knoll, W., & Frank, C. (2001). Polymer-supported lipid bilayers on benzophenone-modified substrates. *Biomacromolecules*, 2, 70–79.
- [Shimomura & Sawadaishi, 2001] Shimomura, M. & Sawadaishi, T. (2001). Bottom-up strategy of materials fabrication: A new trend in nanotechnology of soft materials. *Current Opinion in Colloid and Interface Science*, 6(1), 11–16.

- [Shipley, 1973] Shipley, G. G. (1973). 'Recent X-ray diffraction studies of biological membranes and membrane components' in 'Biological Membranes', volume 2, (pp. 1–89). Academic Press: London.
- [Sigl et al., 1997] Sigl, H., Brink, G., Schulze, M., Wegner, G., & Sackmann, E. (1997). Assembly of polymer/lipid composite films on solids based on hairy rod LB-films. *European Biophysical Journal*, 25, 249.
- [Silvius, 1982] Silvius, J. R. (1982). 'Thermotropic Phase Transitions of Pure Lipids in Model Membranes and their Modification by Membrane Proteins' in 'Lipid-Protein Interactions', volume 2, (pp. 239–281). Wiley - Interscience: New York.
- [Simons & Ikonen, 1997] Simons, K. & Ikonen, E. (1997). Functional rafts in cell membranes. *Nature*, 387, 569–572.
- [Singer & Nicolson, 1972] Singer, S. & Nicolson, G. (1972). The fluid mosaic model of the structure of cell membranes. *Science*, 175, 720–731.
- [Solletti et al., 1996] Solletti, J. M., Botreau, M., Sommer, F., Duc, T. M., & Celio, M. R. (1996). Characterization of mixed miscible and nonmiscible phospholipid Langmuir Blodgett films by atomic force microscopy. *Journal of Vacuum Science and Technology, B*, 14(2), 1492–1497.
- [Soumpasis, 1983] Soumpasis, D. (1983). Theoretical analysis of fluorescence photobleaching recovery experiments. *Biophysical Journal*, 41, 95–97.
- [Spinke et al., 1992] Spinke, J., Yang, J., Wolf, H., Liley, M., Ringsdorf, H., & Knoll, W. (1992). Polymer-supported bilayer on a solid substrate. *Biophysical Journal*, 63, 1667–1671.
- [Spratte et al., 1994] Spratte, K., Chi, L. F., & Riegler, H. (1994). Physisorption instabilities during dynamic langmuir wetting. *Europhysics Letters*, 25(3), 211–217.
- [Spratte & Riegler, 1994] Spratte, K. & Riegler, H. (1994). Steady state morphology and composition of mixed monomolecular films (Langmuir monolayers) at the air/water interface in the vicinity of the three-phase line: Model calculations and experiments. *Langmuir*, 10, 3161–6173.
- [Springer, 1995] Springer, T. A. (1995). Traffic signals on endothelium for lymphocyte recirculation and leukocyte emigration. *Annual Review of Physiology*, 57, 827–872.
- [Steinhoff et al., 2003] Steinhoff, G., Purrucker, O., Tanaka, M., & Eickhoff, M. (2003). $\text{Al}_x\text{Ga}_{1-x}\text{N}$ - a new material system for biosensors. *Advanced Materials*, 13(11), 841–846.
- [Tamm & McConnell, 1985] Tamm, L. & McConnell, H. (1985). Supported phospholipid bilayers. *Biophysical Journal*, 47, 105–113.
- [Tanaka et al., 2001] Tanaka, M., Kaufmann, S., Nissen, J., & Hochrein, M. (2001). Orientation selective immobilization of human erythrocyte membranes on ultrathin cellulose films. *Physical Chemistry Chemical Physics*, 3, 4091–4095.
- [Tanaka et al., 2004] Tanaka, M., Wong, A. P., Rehfeldt, F., Tutus, M., & Kaufmann, S. (2004). Selective deposition of native cell membranes on biocompatible micropatterns. *Journal of the American Chemical Society*, 126, 3257–3260.

- [Théato & Zentel, 2000] Théato, P. & Zentel, R. (2000). Formation of lipid bilayers on a new amphiphilic polymer support. *Langmuir*, 16, 1801–1805.
- [van Deenen et al., 1962] van Deenen, L. L. M., Houtsmuller, U. M., de Haas, G. H., & Mulder, E. (1962). Monomolecular layers of synthetic phosphatides. *Journal of Pharmacy and Pharmacology*, 14(7), 429–444.
- [Vaz et al., 1985] Vaz, W. L. C., Clegg, R. M., & Hallmann, D. (1985). Translational diffusion of lipids in liquid crystalline phase phosphatidylcholine multibilayers. a comparison of experiment with theory. *Biochemistry*, 24, 781–786.
- [Vaz et al., 1984] Vaz, W. L. C., Goodsaid-Zalduondo, F., & Jacobson, K. (1984). Lateral diffusion of lipids and proteins in bilayer membranes. *FEBS Letters*, 174(2), 199–207.
- [Velandar et al., 1992] Velandar, W. H., Madurawe, R. D., Subramanian, A., Kumar, G., Sinai-Zingde, G., Riffle, J. S., & L., O. C. (1992). Polyoxazoline-peptide adducts that retain antibody avidity. *Biotechnology and Bioengineering*, 39(10), 1024–1030.
- [Vuilleumier et al., 1995] Vuilleumier, R., Ego, V., Neltner, L., & Cazabat, A. (1995). Tears of wine: The stationary state. *Langmuir*, 11, 4117–4121.
- [Wagner & Tamm, 2000] Wagner, M. & Tamm, L. (2000). Tethered polymer-supported planar lipid bilayers for reconstitution of integral membrane proteins: Silane-polyethyleneglycol-lipid as a cushion and covalent linker. *Biophysical Journal*, 79(3), 1400–1414.
- [Wagner & Tamm, 2001] Wagner, M. & Tamm, L. (2001). Reconstituted syntaxin1A/SNAP25 interacts with negatively charged lipids as measured by lateral diffusion in planar supported bilayers. *Biophysical Journal*, 61, 266–275.
- [Warriner et al., 1996] Warriner, H. E., Idziak, S. H. J., Slack, N. L., Davidson, P., & Safinya, C. R. (1996). Lamellar biogels: Fluid-membrane-based hydrogels containing polymer lipids. *Science*, 271(5251), 969–973.
- [Warriner et al., 1998] Warriner, H. E., Keller, S. L., Idziak, S. H. J., Slack, N. L., Davidson, P., Zasadzinski, J. A., & Safinya, C. R. (1998). The influence of polymer molecular weight in lamellar gels based on PEG-lipids. *Biophysical Journal*, 75, 272–293.
- [Waugh, 1982a] Waugh, R. E. (1982a). Surface viscosity measurement from large bilayer vesicle tether formation. I. Analysis. *Biophysical Journal*, 38, 19–27.
- [Waugh, 1982b] Waugh, R. E. (1982b). Surface viscosity measurement from large bilayer vesicle tether formation. II. Experiments. *Biophysical Journal*, 38, 29–37.
- [Winter, 2002] Winter, R. (2002). Synchrotron X-ray and neutron small-angle scattering of lyotropic lipid mesophases, model biomembranes and proteins in solution at high pressure. *Biochimica et Biophysica Acta*, 1595, 160–184.
- [Woese & Fox, 1977] Woese, C. R. & Fox, G. E. (1977). Phylogenetic structure of the prokaryotic domain: The primary kingdoms. *Proceedings of the National Academy of Sciences of the United States of America*, 74, 5088–5090.

- [Wohlfarth & Wohlfarth, 2001] Wohlfarth, C. & Wohlfarth, B. (2001). 'Viscosity of Pure Organic Liquids and Binary Liquid Mixtures' in 'Landolt-Börnstein - Numerical Data and Functional Relationships in Science and Technology - New Series', volume IV / 18A, chapter 3.1.2, (pp. 263–266). Springer-Verlag: Berlin.
- [Wong et al., 1999] Wong, J. Y., Majewski, J., Seitz, M., Park, C. K., Israelachvili, J. N., & Smith, G. S. (1999). Polymer-cushioned bilayers. I. A structural study of various preparation methods using neutron reflectometry. *Biophysical Journal*, 77, 1445–1457.
- [Woodle et al., 1994] Woodle, M., Engbers, C., & Zalipsky, S. (1994). New amphipatic polymer-lipid conjugates forming long-circulating reticuloendothelial system-evading liposomes. *Bioconjugate Chemistry*, 5(6), 493–496.
- [Yaminski et al., 1997] Yaminski, V., Nylander, T., & Ninham, B. (1997). Thermodynamics of transfer of amphiphiles between the liquid-air interface and a solid surface-wetting tension study of Langmuir-Blodgett films. *Langmuir*, 13, 1746–1757.

Vielen Dank...

an alle, die zum Gelingen dieser Arbeit beigetragen haben:

Prof. E. Sackmann für seine Begeisterung für Physik und die Möglichkeit diese Dissertation durchzuführen (“Florian? Nein, Oliver!”).

Motomu Tanaka, für sein Ideenreichtum und für das einmalige Arbeitsklima in seiner Gruppe.

Anton Förtig und **Rainer Jordan** für die Synthese der Lipopolymere, ohne die meine Dissertation nicht durchführbar gewesen wäre, für die sehr gute Zusammenarbeit und für die vielen Diskussionen.

Florian Rehfeldt und **Michael Nikolaides** für die Freundschaft, die uns seit Beginn des Studiums verbindet, und ohne die einige Herausforderungen des Studiums und der Promotion kaum zu meistern gewesen wären.

Den “Lipidlern“ und “Filmwaaglern“ **Matthias F. Schneider** und **Heiko Hillebrandt** für die Hilfe bei Theorie und Praxis und für die außerwissenschaftlichen Aktivitäten.

Monika Rusp für die Aufreinigung von Integrin, die Präparation von Integrinvesikeln, die Hilfe bei Chemiesachen, ...

Stefanie Gönnenwein für die Starthilfe beim FRAPen und die Adhäsionsexperimente.

Stefan Kaufmann und **Michael Bärmann** für die Beantwortung meiner biologischen/biochemischen Fragen.

Hulda Kirpal, **Gabi Chmel**, **Claudia Antrecht** und **Karin Vogt** für die Hilfe bei Chemie-Fragen.

Den Rest der Motomu-Gruppe (ehemalige, jetzige, zukünftige): **Uwe Tutus**, **Jochen Hermann**, **Thomas Schubert**, **Manu Schneck**, **Fatima Al Ali**, **Klaus Adlkofer**, **Kirstin Seidel**, **Daniel Gassull** und **Raphael Oliveira** für die wissenschaftliche Zusammenarbeit und die vielen Diskussionen und Aktivitäten.

Jörg Schilling, **Felix Linke** und **Rainer Tharmann** für die Lösung meiner Computerprobleme (Hardware, Software, OpenBox, ...).

Rudi Lehrhuber als fähigen Werkstattmeister.

Allen anderen E22ern für die Zusammenarbeit und die gute Stimmung am Institut und auf der Winterschule.

Der **Kaffeecke** und all diejenigen, mit denen ich dort Kaffee/Bier getrunken habe, für die erfüllten Pausen bei und nach der Arbeit.

Georg Steinhoff und **Martin Eickhoff** für die gute Kooperation im GaN-Business.

Raimund Gleixner für die FLIC-Experimente, und **Prof. P. Fromherz** für die Möglichkeit diese in seinem Institut durchzuführen.

Besonderer Dank gilt **meinen Eltern** und **meiner Oma** für die langjährige Unterstützung.

Curriculum Vitae

Oliver Purrucker

Date of birth: March 22nd, 1975

Place of Birth: Hof/Saale, Germany

University Education

- | | |
|-------------|--|
| 2001 - 2004 | PhD thesis at the Lehrstuhl für Biophysik E22, Technische Universität München, Germany. |
| 1995 - 2000 | Study of physics (“Allgemeine Physik“) at the Technische Universität München, Germany.
Degree: “Dipl.-Phys. Univ.“.

Diploma thesis at the Lehrstuhl für Biophysik E22, Technische Universität München, Germany.
Title: “Deposition of Model Cell Membranes on Silicon - Silicon Dioxide Electrodes and Functional Incorporation of Gramicidin: An AC Impedance Spectroscopy Study“. |

Military Service

- | | |
|-------------|---|
| 1994 - 1995 | 3. Gebirgsjägerbataillon 231, Bad Reichenhall, Germany. |
|-------------|---|

Primary Education

- | | |
|-------------|--|
| 1985 - 1994 | Comprehensive secondary school: Gymnasium Wunsiedel (“Mathematisch-naturwissenschaftlicher Zweig“), Germany.
Degree: “Allgemeine Hochschulreife“. |
| 1981 - 1985 | Primary school: Grundschule Weißenstadt, rural district of Wunsiedel, Germany. |

Publications

Purrucker, O., Förtig, A., Lüdtke, K., Jordan, R., and Tanaka, M. (2004). Confinement of Transmembrane Cell Receptors in Tunable Stripe Micropatterns. *Journal of the American Chemical Society*, accepted.

Purrucker, O., Förtig, A., Jordan, R., and Tanaka, M. (2004). Supported membranes with well-defined polymer tethers - incorporation of cell receptors. *ChemPhysChem*, 5, 327 - 335.

Purrucker, O., Hillebrandt, H., Adlkofer, K., and Tanaka, M. (2001). Deposition of highly resistive lipid bilayer on silicon-silicon dioxide electrode and incorporation of gramicidin studied by ac impedance spectroscopy. *Electrochimica Acta*, 47, 791 - 798.

Steinhoff, G., Purrucker, O., Tanaka, M., Stutzmann, M., and Eickhoff, M. (2003). $\text{Al}_x\text{Ga}_{1-x}\text{N}$ - A New Material System for Biosensors. *Advanced Functional Materials*, 13, 841 - 846.

Tutus, M., Purrucker, O., Adlkofer, K., Eickhoff, M., Tanaka, M. (2004). Electrochemical Stabilization of Crystalline Silicon with Aromatic Self-Assembled Monolayers in Aqueous Electrolytes, submitted.

Förtig, A., Jordan, R., Purrucker, O., and Tanaka, M. (2003). 2-alkyl-2-oxazoline lipopolymers for the construction of polymer tethered lipid bilayers. *Polymer Preprints*, 44, 850 - 851.

Förtig, A., Jordan, R., Graf, K., Schiavon, G., Purrucker, O., and Tanaka, M. (2004). Solid-supported biomimetic membranes with tailored lipopolymer tethers. *Macromolecular Symposia*, 210, 329 - 338.

Tanaka, M., Rehfeldt, F., Schneider, M. F., Mathe, G., Albersdörfer, A., Neumaier, K. R., Purrucker, O., and Sackmann, E. (2004). Wetting and Dewetting of Extracellular Matrix and Glycocalix Models. *Journal of Physics: Condensed Matter*, accepted.